IMPERIAL COLLEGE OF SCIENCE, TECHNOLOGY AND MEDICINE

Faculty of Engineering

Department of Chemical Engineering

CERAMIC HOLLOW FIBRE CATALYTIC CONVERTERS FOR AUTOMOTIVE EMISSIONS CONTROL

NUR IZWANNE BINTI MAHYON

A Thesis Submitted for the Degree of Doctor of Philosophy and the Diploma of Imperial College London

DECLARATION OF ORIGINALITY

I hereby declare that this thesis and the work reported herein was composed by and originated entirely from me. Information derived from the published and unpublished work of others has been cited, acknowledge in the relevant text and related references are included in this thesis.

Nur Izwanne Binti Mahyon

Imperial College London,

October 2019

ABSTRACT

The development of ceramic hollow fibre catalytic converters for the control of automotive emission has been presented in this thesis. Attempts have been made to understand the different factors such as the fabrication of the substrate, the effects of the washcoat packing, the variations of the catalytic reactions at different catalyst formulations, and the evaluation of the pressure drop in the new substrate structure, since these factors may cause a real hindrance in the development of a new ceramic hollow fibre catalytic converter. An asymmetric ceramic hollow fibre substrate was fabricated through the extrusion process, assisted by a phase-inversion. The produced substrate resulted in a hollow fibre with an array of microchannels with almost double the hydraulic diameter of the commercial 400 cells per inch square (CPSI) honeycomb monolith, which lead to less pressure drop in the system. The hollow fibre substrate can offer a tremendous increase in the geometric surface area (GSA), which is beneficial for catalyst layer deposition. With the new structure, a new washcoating technique has been proposed. A loosely packed washcoat in the microchannel has been identified as the best configuration. After the successful conversion of CO at a low light-off temperature and low precious metal loading, two perovskite catalysts have been synthesised, and their catalytic activity in the hollow fibre catalytic converter has been assessed. This result indeed highlights the advantage of the new proposed structure for catalytic converters in order to control tailpipe emissions.

ACKNOWLEDGEMENTS

First of all, a tremendous thanks to all those who freely gave their time, advice, encouragement and trust throughout my PhD journey.

I would like to thank my supervisor, Professor Kang Li and Professor Ricardo Martinez-Botas for their guidance, patience and experiences that gave shape and direction to my studies. Thank you for sharing your immense knowledge and enthusiasm to carry with me as inspiration.

Not to forget, I am truly indebted to all my colleagues, especially to Dr Zhentao Wu and Dr Tao Li who have carefully reviewed the journal papers and different parts of this thesis and shared their extensive experience and knowledge on the subject. To the members of Kang Li's group, Fairus, Farah, Lucy, Tong Rong, Dr Bo, Dr Huang Kang, Vatsal, and Marc, and the members of the Turbocharger Ricardo's group, thank you for creating such a lively knowledge-sharing environment.

For my parents, Mahyon Mohd Kasan and Rosmah Abu Bakar, my siblings, relatives and my in-laws, my heartfelt thanks to all of you for your perseverance and relentless encouragement, prayers and support for me to help me be the first in the family to pursue a PhD.

I am grateful to my employer, Universiti Teknologi Malaysia and the Ministry of Higher Education Malaysia, for their financial support, which made my pursuit of PhD possible. To my research group LoCARtic UTM, Dr Srithar Rajoo, Dr Chiong, Nur Izrin, Ryan, Fad, Kim, and all other members who have helped me during my research time at LoCARtic, I am

thankful for your kindness and generosity. I would like to acknowledge the research funding provided by EPSRC in the United Kingdom.

Next, a thank-you to my special friends, Irina Harun and Nuraini Daud for being there at all times for almost everything. The time I spent in London would have definitely been more difficult without the assistance and friendship of the Vellacott members, the Beaumont roommates, the Sri Rahayu's badminton group, and not to forget, Kajol (Farhan) and Joshi (Ramizah) for always being so entertaining.

Despite the errors that still exist here and there which are entirely my responsibility, this thesis would not have been this thesis without the help of those who have had proof-read it. Thank you for your generosity with your time.

LIST OF PUBLICATIONS AND CONFERENCE PRESENTATIONS

N.I. Mahyon, T. Li, R. Martinez-Botas, Z. Wu, K. Li, A new hollow fibre catalytic converter design for sustainable automotive emissions control, Catalysis Communications, 120 (2019), 86-90.

N.I. Mahyon, T.Li, B. D. Tantra, R. Martinez-Botas, Z.Wu, K. Li, Integrating Pd-Doped Perovskite Catalysts with Ceramic Hollow Fibre Substrate for Efficient CO Oxidation, Journal of Environmental Chemical Engineering, submitted.

N.I. Mahyon, T. Li, Ricardo F. Martinez-Botas, K. Li, Ceramic Hollow Fibre Catalytic Converters for Automotive Emissions Control, Presented at 9th International Membrane Science and Technology Conference, 5-8 December 2016, Adelaide, Australia.

(Won The Best International Student Presentation Award)

N.I. Mahyon, T. Li, Ricardo F. Martinez-Botas, K. Li, Ceramic Hollow Fibre Catalytic Converters for Automotive Emissions Control, Presented at WCX: SAE World Congress Experience Conference, 10-12 April 2018, Detroit, Michigan, United States of America.

N.I. Mahyon, T. Li, Ricardo F. Martinez-Botas, K. Li, Ceramic Hollow Fibre Catalytic Converters for Automotive Emissions Control, Presented at 2nd Malaysia-Singapore Research Conference, 25 March 2017, Cambridge, United Kingdom.

(Won The Best Poster Presentation Award)

TABLE OF CONTENTS

LIST OF TABLES

LIST OF FIGURES

CHAPTER 1

Introduction

1.1 Background

A report published in 2011 by the World Energy Council (WEC) states that the global transportation sector is expected to face an intensification of unprecedented challenges in the four decades between 2010 to 2050. The Global Transport Scenarios to 2050 has been built to examine the future of this industry that would be profoundly affected by several factors such as global economic growth, demographic trends and any future technological breakthroughs [1]. The proliferation of the transportation industry, driven by population demands, is predicted to cause an increase in global emissions if left unchecked. Further, it is expected that by the year 2050, carbon dioxide (CO_2) emissions will increase by nearly 79%, approximately 12 Gt CO_2eq/year, which is subject to government intervention in a low-carbon transport policy [2]. The aforementioned figure is alarming and has put pressure on policymakers to pursue strict emission regulations within a tighter range of concentration, as a mitigation measure.

Tailpipe emissions originating from an internal combustion engine (ICE) emit a number of combustion by-products. Under normal engine operating conditions, the following is observed as the typical composition of the gases emitted (See Table 1.1).

Table 1.1 Typical exhaust gas composition at normal engine operating condition for gasoline [3]

Major Constituents	Composition
Water, H_2O	10 vol.%
Carbon dioxide, CO_2	10 vol.%
Unburned hydrocarbons, HCs	350 vppm
Oxygen, O_2	0.5 vol.%
Carbon Monoxide, CO	0.5 vol.%
Nitrogen oxides, NOx	900 vppm
Hydrogen, H_2	0.17 vol.%

CO, HCs and NOx are the major pollutants from the exhaust. CO and HCs are formed as a result of incomplete combustion, while combustion at a sufficiently high temperature and pressure produces NOx. Exposure to CO causes detrimental health risks when inhaled, since CO restricts the level of oxygen in the blood and causes further suffocation of the organ through the displacement of oxygen. Also, high concentrations of CO may lead to unconsciousness or even death. HCs and NOx, on the other hand, are responsible for environmental hazards since a reaction between the two compounds and sunlight produces ground-level ozone, which is a major component of smog and other secondary pollutants. Photochemical smog causes a series of respiratory diseases and further leads to the irritation of the eyes, reducing visibility [4,5]. Considering the health and environmental impacts caused by these compounds, the development of exhaust treatment technologies is crucial for minimizing the risks posed by automotive ICE emissions.

To address the risks discussed above, tailpipe emission control devices, known as catalytic converters, have been used to treat internal combustion engine products and convert them into innocuous gases such as CO_2, water (H_2O) and nitrogen (N_2). A tailpipe control device was first invented during the 1950s by the French mechanical engineer Eugene Houdry, an expert in catalytic oil refining [6]. Early published studies concerning smog in Los Angeles brought Houdry's attention to these issues, who then focused on trying to reduce the health risks associated with the increasing levels of air pollution caused by the burgeoning automobile and industrial sectors. Widespread use of the catalytic converter only began in the mid-1970s after the U.S. Environmental Protection Agency (EPA) enabled strict regulation, requiring every gasoline-powered vehicle manufactured 1975 onwards to be equipped with a catalytic converter [7]. Further research was expected to improve the initial designs of the catalytic converter. The original design operated as a two-way converter where it targeted the oxidation of CO and hydrocarbons only. The current generation of the catalytic converter is capable of nullifying CO, HCs and NOx simultaneously, and is known as the three-way catalytic converter. Interestingly, catalytic converters do not have an application in a vehicle exhaust system only, but also have broader uses in emission control for electrical generators, mining equipment, locomotives and aeroplanes.

The conventional catalytic converter is a honeycomb structure in a monolithic configuration made of ceramic or metal components coated with metal catalysts from the Platinum Group Metals (PGM), where the constituent elements are usually platinum (Pt), rhodium (Rh), and or palladium (Pd), subsequently encased in a stainless-steel container. The honeycomb monolith design provides a parallel flow channel for contact between the reactant and catalyst, limiting unnecessary back-pressure in the system. The metal active catalyst layer, also known as a catalytically active washcoat, consists of a high surface area material impregnated with a

catalyst. There are two different types of catalysts at work; an oxidation catalyst and a reduction catalyst. Although the research on catalytic converters has been extended to study different types of non-PGM catalysts and compatible oxygen storage material washcoats, this research is still in the experimental stage [8–11]. Nonetheless, the main concern with the non-PGM is their susceptibility towards deactivation due to the sulphur originating from diesel fuel especially, further making such metals unfavourable for long-term usage. Hence, highly valuable and expensive PGMs remain the preferred choice of catalyst after significant experimentation with cheaper alternatives has yielded inferior results [12].

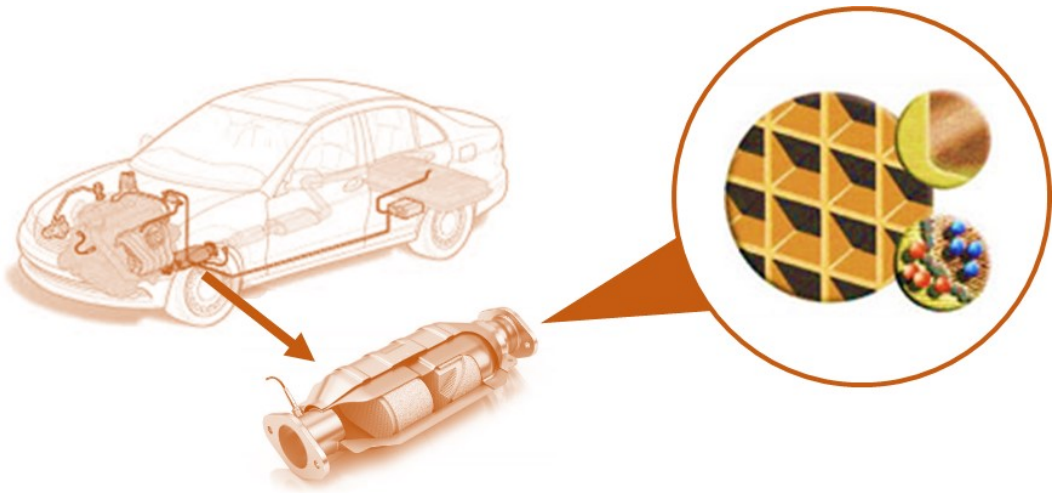

Figure 1.1 Diagram of catalytic converters and its position in the cars

The uncertainty around the future of PGM is largely due to the progressive depletion of the rare metals used. Further, the price volatility of PGM would restricts commercial use of this material for long term [13]. One solution is to reduce the amount of PGM in catalytic converters without affecting their efficiency and performance. As catalytic performance is directly proportional to the contact of the active sites with the reactants, a larger surface area for deposition is required in order to optimise this interaction. This can be achieved by increasing the geometric surface area (GSA) of the substrate on which the catalytic washcoat can be

deposited evenly. A common practice to improve the GSA is by increasing the number of cells per inch square (CPSI) of the monolith [14]. However, this method draws a much higher pressure-drop because of increased flow restriction at the catalyst entrance. Therefore, it is crucial that any optimisation of the substrate takes into account two conflicting requirements: (1) the increase of contact area between the gas and the catalyst and, (2) minimisation of pressure loss across the gas flow path [15].

In this thesis, a novel ceramic hollow fibre was fabricated using a single-step phase-inversion extrusion technique. A hollow fibre containing microchannels was used as a new substrate for the application of catalytic converters in pursuance of controlling automotive emissions. The availability of microchannels in the substrate has been proven to offer high GSA without having to restrict the open area entrance for the fluid to pass through, thus, improving the back-pressure condition of the engine. With a significant GSA at hand, the deposition of the active material was done at a notably lower amount than the conventional formulation, reducing the PGM loadings in the new system. The study also explored the most favourable packing conditions of the catalyst in the substrate to fully utilise the active sites and to minimise the mass transfer resistance during the operation. Catalytic performances were carried out to evaluate the conversion efficiency by using CO for a sample reaction.

After the success of the ceramic hollow fibre catalytic converter using a palladium-only catalyst, an attempt to further reduce PGM loading in the catalytic converter led the research to synthesise a palladium-doped perovskite. Finally, two types of palladium-doped perovskites were synthesised in-house, and their conversion performance was studied and discussed.

1.2 Thesis Objectives

The primary objective of this thesis is to develop ceramic hollow fibres for catalytic converters containing a substantially reduced volume of Platinum Group Metals (PGM), for emission control from light-duty vehicles. In this study, ceramic hollow fibres containing microchannels with a high geometric surface area are used as a substrate for catalytic converters. These were fabricated through a phase inversion assisted single-step extrusion process. In order to achieve the primary objective of the study, the following milestones were set to ensure the completion of the project:

i. To fabricate defect-free ceramic hollow fibre substrates using a single-step extrusion process

Porous ceramic hollow fibre substrates were fabricated by the extrusion phase inversion process, using a single orifice spinneret. This step was aimed towards producing a hollow fibre with high porosity and open micropores in the inner surface with a relatively high mechanical strength, for use as a substrate incorporated with the active metal catalyst.

ii. To study the effects of the washcoat loadings and the packing of the hollow fibre microchannels on the catalytic reaction of CO oxidation.

Catalytic performance is not only affected by the reactivity of active metals being used. In catalytic converter applications, the washcoat layer also plays a significant role. The thickness of this layer affects the conversion performance resulting from the existence of the mass transfer resistance in the system. Different washcoat loadings and packing conditions lead to a difference in the mass transfer regime during the reaction. Thus,

finding the best condition for the washcoat packing is vital towards ensuring optimal catalyst utilisation.

iii. To determine a washcoat and catalyst deposition technique for an even distribution of the active sites onto microchannels.

Catalytic converters are made of monolith support deposits with washcoat and catalysts. As the new proposed design contained open microchannels, deposition and impregnation of active layers required modifications from conventional practice. Different deposition and impregnation techniques were investigated to achieve well-dispersed and highly distributed active catalyst sites.

iv. To explore the options of available low Platinum Group Metals as a potential three-way catalyst.

Price volatility and the scarcity of PGM makes finding a suitable substitute for this type of catalyst compelling. A Perovskite oxide has proven to have interesting properties. One of the properties of a perovskite oxide is the enhancement of the thermal stability of the easily sintered PGMs while maintaining their reactivity. For this reason, two types of perovskite oxides containing different metals were synthesised. The catalytic activity of precious catalysts and perovskite catalysts was studied by measuring the oxidation reaction of carbon monoxide.

1.3 Thesis Structure and Organisation

This thesis is composed of seven chapters discussing the process and steps taken to use ceramic hollow fibres as the new substrate for catalytic converter applications. The process starts with

the fabrication of alumina ceramic hollow fibres as the new substrate design for the catalytic converters. The effects of the washcoat packing inside the microchannels on the CO oxidation performance are studied, followed by the performance of low PGM perovskite oxides catalyst in the hollow fibre substrate. Figure 1.2 presents the overall flow of the thesis.

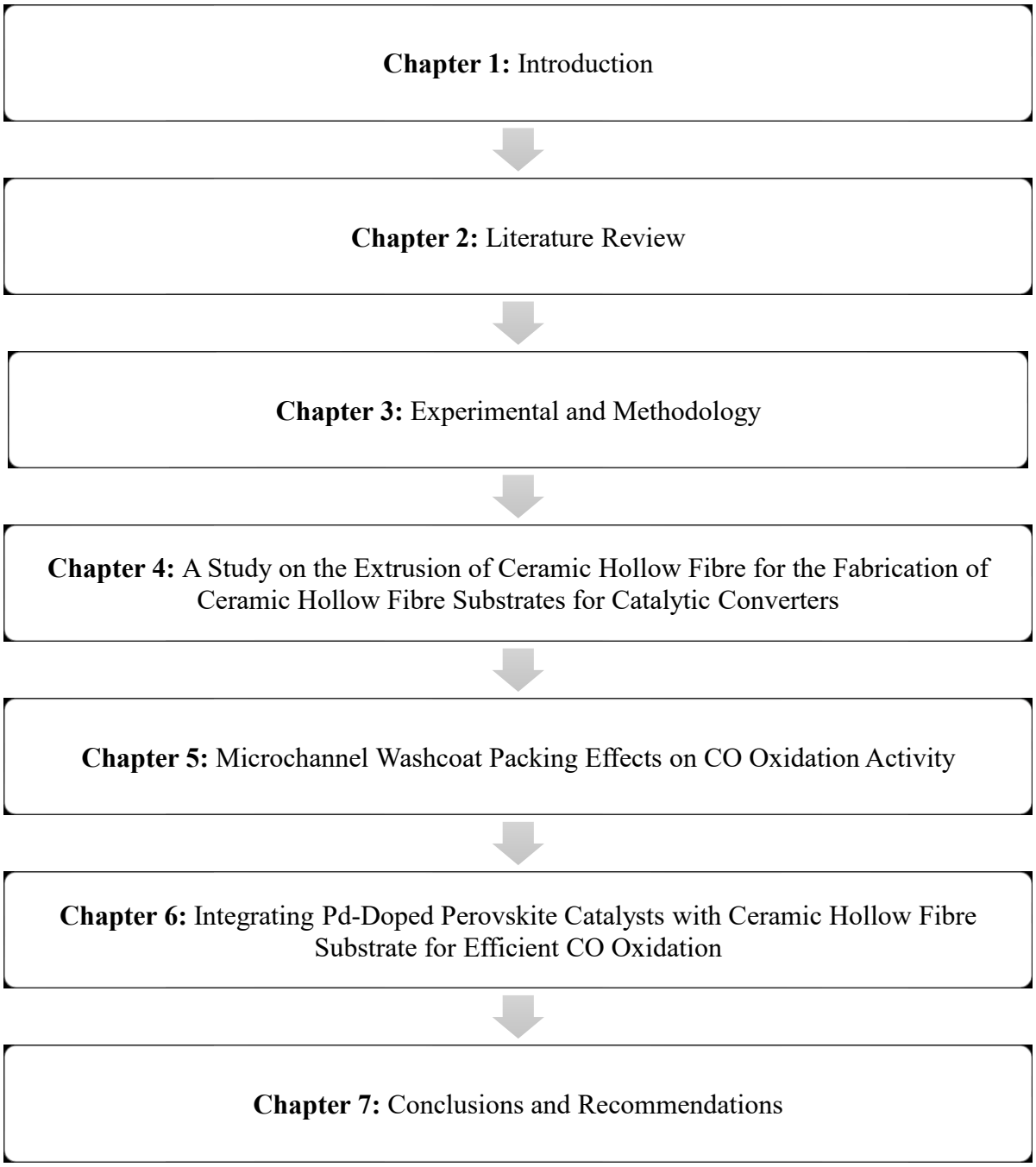

Figure 1.2 Overall structure of the thesis

A brief history and introduction of catalytic converters is summarised in **Chapter 1**. This chapter includes the discussions on the objectives of the study and an overview of the thesis. Subsequently, **Chapter 2** presents the literature review, which provides a more comprehensive discussion on the topic concerning catalytic converter components as well as the existing and the current development of the topic. Catalyst studies and challenges that have yet to be overcome in tailpipe emission treatments are also examined in the review of the literature. Further, ceramic hollow fibre fabrication through phase inversion technique is discussed. The discussion also extends to the application of an emerging perovskite oxide as a new potential catalyst, to substitute the commercially used PGM catalyst.

Chapter 3 lists all materials used in the process, methodology, characterisations and experimental procedures applied to achieve the aforementioned objectives of the study.

Chapter 4 presents the process and success rate of fabricating new ceramic hollow fibre substrates for catalytic converters through the extrusion technique assisted by phase inversion. The formation of the microchannel, through this technique, the morphological evaluation and the structural improvement, as compared to the typical honeycomb structure, is also discussed in this chapter.

Chapter 5 discusses the relevant processes after the success of the substrate fabrication. The chapter discusses the effects of the washcoat packing inside the microchannel. Since a ceramic hollow fibre is new in the use of a catalytic converter application, the configuration and an effective washcoat layer is critical to the study. In addition, CO oxidation reactions were carried out, and their performance was evaluated.

Chapter 6 maintains continuity with the studies concerning the washcoat effect in Chapter 5, examining the objective of reducing the content of PGM applied to the catalytic converter system. For this process, palladium doped perovskites were synthesised, and their morphology, structural and reactivity were characterised. Their reactivity was evaluated by CO oxidation also as a sample reaction, and the effects of the packing configuration in the hollow fibre substrate were compared with the packed-bed packing. Mass transfer limitations in the washcoated hollow fibre substrates are further discussed in the chapter.

Finally, all findings from the study are summarised in **Chapter 7**. A discussion is presented on the methodologies and outcomes within this thesis, and recommendations are made for future research.

CHAPTER 2

Literature Review

This section presents a comprehensive review of the literature concerning automotive emissions and the fundamentals of catalytic converters. Furthermore, a detailed discussion of the challenges and limiting factors that affect the performance of catalytic converters is presented. Additionally, recent advancements in the three-way catalyst technology and principles of an induced-phase inversion substrate fabrication are also presented in this section.

2.1 Automotive Emissions

The term automotive was derived from the Greek and Latin words, *autos* meaning self in Greek and *motivus* (of motion) in Latin. These two words were joined together and the term automotive was coined, referring to any form of a self-propelled vehicle. The present-day understanding of automotive often relates to vehicles powered by an internal combustion engine (ICE). The ICE plays an essential role in the automotive industry, largely due to its simplicity, robustness and high thermal efficiency [15]. They can be categorised under two major engine-forms, namely, the petrol ICE and diesel ICE. The working mechanism differs

in the two engines. Diesel combustion is initiated under a certain pressure and temperature. This is known as the compression ignition (CI) engine. On the other hand, petrol or gasoline is ignited by a spark that ignites the premixed fuel-air in the combustion chamber and is known as a spark ignition (SI) engine. Other significant differences between CI and SI engines are their efficiency and emission levels. Since CI engines have a high compression ratio, these engines are thermally efficient compared to the SI engines. However, emissions from SI engines are comparatively greener and easier to treat. Going forward, this review will focus on emissions originating from petrol ICE.

Exhaust from motor vehicles contain a complex mixture of chemicals. These chemicals in gas form include carbon monoxide (CO), hydrocarbons (HC), and nitrogen oxide (NOx), and in solid form include particulate matter and solid or liquid aerosol, which in turn includes volatile organic compounds (VOC) and semi-volatile organic compounds (SVOC) [5,16]. These substances undergo chemical reactions with components present in the atmosphere. Such interactions increase the existing level of air pollution. They also result in the creation of a secondary pollutant, which aggravates the health and environmental risks associated with these exhaust emissions. Under normal engine conditions, the primary tailpipe emissions contain CO (0.5 vol.%), HCs (350 vppm) and NO (900 vppm) [3]. It is impossible to get 100% efficiency from the combustion process due to limitations arising from Air-to-Fuel (A/F) mixing and cooling effects from the cylinder wall and as a result it leads to the formation of by-products. Combustion under lean mixture produces less CO and HCs, but engines suffer from low power output. Rich combustion, on the contrary, leads to a low fuel economy and higher output of CO and HCs, while combustion at a high temperature, if accompanied by sufficient pressure, forms NOx emissions. Figure 2.1 illustrates the correlation between emission levels and engine power.

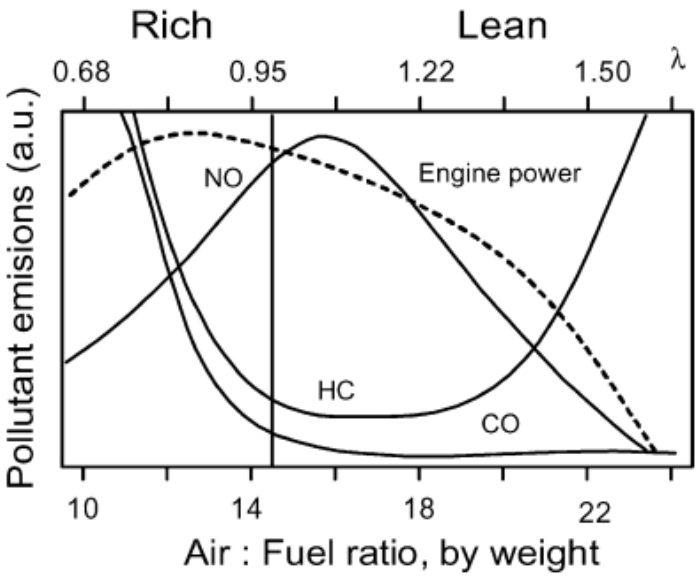

Figure 2.1 Effect of A/F ratio (w/w) on engine emissions and output power [17]

When inhaled, CO competes with oxygen for available binding sites in haemoglobin, which causes a reduction in oxygen transport and release in the body. Exposure to low concentrations of CO can cause dizziness, headache and nausea. A short report published by Townsend et al. on prolonged exposure to low concentrations of CO argues that there might be a possibility of neurological effects on the brain [18]. But the results from the report are still contentious since transient exposure does not have a lasting effect. Nevertheless, chronic exposure to CO may lead to unconsciousness or even death. While CO is considered primarily as a direct hazard to health, NOx, which usually relates to nitrogen monoxide (NO) and nitrogen dioxide (NO_2) as the main constituents, are the primary pollutants of the atmosphere. NOx and its main constituents are believed to be the major contributors to acid rain, photochemical smog, tropospheric ozone, depletion of the ozone layer and global warming [19]. Reactions with readily available compounds in the air produce secondary pollutants. For example, in the presence of sunlight and a VOC compound, smog is formed. This secondary pollutant is not only environmentally harmful but is also toxic to human health, as it can irritate the eyes and

the nasal passage, causing damage to the lungs in the short-term while exhibiting carcinogenic properties with long-term exposure [20–22].

In 2012, the World Health Organisation reported an estimated 7 million deaths annually worldwide, caused by air pollution [23]. For the record, automotive emissions contribute 14% to the source of pollutants, especially in urban areas [24]. The deaths value has more than doubled from the previous year's estimates after a wider demographic was taken into account and with the use of improved measurements and technology. The risk factor is greater than expected and requires urgent attention towards cleaning the air. However, reducing global transport emissions is a challenge, especially with the increase in the demand and supply for private vehicles. Hence, structured mitigation measures with the involvement of different bodies is needed to be carried out and updated regularly, in order to ensure that the problem is contained without affecting the global economic growth of the automotive sector.

2.2 Emissions Control

Implementation of the Clean Air Act in 1970 in the United States changed the landscape of emission control strategies around the globe [25]. This initiative has driven countries such as Japan, Europe and several other countries to set up their own emission regulations, in order to address and mitigate the same concerns over increasing health and environment threats originating from vehicles emissions. Many international agencies worldwide have pledged to contribute to helping control air pollution and climate change caused by automotive emissions. These agencies include the Environmental Protection Agency (EPA), Organisation for Economic Co-operation and Development (OECD), Intergovernmental Panel on Climate

Change (IPCC), International Energy Agency (IEA), European Environmental Agency (EEA) etc. Their efforts include advancing technological developments, creating several model structures, organising the structure of traffic and specific emphasis on making several legal arrangements to review current legislation on emission control [26]. Such legislations aim to control and limit the discharge of noxious gases from internal combustion engines and other components. Stringent emission regulations have pressurised key players in the automotive industry to manufacture greener vehicles, predominantly by improving their emission control devices. These improvements are usually a response to government regulations, either through direct environmental regulations or through health and safety regulations. Additionally, global awareness of health and environmental issues, regardless of the level of air pollution, has increased. Therefore, if carmakers do not commit to the current trend, they will loose their grip on the market.

With the intention of keeping noxious emissions under control, different techniques have been proposed and tested. Progress concerning ICE technological improvements can be broadly divided into two sections: (i) to make ICE more efficient, and (ii) to improve the exhaust treatment system. These two systems are also interdependent. An efficient ICE configuration can lead to emission of fewer pollutants, while a good design of tailpipe emission control devices can help improve engine performance while cleaning the air simultaneously. Advancements in modern internal combustion engines focus on producing a fuel-efficient system, with the innovation of fuel injection integration with computer controls. Such advanced technology includes direct injection, cooled exhaust gas recirculation (C-EGR), high compression ratio (CR), Atkinson cycle, stop-start technology, cylinder deactivation, advanced turbocharging and mild hybridisation [3,27].

Direct injection enables fuel efficiency which promotes ultra-lean burn through highly pressurised gasoline, injected directly into the combustion chamber. C-EGR function is to lower NOx emissions by recirculating a portion of the exhaust gas back to the engine chambers, hence, lowering the combustion temperature. Stop-start technology uses a computer to detect when the car is in a stationary position to reduce fuel consumption and emissions. However, the stop-start technology has caused concern over the life of the engine's bearings and its durability, especially with increasing metal-to-metal bearing contact due to the stop-start rotations. Advanced turbocharging, on the other hand, is seen as the most interesting option in an ideal condition. Turbocharging would be able to offer a high-power density engine at low fuel cost [28,29]. Even though the featured technologies claim to be able to reduce emissions, one way or the other, issues with the efficiency of these technologies are inevitable. Hence, the exhaust purification device recognised as a catalytic converter is still an essential part of the emissions control system.

2.3 Catalytic Converters

In the 1950s, German engineer Eugene Houdry invented the first catalytic converter. Introduction of the technology to the automobile sector began in the mid-1950s. During this time, we saw a limited adoption of this system in cars due to the presence of a number of catalyst poisons originating in the fuel, especially Tetraethyl lead, which could effectively disable the catalyst. After strict regulations demanded the removal of lead from gasoline, widespread development of the technology led to the first production of a catalytic converter in 1973. Early research agreed upon a set of design and performance criteria for guidance when designing a catalytic converter. The listed criteria included (i) a reasonable life cycle cost of the device, which covers equipment and maintenance cost, (ii) a robust device which would be

able to run for at least 12,000 miles without any major equipment replacement and with low maintenance, (iii) creation of converters of a size that adapt to the space available in the conventional automobile design, (iv) the condition that the device should not impose a back-pressure more than 25% and should not impact fuel consumption or the vehicle's performance, and (v) that the catalytic converter should be able to maintain an emission level of HCs less than 275 ppm and 1.5% by volume of CO for a minimum of one year or the first 12,000 miles of operation [30]. Though it was introduced in the 1960s, the rules from this set of guidelines are still relevant for the modern catalytic design, with an even tighter specification.

Catalytic converters are regarded as a vital component in every internal combustion engine. The development of catalytic converters was expedited by the change in fuel composition and the advancement in engine management and automation control systems. Initially, after-treatment systems only targeted CO and unburned hydrocarbons, which were treated with a simple oxidation reaction system known as a two-way system. The basic converters commonly comprise of Pt-Pd/Al_2O_3 catalysts to assist in the conversion process. The two-way catalytic converter is also known as an oxidation converter. The oxidation converter has two simultaneous processes that allow the oxidation of carbon monoxide (CO) to less harmful components, such as carbon dioxide (CO_2) and oxidising hydrocarbons to CO_2 and water (H_2O) [31]. It operates at relative efficiency with lean fuel. However, since it only has a two-way reduction capacity, the oxidation converter is ineffective in controlling the oxides of nitrogen (NOx), which needs a more complex reduction reaction. Thus, the two-way catalytic converters have been superseded by the three-way converters (TWC).

The schematics of the three-way catalytic converters are shown in Figure 2.2. A TWC has the additional advantage of controlling the emission of nitrogen oxides (NOx), greenhouse gases

which are precursors to acid rain, and currently the most ozone-depleting substances [32]. In comparison to the two-way catalytic converter, which only works based on oxidation reaction, a TWC has three simultaneous tasks:

i) Oxidation of carbon monoxide to carbon dioxide:

$$O_2 + CO \rightarrow 2CO_2 \quad [2.1]$$

ii) Oxidation of unburned hydrocarbons (HC) to carbon dioxide and water:

$$C_xH_{2x} + O_2 \rightarrow H_2O + CO_2 \quad [2.2]$$

iii) Reduction/three-way

$$2CO + 2NO \rightarrow 2CO_2 + N_2 \quad [2.3]$$

$$HC + NO \rightarrow CO_2 + H_2O + N_2 \quad [2.4]$$

$$2H_2 + 2NO \rightarrow 2H_2O + N_2 \quad [2.5]$$

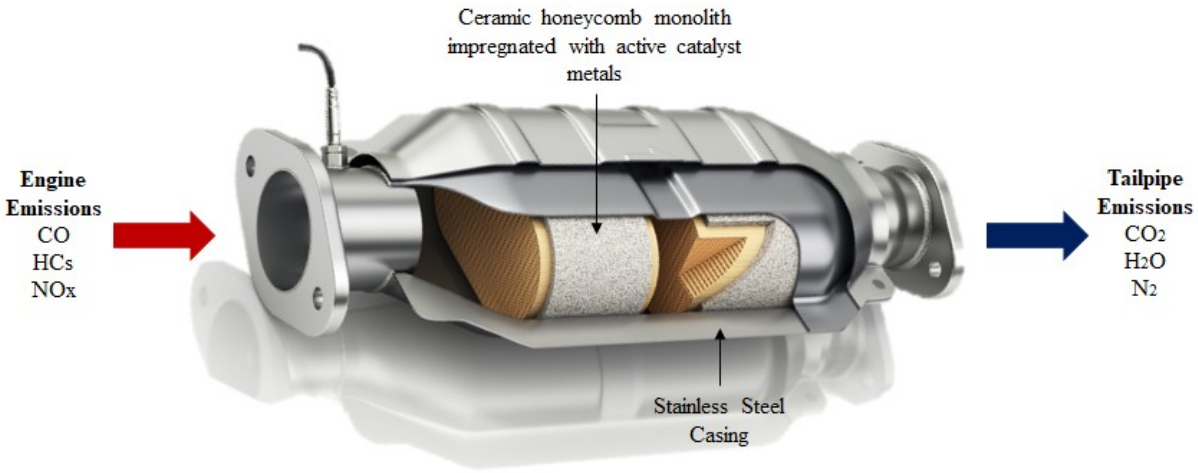

Figure 2.2 Schematic of a three-way catalytic converter [33]

As presented in Figure 2.2, there are two sections of substrate blocks. Some designs use this system configuration, while some combines it into one monolith block, in accordance with their catalytic formulation. For the above diagram, the first section of the honeycomb monolith is designed for the reduction reaction. In this case, a mixture of platinum (Pt) and rhodium (Rh) are used to reduce NOx emissions. In the second part of the catalytic converter, unburned hydrocarbon and carbon monoxide are oxidised by burning them over the platinum (Pt) and palladium (Pd) catalysts. The stoichiometric-burn engine is required to be paired with the TWC to ensure that the number of unwanted combustion products can be reduced as much as possible. The appearance of a catalytic converter is almost similar to a muffler. But the structure of a catalytic converter comprises of three main components, which are the substrate or monolith, the washcoat layer, and active metal catalysts.

2.4 Catalytic Converter Components

The selection of materials for catalytic converters is considered as a complex task, as various parameters need to be carefully weighed. A mismatch of components may lead to a failure of the system to effectively deliver its task. Firstly, it is essential for each component material to have the closest possible thermal expansion coefficient value, in order to minimise the thermally induced stress between each component and to avoid subsequent cracking problems. As catalytic converters operate in environments that are harsh, the stability of the materials is an imperative consideration. The materials should have the ability to maintain stability in a redox reaction environment, while possessing a high degree of toughness and strength. Additionally, the cost of the materials also affects the selection procedure for economic reasons. The three main components in a catalytic converter system, namely the monolith, the washcoat and the catalyst are briefly discussed in the next section. This discussion starts with the latter component, since the catalyst is the main component of the reaction process.

2.4.1 Catalyst

In 1835, Baron J. J. Berzelius coined the term Catalysis, which describes the property of a material that can promote and speed up chemical reactions without itself being consumed. With the addition of a catalyst in the system, lower energy is required to activate the transition state, as shown in Figure 2.3. In other words, a catalyst facilitates the stretching and breaking of a bond by lowering the activation energy, E_a. Not only does it facilitate the reaction through activation energy, but a catalytic reaction also provides an alternative mechanism path for the reaction. By having fewer energy pathways as compared to the uncatalysed reaction, the chemical processes can be carried out at a lower temperature and/or pressure. Also, there are

two types of catalysts; positive catalysts, which can accelerate reactions or negative catalysts which may retard chemical reactions. Out of these two, the positive catalyst is more commonly used in research and application.

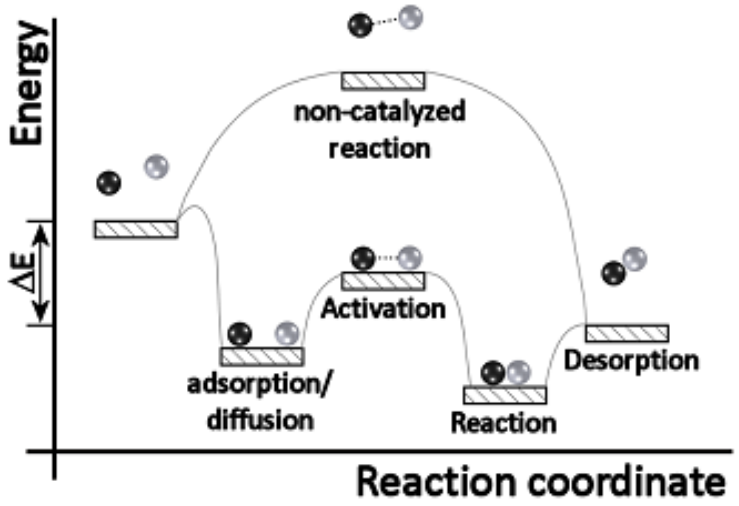

Figure 2.3 Generic potential energy diagram for chemical reactions [34]

Activation Energy, ΔE, kilojoules per mole ($J.mol^{-1}$)

The performance of a catalyst is evaluated based on the rate of the reactions and their selectivity towards the production of the desired product. The constant for the rate of reaction, *k*, can be expressed in an Arrhenius expression as;

$$k = Ae^{-E_a/RT} \qquad [2.6]$$

A: frequency factor or pre-exponential factor, *e*: mathematical quantity, *Ea*: activation energy ($J.mol^{-1}$), *R*: universal gas constant ($J.mol^{-1}.K^{-1}$), *T*: absolute temperature, K.

Catalysis may be classified into two categories: (i) homogeneous catalysis, where the reactants and the catalyst are in the same phase, e.g., both are in the liquid phase and (ii) heterogeneous catalysis where reactants and the catalyst are present in different phases, e.g., solid-liquid or

solid-gas states. Homogeneous catalysis is the least favourable since the same phase reactions lead to the need for additional separation steps to extract the product. Hence, the heterogeneous reaction has been the main research area for catalytic application. Since the reactants and the catalyst are in different phases, handling heterogeneous catalysis at various operating environments is easier. Furthermore, the end-product does not get contaminated by the catalyst residue [35]. The mechanism of a heterogeneous catalyst involves contact between the reactants and a solid material. In the case of automotive catalysts, the two phases are between the solid surface of the metal catalyst, while the exhaust reactants are in the gas phase.

Heterogeneous catalysis is a surface reaction where various factors have been shown to result in different catalytic behaviours. Such factors may include particle size, shape, chemical composition, metal-support, and interaction with metal-reactants [36]. The catalysts are generally made from metals or metal oxides where the key to a greater reaction is the surface area of the catalyst. To further understand the correlation between the surface metal and reactions, investigations regarding the adsorption and desorption on the metal surface has been carried out extensively. The research has yielded various proposed reaction mechanisms. The most discussed reaction mechanisms include i) Langmuir-Hinshelwood, ii) Eley-Rideal, and iii) Mars-Van Krevelen mechanisms. Steps for each of the reaction mechanism is presented in Figure 2.4.

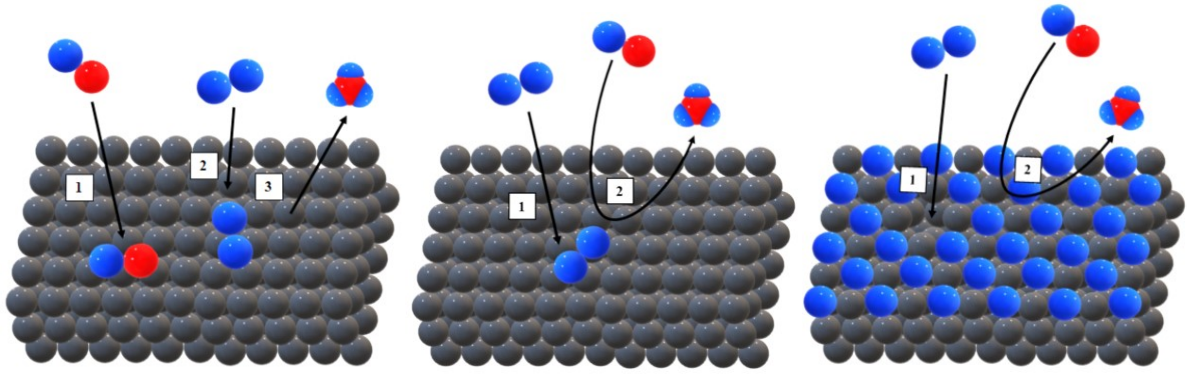

(a) **(b)** **(c)**

Figure 2.4 Surface reaction mechanism (a) Langmuir-Hinshelwood, (b) Eley-Rideal, (c) Mars-Van Krevelen

The general theory of a reaction surface mechanism involves adsorption of the reactant molecules from the bulk fluid to the catalyst surface. The adsorption may later occur either through associative adsorption or dissociative adsorption. The reaction then occurs on the surface to produce the product and finally, desorption of the product from the catalyst surface to the bulk fluid. In the Langmuir-Hinshelwood mechanism, both reactants adsorb on the catalyst surface first, and the reactions take place thereafter. For the Eley-Rideal mechanism, only one reactant adsorbs on the surface, and the other reactants interact with the gas phase before being desorbed. Mars-Van Krevelen, on the other hand, is different from the first two. Here, the surface itself is involved in the reaction, where a vacancy in the support layer is created during the reaction. This space is then filled by reactants from the bulk fluid and the reaction occurs as in the Eley-Rideal mechanism, before desorption takes place. Among these three, Langmuir-Hinshelwood and Eley-Rideal mechanisms are more commonly discussed.

The overall rate of reaction is limited by the slowest step in the mechanism, which is either the diffusion step comprises of the adsoption and desorption or the reaction step. If the catalyst is highly active, diffusion from the bulk to the catalyst surface could limit the overall reaction.

And if the diffusions are fast, the reaction step may restrict the total conversion. Each catalyst has its intrinsic reaction rate value. Considering the presence of adsorption steps, the actual rate may be lower than the intrinsic value due to the transport phenomena. For example, in the case of CO oxidation, it is well documented that the reaction proceeds via the Langmuir-Hinshelwood mechanism, and is dependent on the temperature and partial pressure. At a lower temperature, chemisorbed CO may build up coverage on the catalyst site and for the O_2 to be dissociatively adsorbed, CO needs to be desorbed from the site first [37]. This results in a first-order reaction in O_2 and a negative first-order reaction dependence on CO; where for the negative order, the increase of reactant or product's concentration means a decrease in the rate of reaction [38]. This is also known as a CO-inhibition reaction. However, when the reaction is subject to a highly oxidising condition with low CO concentration, the reaction falls under positive first-order in CO. The first-order reaction, in this case, typically represents high reaction activity; thus, the global reaction kinetics is limited by the mass transfer resistance.

It is known from reaction kinetic studies that the selection process for the type of catalyst to be used in any system relies not just on the chemical properties of the catalyst. Physical properties need to be considered too. Porosity, surface area over volume ratio, and particle size are the major criteria to look into [3]. As the reaction takes place at the surface, maximising surface area for exposure with the reactants is highly beneficial. There are two types of mass transfers at play during a reaction; i) internal mass transfer, and ii) external mass transfer. The external mass transfer occurs at the support layer while the internal mass transfer is related to the porosity of the catalyst particle. A highly porous catalyst is preferable to minimising mass transfer from the bulk fluid to the catalyst surface. For this reason, preparation of a metal catalyst with the right catalyst cluster is important.

Although various factors may have an impact on the overall catalytic performance, the two most important factors are the catalyst temperature and space velocity. Since a catalyst needs an intrinsic value of energy to get activated, the supply of energy from temperature is critical. Without enough activation energy, the chemical reaction cannot be initiated. The space velocity, on the other hand, correlates to the residence time. In a catalytic converter, the residence time is quantified by the Gas Hourly Space Velocity (GHSV). Equation 2.7 shows the definition of GHSV in the catalytic process:

$$\text{GHSV } (\text{h}^{-1}) = \frac{\text{Exhaust flow } (\text{m}^3\text{h}^{-1})}{\text{Catalyst volume } (\text{m}^3)} \qquad [2.7]$$

Based on this correlation, the relationship between GHSV and catalytic performance can be understood. At high GHSV, catalyst performance is low. Since the rate of exhaust flow is high, the contact time between the reactants and the surface catalyst is short. The short contact time restricts the completion of the catalytic reaction, leading to a lowered performance. Understanding space velocity in relation to catalytic performance is also useful especially in a catalytic converter system where operating conditions of the ICE is within a fixed region. For example, with a high flow of exhaust gases, space velocity would be massive. Therefore, in order to ensure that the system yields an acceptable conversion level, mounting of a proper amount of catalyst into the system may be helpful in designing a better converter.

The efficiency of a catalyst can be quantified by different methods. Turn-over Frequency (TOF) is one of the standard measurements. It measures the number of moles transformed by one mole of the active site per hour. Another common way of measuring performance is through the light-off temperature curve profile. The acceptable definition of the light-off temperature is the temperature at which the conversion of reactants reaches 50 %. But Lee and

Trimm argued that it would be well suited to define the temperature at which the reaction rate becomes mass transfer limited [39]. Performance measurement with this method is largely used for catalytic converter evaluations where a standardized method makes comparisons between different catalysts easy.

Various types of metal catalysts can be used in heterogeneous catalysis. As an early selection is a matter of trial and error, the choice of catalyst depends upon several vital characteristics. Amongst them, the selectivity of a catalyst towards the reactant species and the catalyst reactivity are of foremost importance. For a catalytic converter system, it has been recognised that the best metal catalyst for the reactions would be the Platinum Group Metals (PGM) catalyst.

2.4.2 Platinum Group Metals (PGM) Catalyst

Platinum Group Metals (PGM) is widely used as a catalyst in the TWC system where simultaneous conversion of polluted exhaust gases are required. Some may interchangeably be referred to as precious metals or noble metals. Platinum (Pt), palladium (Pd) and rhodium (Rh) are the best combinations of PGM in the TWC system assisted by other promoters and stabilisers such as alumina and ceria. PGM is a rarely occurring material with limited availability in the earth's crust. Out of the three main PGM, palladium is the most abundant, usually following the sequence Pd > Pt > Rh with each metal constituting on average 15 ppb, 5 ppb and 1 ppb respectively [13,40]. Figure 2.5 represents the distribution of elements in the earth's crust.

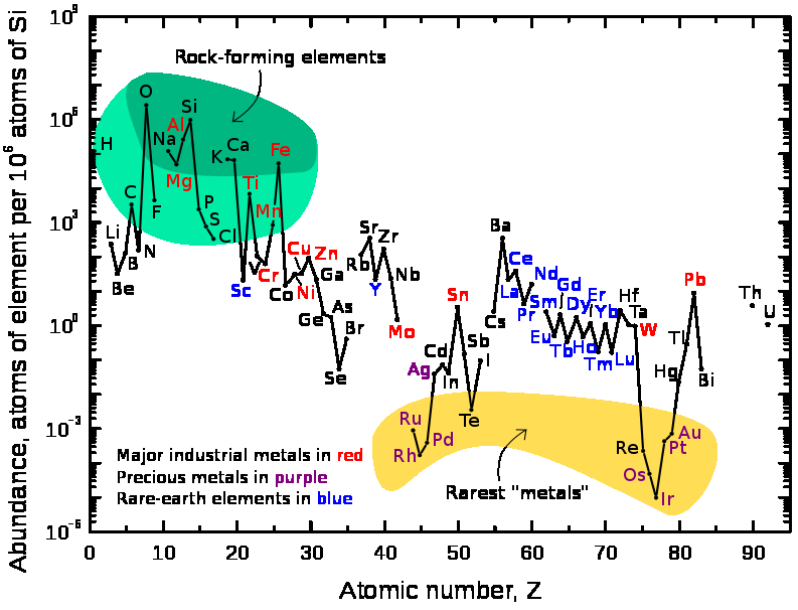

Figure 2.5 Distribution of chemical elements in the Earth's crust [41]

The scarcity of PGM is seen as the biggest challenge in the long term. With demand increasing every year, a depletion in the total reserves can be observed. PGM is already expensive in the current market. But with an uncertain supply chain coupled with the difficulties of metal extraction from depleting concentrated ores, PGM prices will only shoot up further. To tackle the challenge of economic feasibility regarding the use of PGM in catalytic converter applications, Pd only TWC catalyst has been developed. Pd is known to have the ability to conduct both oxidation and reduction processes, plus its abundance and relatively cheaper price compared to Pt and Rh has contributed to the development of Pd only TWC [42].

A palladium only catalyst has been developed to reduce reliance on Pt and Rh. In 1994, the first-ever Pd only TWC was put into application by the Ford Motor company. The formulation managed to meet emission regulations, which were considered the most stringent during the time [43]. Since then, a lot of studies have been carried out to comprehend the reaction mechanisms of Pd. The affinity of Pd for oxygen is much higher than its affinity for Pt and Rh;

thus, it is capable of adsorbing more oxygen which results in a better oxidation catalyst. But the question of performance over the reduction capability of Pd is still debatable. Pd has been proven to undergo a self-poisoning mechanism especially in the presence of heavy hydrocarbons. Heavy hydrocarbons typically result from rich-fuel combustion, where the NOx concentration is high. In such a condition, the ability of Pd to reduce NOx may get retarded. However, with a proper catalyst design and formulation, it would be possible for Pd to have a reduction performance better than Rh. As found by Holes et al. the addition of CeO_2 into Pd supported γ-Al_2O_3 results in NO reduction reaction rate of at least one order magnitude higher [44].

Pd can be integrated into the support layer by means of different metal configurations, either in the form of a cluster, nanoparticle, or a single atom. Recently, a lot of research has been focused on optimising catalytic operations by a supported single atom. It is claimed that the single-atom configuration could expose the well-defined active sites to optimally involve in a reaction, resulting in a catalyst with high efficiency. The challenge with single-atoms however, is their adhesion to the support layer. Improper anchoring could lead to metal aggregation forming clusters or bigger particles during synthesis or operation [45]. It has been proven that placing a high importance on the preparation technique can ensure an optimised catalytic performance so that the catalyst can have high stability even at harsh operating conditions.

2.4.2.1 Preparation of Supported Catalyst

In the development of catalytic converters, the deposition of a catalyst onto its substrate is of great significance. In order to produce a thin and well-dispersed catalyst on the support surface, various impregnation methods have been carried out and proposed. This crucial step is the most delicate part as improper impregnation techniques may lead to a failure to activate the catalyst sites for the reaction process, while excessive impregnation is a waste of material since some layers are out of reach and beyond any contact with reactants. The issue of catalyst distribution homogeneity could worsen during the drying protocol where catalyst redistribution would occur due to the capillary forces or due to weak adhesion to the support which causes accumulation of the catalyst in a particular region. In addition, when the support is in a monolithic structure, high cell density support may induce difficulties in distribution due to the surface tension of the catalyst precursor solution [46]. The low concentration of a catalyst over the volume of a monolithic support also makes it a challenge to distribute the catalyst along the monolith length. One example for consideration is the initial concentration of the metal precursor. It has to be below the supersaturation point as otherwise, premature deposition of particles in the bulk amount may occur [47]. The distribution, however, could be controlled with a proper preparation technique. Figure 2.6 shows a general observation of an active phase distribution on the commercial monolith.

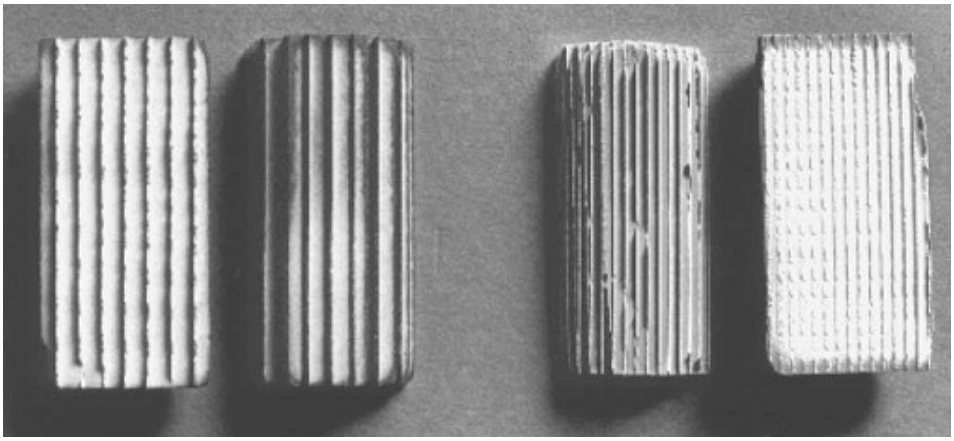

Figure 2.6 General observation of an active phase distribution by impregnation on commercial monolith [48]

The selection of methods to be used to incorporate a catalyst into support depends on the type of precursor, the nature of the catalyst and the active phase concentration. Based upon the selected method, the time, temperature, pH and concentration of the catalyst will result in unique distribution models and physical properties of the catalyst such as porosity, particle size, etc. Four most typical distributions models are i) uniform, ii) egg-shell, iii) egg-white, and iv) egg-yolk [46,49]. Generally, there are three categories in catalyst preparation [50]:

i) Preparation of the primary solid through either one of these main techniques (deposition, precipitation and co-precipitation, gel formation, selective removal).

ii) Primary solid processing through drying, thermal decomposition of the precursor salts, or calcination.

iii) Catalyst activation such as through reduction to metal, the formation of sulphides, or deammoniation.

In the first step, contact must be made between the aqueous catalyst solution and the support. Interactions between these two will dictate the level of distribution homogeneity. A palladium catalyst can be supported by a range of materials such as carbon, oxides and silica. But above all, oxidic support is seen as the best combination for palladium. That is because the oxidic support contains a hydroxylated surface with the presence of unsaturated metal sites which may act as Lewis-acidic centres. γ-Alumina is the most used support for Pd. Metal complexes show a well-defined reactivity towards the surface group of γ-alumina [49]. Functional interactions between the support are critical for an even catalyst distribution. Amongst the widely used techniques for a structured catalyst preparation are the sol-gel, deposition-precipitation, ion exchange and wet impregnation.

Haber et al., Perego and Villa described the general guidelines for each of the catalyst preparation method in their publication [50,51]. Some techniques possess unique advantages over the others. Sol-gel, for example, is seen to be better over precipitation due to a better control over surface area, pore volume and pore size distribution [51]. But the deposition-precipitation method, on the other hand, can produce a catalyst with a high component distribution, processes at low temperature and is low cost [52]. Sol-gel and deposition-precipitation methods can incorporate a catalyst in the interstitial regions which, however, is less beneficial for a catalytic converter with a structured catalyst. For this, the impregnation method is preferable since, through impregnation, the metals are dispersed on the surface of the support. With impregnation, the number of metals used can be reduced, and the process is more straightforward. However, the control of the metal distribution is critical with impregnation to ensure that the catalyst sites can be optimally utilised.

Finally, the drying and calcination protocol is critical to creating an anchor between the catalyst and the support. Inappropriate techniques and calcination temperature profile would cause catalyst redistribution and poorly anchored metal particles on the surface. The former issue will create uneven reaction spots during the operation while the latter may accelerate the performance deterioration with the loss of catalyst, especially at a high vibrational engine operation. In addition, an environmentalist has started to question the effects of PGM pollutants in the air, originating from automobiles. With careful investigation and preparation techniques, the aforementioned challenges can be reduced to a tolerable limit.

The issue of price volatility and limited availability of precious metals have triggered various attempts to reduce the dependability on the PGM in three-way catalytic applications. Vibrant ongoing research on PGM catalyst substitution now focuses on perovskite catalysts. Interest in utilising the unique regenerative properties of perovskites started since the 1970s initiated by the publication in Nature regarding their possible applications in exhaust treatment [53]. Since then, the exploration of perovskite behaviours and their potential as catalytic converters have taken place with - vigour.

2.4.3 Perovskite Oxide as A Three-way Catalyst

Perovskite's attractive characteristics have attracted a lot of attention towards using this type of material for numerous applications. A perovskite is known for its flexibility, adaptability, thermal stability, abundant availability and most importantly for its low cost [54,55]. With these features, a perovskite has the potential to cover areas such as magnetic, electronic, structural, and catalytic application. The versatility of a perovskite in terms of their chemical and physical properties is owed to their structural and compositional flexibility. The perovskite

structure consists of a general ABO_3 formulation, with a large cation at a 12 coordinated A site, 6 smaller cations in the B site and an anion, most often oxygen [56]. Almost all elements in the periodic table can accommodate the perovskite structure. But the common A-site occupier has the rare earth elements such as La, Na, Ca, Sr or Ba. To tailor a perovskite's properties, the A site and B site can be substituted by related materials having the required characteristics. But research has shown that the A site substitution does not have significant impact on the change of properties since the substitution of the A site cannot change the perovskite's oxidation state. The B site substitution however, can create an oxygen vacancy that leads to the alterations of a perovskite's properties [57,58].

The substitution, however, can be done only to a certain extent. An ideal perovskite structure is in the cubic crystal packing which corresponds to the "*tolerance t"* factor of 1. But with a component substitution with varied sizes of atoms, there will be a distortion in the packing creating other structures. The stability of a perovskite can be measured by the Goldschmidt "*tolerance t*" factor. The *t* value determines structural symmetry and can also affect their dielectric properties [58]. It can be expressed as;

$$t = \frac{R_A + R_O}{\sqrt{2}(R_B + R_O)} \qquad [2.8]$$

where R represents crystal radii for

R_A: cations A, R_B: cations B, R_O: anion O

Any deviation of *t* value from 1 means that the structure is of low symmetry. When the *t* is less than one, it describes a perovskite with larger B-site cations, while a *t* larger than one represents a perovskite with larger A-site cations. When either site is bigger, the other site cation

accommodates the free spaces by tilting and forming different crystal structures such as octahedra, tetragonal, rhombohedral, orthorhombic etc. Perovskite structures can be created with *t* values in the range of 0.9 to 1.10 [58].

The term 'Intelligent Catalyst' was introduced by Tanaka et al. to represent a perovskite with regeneration abilities [2]. This intelligent catalyst has been proven to react accordingly with the environmental input [59]. PdO is formed after an oxidation treatment and a switch to a reduction environment produces a metallic Pd. The segregation of Pd into and out of the perovskite structure, which happens according to the redox environment is due to the presence of Pd as a solid solution in the perovskite lattice. The claim is made that with an XPS analysis showing an abnormal binding energy with Pd in the perovskite crystal results in a binding energy higher than that of bivalence. Pd metal movement in the lattice of a perovskite during oxidation and reduction atmosphere is believed to contribute to the maintenance of its performance in the long run [60]. This movement can suppress the growth of the Pd particle, which is usually caused by sintering effects due to the high-temperature operation. The flexibility of the perovskite framework to accommodate the metal migration from one site to another, reversibly, have been proven by many researchers [61–65]. The capability of a perovskite catalyst to sustain its size, thus offering a better ageing condition is seen as a considerable advantage of this catalyst over the conventional PGM

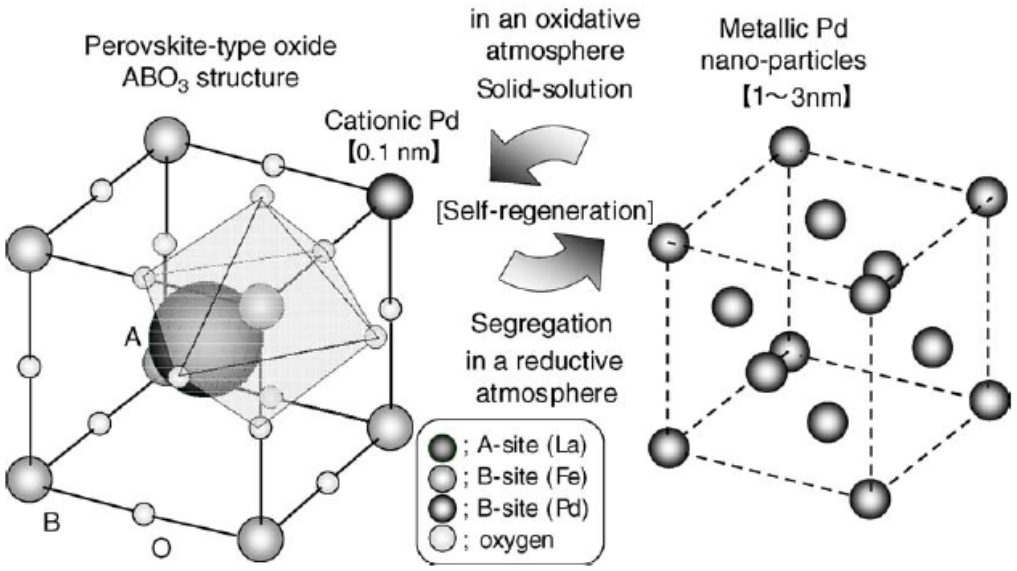

Figure 2.7 Representative of the self-regenerative function of a perovskite catalyst [61]

Even with a proven regenerability of a perovskite, many are still sceptical about its usefulness in a catalytic converter application. The focal attention is on a perovskite's resistance to sulphur poisoning. Exposure to SO_2 creates chemically bonded compounds such as sulphates, sulphites and/or sulphides depending on the condition of the environment it is exposed to [66]. The reaction is irreversible and may deactivate a perovskite catalyst. As the heterogeneous reaction is based on a surface reaction, a decrease in oxygen permeation of 80% was observed after the LSCF perovskite sample was exposed to SO_2 [67]. The exposure causes a change in the surface morphology with corrosion like effects up to several tens of micrometres in depth. The emerging porous surface is non-ionic conductive and inactive to surface exchange reactions. This leads to a loss in the perovskite surface of properties that are beneficial for a reaction process.

Different techniques have been applied in order to investigate the perovskite poisoning mechanism and to stop the deactivation process from occurring. Promoters could be added to the formulation to add shields or to offer optional routes for SO_2 to react with, instead of

reacting with the active sites. Even though it is impossible to prevent the poisoning completely, it is possible, at least, to delay the process. Although thousands of combinations are possible in a perovskite catalyst, including noble metals in the formulation is the best option. Inclusion of PGM in the perovskite formulation can not only increase the reactivity of the catalyst but can also prolong the lifetime of the perovskite catalyst in the exhaust environment. The issue of reactivity and poisoning of the perovskite catalyst has slowed down the utilisation of the material in catalytic converter applications. But with an introduction of fuel with lower sulphur content, an increased interest in using a perovskite as a catalyst in the TWC system is seen and the momentum in research has returned. The most researched perovskite for this application is the lanthanum-based perovskite.

2.4.3.1 Lanthanum Based Perovskite Oxides

Until the present date, out of the many options of transition-based metal perovskites, lanthanum based perovskite has been shown to produce the highest reactivity for an oxidation process, when coupled with Co, Mn, Fe, Cr or Ni in their B sites [68]. Early studies on lanthanum-based catalysts focus on the interactions and stabilising effects from using lanthanum as the catalyst support and additive. Studies have shown that the incorporation of lanthanum into PGM could delay metal sintering due to synergistic stabilising effects. Inclusion of Pd metal into a perovskite lattice could not only enhance the Pd's thermal stability but the perovskite's unique lattice containing oxygen chemistry could also be beneficial for the reaction process. PGM could be added into the perovskite support through two major routes; either supported on the perovskite, or doped into the perovskite lattice. The first method is proven to give a higher conversion efficiency since a precious metal catalyst is in direct contact with the reactants. However, the latter route produces a much more stable catalyst even after undergoing a harsh

ageing routine. Interestingly, Malamis et al. reported that initial testing showed a better reaction profile on the Pd supported perovskite [53]. However, after the ageing cycle, catalytic activity became similar for both conditions, the doped and the impregnated catalyst. As the supported catalyst is prone to sintering problems, eventually the Pd doped perovskite offers a better template for long term operations.

A perovskite is generally formed at an elevated temperature, where the most common method of synthesis is through the solid-state oxide synthesis. This method is easy, but the use of high temperature leads to the formation of a large particle and a less active catalyst. For applications in electrical and electronic environments, this should not possess any problem. But when the use of the perovskite involves the need for high surface area, the solid-state synthesise method is not suitable. That being the case, efforts have been made to develop a method of synthesis that can produce smaller sized perovskites with high surface area and high porosity [54].

Such developed perovskite synthesis methods includes co-precipitation, citrate sol-gel method, solution combustion synthesis (SCS), high-pressure synthesis and mechanically activated synthesis [58]. Amongst all these methods, the most researched method for TWC applications is the citrate sol-gel method. The advantage of the sol-gel method over the others is due to the processability to produce particles with a small size and high specific surface area. Through this process, the addition of ethylene glycol is claimed to prevent further growth of the particles as their surfactant properties absorb on the surface of the growing crystallites thus forming smaller particles with a higher surface area [69]. The Citrate method involves the addition of citric acid in stoichiometric amounts to form a ‘stable chelate complex’. Typically, aqueous metal salts such as nitrates are used with the addition of bases to modify the pH and enhance cation biding to the citrate [70]. The gelation process is achieved with the removal of water by

pyrolysis in air. The formation of a homogeneous chelate complex solution is the main advantage which contributes to the even distribution of active sites and small crystallite size.

2.4.4 Catalyst Deactivation

In time, a catalyst will face a decline in its activity, subject to its deactivation mechanism. The deactivation may occur either due to ageing caused by a crystal structure transformation, irreversible poisoning on the active sites, or by fouling or coking. Depending on the environment the catalyst is exposed to, the rate of deactivation can vary accordingly. In a catalytic converter, the two main common deactivation routes are ageing and poisoning. With high temperatures coupled with rigorous fluctuations of the environment in the exhaust stream, the catalyst is prone to getting sintered. The sintering effects may change the catalyst crystallinity and its particle size, typically creating a larger particle. This phenomenon causes a loss in surface active sites thus reducing the conversion ability. The sintering effect not only affects the catalyst particles but also the catalyst support which is exposed to this problem. In order to prevent any premature ageing and/or to delay the ageing process, the support of stabilisers can be added to the catalyst formulation. The most commonly used stabilisers are lanthanum. Lanthanum promoters which were added to alumina support can retain their initial surface area, which was believed to proceed via i) the formation of a lanthanum aluminate and ii) the nucleation of a cubic $LaAlO_3$ on the surface of the alumina [71].

Most cases of catalyst poisoning are caused by sulphur. Sulphur is a natural component in crude oil. As it can lead to an impairment of the emissions treatment device, the level of sulphur is reduced tremendously in the oil refining stage. The remaining traces, however, can cause

poisoning of the catalyst. Poisoning in catalytic converters happen when the sulphur compounds react with the catalyst surface and create sulphur-metal bonding which is irreversible, for example, the formation of a stable $PdSO_4$. Sulphur can also be absorbed on the metal support, but the acidity of the support such as Al_2O_3 is rather strong so the S^{2-} transformation into SO_4^{2-} on the support surface is unfavourable. The affinity towards PGM particles is higher.

On the other hand, it is reported that PGM can be added to the perovskite lattice not only to increase their catalytic reaction but also to delay the deactivation process [72]. By incorporating Pd into the perovskite lattice, the Pd surface is hindered; thus, lanthanum sulphates are formed instead of the $PdSO_4$. Tiancun et al. has discussed that the influence of sulphur on the supported catalyst is different than that on the unsupported catalyst [73]. For this reason, formulating a suitable supported catalyst can be beneficial towards reducing the rate of catalytic activity degradation.

Hitherto, PGM is still the most reliable TWC. But with a proper selection of materials and the technique of synthesis, a perovskite catalyst can be among the best candidates to reduce reliance on PGM with their versatile properties. Such properties include the thermal stability of a perovskite where it is highly needed for catalytic application in the exhaust stream where thermal fluctuations are high. On the other hand, with a perovskite as a TWC, substantial reduction of PGM is possible by altering the B-site cation substitution, without sacrificing conversion efficiency of the catalyst. For these reasons, research to expand perovskite usability in catalytic converters would be hugely beneficial.

2.4.5 Washcoat

The washcoat layer, also known as the refractory oxide layer, is desirable as it provides a high specific area for deposition of the active catalyst layer and serves as a platform for better catalyst adherence [74]. Furthermore, this layer is engineered to act as a physical barrier which can provide maximum resistance to undesired reactions and contaminants. The optimum thickness of 20 – 60 μm is designed to keep the diffusion resistance to a minimum so that reactant gases can reach the active sites more easily. The configuration of the washcoat in the catalytic converter is illustrated in Figure 2.8. This washcoat layer, also considered as a secondary support for the system, is commonly a high surface area oxide such as γ-alumina which also possesses a high porosity, Lewis acidity and basicity properties that can improve catalyst interactions for better reactivity [75]. Yet, γ-alumina is known to be prone to phase transformation to α-alumina, a thermodynamically stable phase, especially after prolonged exposure to a temperature higher than 800 ºC. The phase transformation is believed to be caused by a nucleation-and-growth mechanism and could be accentuated with the presence of steam [76]. Particle growth leads to a loss of surface area, which may also cause catalyst deactivation. Therefore, a lot of material research has been carried out to improve the thermal stability of the γ-alumina washcoat layer. Among the heavily researched stabilisers are ZrO_2 and La_2O_3 [71,77,78].

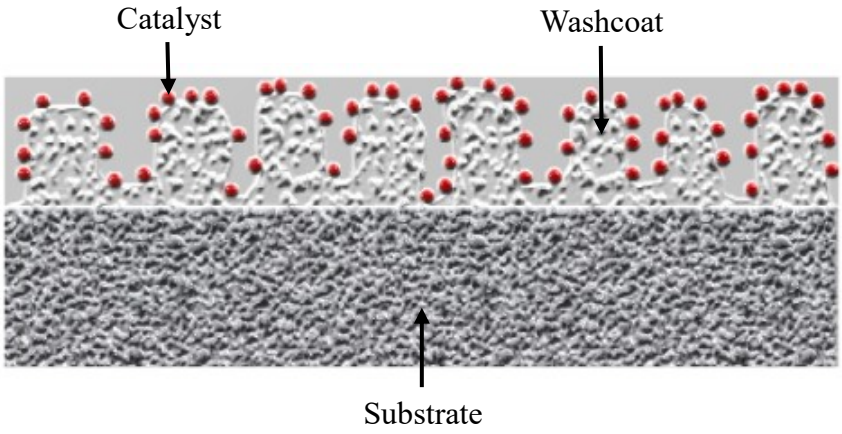

Figure 2.8 Basic components of catalytic converter

Besides the introduction of a thermal stabilising agent to the washcoat layer, the most promising promoter in the TWC system since the 1980s, cerium oxide (CeO_2), is added in the system. Cerium oxide, also known as ceria, is an essential component due to its high oxygen storage capacity (OSC) properties [79–81]. As this material has an oxidation state of +4 and +3, the ease with which this material switches its states is favourable towards ensuring a stable oxygen release and storage process during operation [82]. To optimise this layer, an additional sensor is needed in the system to adjust the fuel control of the combustion where the O_2 sensor is installed at the inlet mouth and outlet path to monitor the O_2 storage efficiency of the washcoat. That said, however, ceria could lower the thermal strength of alumina and make it prone to getting sintered.

2.4.5.1 Washcoating Technique

A washcoat deposition onto the monolith requires a technique that depends on the properties of the solution used and the interaction between the monolith wall and the washcoat solution.

An unsuitable deposition technique may cause uneven distribution of the washcoat layer and induce an unnecessary mass transfer resistance in the system. In general, there are two types of washcoating methods, which are i) the pore filling of the micropore support, and ii) the deposition of a layer of washcoat on the support surface. The first method involves partial or filled substrate pores with the washcoat. This method can offer the strongest adhesion of washcoat since the particles are fixated inside the pores of the substrate. However, the pore-filling process can be done only with particles having a size smaller than the substrate pores and the amount that can be deposited is limited. For layered washcoating, the technique has more flexibility in terms of the choice of materials and configuration of the layer. However, there are higher delamination chances due to poor adhesion. The various washcoating methods have been introduced below with their own specific benefits and disadvantages. Each technique is described in the following section.

2.4.5.1.1 Colloidal Solution Coating

The colloidal coating works by filling the pores of the monolith. Washcoating steps involve immersion of the monolith in the colloidal solution for the specified time, removal of the excess solution by blowing it with pressurised air, drying of the monolith horizontally at room temperature followed by the final calcination process. Typically, no additional layer is visible through this technique [74]. Total washcoat loading mostly depends upon monolith porosity.

2.4.5.1.2 Sol-Gel Coating

For the sol-gel method, the first stage is the preparation of the sol solution. Then follow the dipping of the monolith, drying and calcination. Since this method involves a crosslinking network between the colloidal particles, the result is better pore filling and adhesion than the

colloidal slurry. However, the thickness of the washcoated layer by this method is limited since the dipping duration does not influence the number of particles that could attach on to the monolith.

2.4.5.1.3 Slurry Coating

The slurry coating is usually done with a particle size in the range of 2 – 5 μm, which is larger than the other two previously mentioned techniques. The necessary steps are generally the same, with an immersion of the monolith in the coating solution, removal of the excess liquid and drying followed by the calcination thermal treatment. The capillary force is responsible for assisting the adherence of the particles onto the monolith surface while pH and viscosity of the solution play a vital role in the strength of the adhesion [83]. Nitric acid is usually used to stabilise the slurry solution, but the addition needs to be done with extra caution as the acid concentration may have a complex influence on the gelation process [84]. Fewer coating repetitions are required in order to get the same weight loading as the other methods. However, this method is sensitive to the viscosity change that occurs after every dipping process. It is critical to ensure the homogeneity of the solution to prevent uneven washcoat distribution.

Other than the conventional washcoating step followed by catalyst impregnation on the surface, the catalytically active layer is prepared separately by direct impregnation of the catalyst into the washcoat material. This supported catalyst is later embedded into the monolith wall, followed by the calcination process. The thermal treatment is needed for better adhesion of the catalytic layer on the monolith. The selection of the washcoating technique, however, is subject to catalytic performance.

2.4.5.2 Mass Transfer in Washcoat Layer

The addition of the washcoat layer is beneficial to the reaction performance where a larger specific surface area is made available for active catalyst deposition. However, since the catalytic reaction undergoes transformations through a diffusion mechanism, an increase in the volume of the washcoat adds a mass transfer resistance to the diffusion pathway. The diffusion of the reactants combined with chemical reactions leads to concentration of gradients that affects reaction rates. As a result, a reduction in the overall conversion efficiency is observed [85]. Apart from the thickness of the washcoat, other factors cause an increase in the mass transfer resistance too. Such factors include the porosity of the washcoat material, packing density and the homogeneity of the washcoat deposition.

In a catalytic converter, where the reaction rate of the catalyst is fast, the limiting rate falls typically in the mass transfer limited region. There are two sources of mass transfer effects within a single channel of the catalytic substrate: i) internal mass transfer inside the washcoat porous structure, and ii) external mass transfer from the bulk fluid to the washcoat layer [86]. The overall steps of the reaction mechanism are shown in Figure 2.9. Before the products can be discharged from the system, the reactants face two stages of mass transfer: i) to reach the active catalyst sites from bulk fluid and ii) to diffuse out from the reaction sites. The more restricted this area is, the longer it takes for gas molecules to travel along the reaction path. Thus, the washcoat layer is designed within a specific range of thickness for better molecular diffusion and to limit the decrease of the open frontal area that leads to additional backpressure [75].

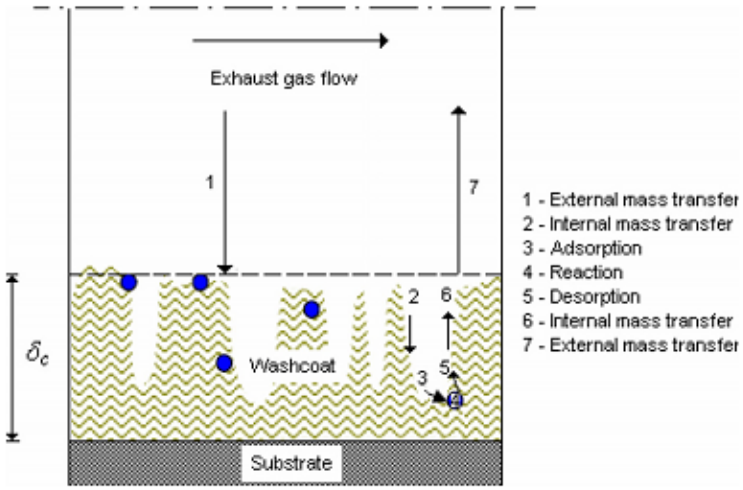

Figure 2.9 A schematic representation of catalytic reaction steps involved in a channel of catalytic converter [87]

δ_c = effective washcoat thickness (m)

The steps of mass transfer movement in the catalytic converter are represented in Figure 2.9. Santos and Costa have listed seven steps accommodating the internal mass transfer and the external mass transfer involved in the TWC system. In this sense, most of the washcoat is designed thin to keep the mass transfer resistance low; however, active sites on the bottom layer may not be as fully utilised as the active sites on the top layer. Due to this, the study of the effects of internal and external mass transfer is critical in this process. The highlighted steps in this process are: i) mass transfer from the bulk fluid to the washcoat layer, ii) internal mass transfer inside the supported catalyst, iii) reactants adsorption on the active sites, iv) molecular reactions, v) desorption from active sites to the washcoat layer, vi) internal mass transfer in the washcoat layer, and lastly vii) external mass transfer of the products to the bulk fluid. Overall catalytic performance is affected significantly by other effects such as the space velocity and the diffusion steps. Also, a small parallel channel of the monolith induces laminar flow inside the channel. In general, there are two types of mass transfers at play: the convective mass

transfer and the diffusive mass transport. Along with mass transfer, momentum and energy transfers are also present and occurs in axial and radial directions [88].

2.4.6 Substrate

Prior to the 1980s, pallet substrate in packed bed configuration was used in the catalytic converters. Although it is known that the packed-bed catalyst has more contact between the reactants and the catalyst surface, this configuration is deemed unsuitable for the application of exhaust treatment as it draws tremendous back-pressure to the engine system. To overcome the above-mentioned difficulties, substrates in monolithic forms have been chosen as the primary structure. A structured substrate that is commonly a ceramic honeycomb monolith has hundreds of interconnected repeated channels, in order to provide a large geometric surface area (GSA) in which the washcoat and precious metal catalyst is incorporated [89,90]. The honeycomb structure of the substrate allows exhaust gases to flow against a maximum substrate surface area where the catalyst reaction occurs. The catalyst must make direct contact with the targeted reactants for the reaction to take place, and the degree of the contact will determine the exhaust conversion efficiency.

Monolith structures are favourable in automotive catalytic combustion considering the high flow rates of exhaust gases and the need for a low-pressure drop in the system. On account of this low backpressure, Reynolds number of more than 300 000 can be used for the setting of flow rate in the system [91]. The open structure of the monolith also offers high geometric surface areas over its volume and thus is more compact than the packed bed. The open structure allows for efficient warming up of the catalyst and conversion is initiated at a shorter period after engine start-up and a shorter diffusion length to the catalyst surface is offered to the

reactants [92]. Also, the packed bed configuration has low resistant to mechanical vibration, which is a norm in automotive operations. Once it undergoes repacking due to the vibrations, the pathways of the reactants change, and this also affects the conversion efficiency. The monolith structure does not face such catalyst repacking phases during operation and is much more stable. The robustness of the monolith structure gives much freedom to configure the orientation of the catalytic converter in the exhaust [89].

A monolithic catalyst substrate is commonly fabricated through the extrusion process and the widely used extruded monolithic supports are made from either metal or ceramic materials. The ceramic monolith became available in the mid-1970s, while the metallic monolith was introduced in the 1990s. The metal monolith is believed to promote a better engine breathing due to its thinner wall structure that leads to a reduced flow restriction as a result of a low solid fraction. It has also been suggested that the light-off temperature for the reaction to take place would be lower for this material as it has a high thermal conductivity along with low heat capacity properties, thus a shorter time for conversion from the initial cold-start engine is required. The standard value of the thermal conductivity of metals is around 25 W/m.K, while for ceramic materials it varies from 0.8 to 5 W/m.K. Besides, metals are seen as more robust and less prone to breakage compared to fragile ceramic materials, and their thermal expansions are a preferred match with the stainless steel shell [91,93]. However, since the thermal expansion of the metal is greater than that of a ceramic material, an adherent of washcoat on the metal surface requires special techniques to prevent the delamination from occurring at high-temperature operations. High melting temperature metals up to 1500 ^{o}C such as Fecralloy (73% Fe, 5% Al, 20% Cr + Ni and Si) is favourable to prevent the disintegration of the monolith support [89]. Figure 2.10 shows a typical ceramic and metal monolith available commercially.

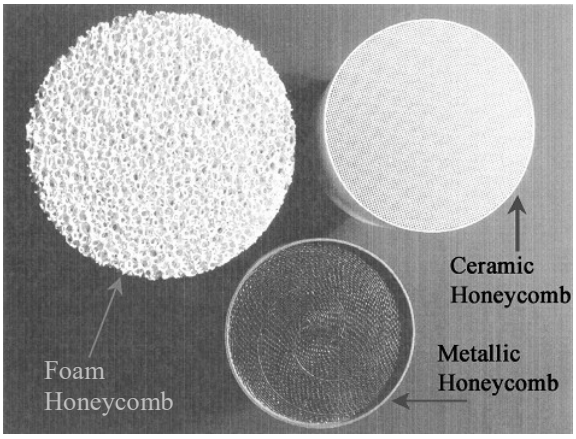

Figure 2.10 Commercially available ceramic and metallic monolith [89]

The durability and a long life span of catalytic converters are attributed to the stainless-steel casing which is responsible for providing support to the monolith. It acts as a cushioned mat which is capable of minimising the expansion and distortion of the monolith from the effects of direct exposure to exhaust gases. Intensive comparative studies by Vaneman on the advantages and disadvantages of the metal monolith in comparison to ceramic monolith have concluded that it was unsuitable for metal to be commercially used as a monolith due to its limited benefits compared to a ceramic monolith [93]. A ceramic monolith has numerous advantages over a conventional metallic monolith that includes excellent interphase mass transfer, insignificant resistance to mass transfer by intraphase diffusion through the catalytic layer, excellent thermal and mechanical properties, straightforward scale-up and other advantages [94]. The strength of metal foils decrease at high-temperature operations and can cause structural deformation. It is also relatively more expensive than the abundant counterparts of ceramic materials and heavier in weight which makes it unappealing for large scale production [93]. Compared to the metallic monoliths which are mostly nonporous, the ceramic monolith can provide satisfactory porosity with a higher specific surface. The ceramic monoliths that are often used in the treatment of exhaust gases are V_2O_5/TiO_2, zeolites, combinations such as TiO_2, V_2O_5 and WO_3, $VOx/TiO_2/SiO_2$, and so on [89,95,96].

Table 2.1 lists the properties of commercially available ceramic and metal monoliths.

Table 2.1 Properties of ceramic and metallic monoliths [91]

Ceramic monoliths				
Cell density per inch^2	200	300	400	600
Wall thickness (mm)	0.3	0.3	0.15	0.15
Channel size (mm)	1.5	1.14	1.14	0.9
Open area (%)	69	63	77	73
Surface area (m^2/m^3)	2200	2740	3088	3790
Metallic monoliths				
Cell density	18			600
Wall thickness (mm)	0.13			0.05
Open area (%)				89

Among all ceramic materials, the most widely used is cordierite, $2MgO\text{-}Al_2O_3\text{-}5SiO_2$**,** since its properties adapt to an excellent monolith. It has a low thermal coefficient expansion, high melting temperatures up to 1465 ºC and superior resistance to oxidation [14,89,91]. Also, alumina is now gaining more attention as a starting material due to its additional high surface area properties. Cordierite melts at 1435 ºC while alumina has a far higher melting point of 2070 ºC. This property makes alumina more attractive as the support since cordierite may get malleable if the operating temperature reaches a sufficiently high level. The chemical properties of alumina such as the availability of the Lewis acid sites and defective spinel

structure due to the removal of a divalent cation and trivalent aluminum cations could potentially enhance metal-support interactions and improve catalytic activity for various reactions [75,97]. The chemical properties also make it possible to impregnate the catalyst on the alumina support without the washcoat layer. Coupled with their physical properties of high strength and excellent thermal stability plus abundant availability, alumina is the best candidate for catalytic converter support [98].

2.4.6.1 Flow Across Monolithic Substrate

The honeycomb monolithic structure is beneficial for its property of mechanical strength because any force applied to the monolith can be uniformly dissipated [99]. The characteristics of a monolith are based on three major variables, such as relative density, cell wall material and geometry of the walls. The flexibility in tailoring these variables offers the possibility of exhibiting a very high stiffness-to-weight ratio in combination with unique thermal, acoustic and energy-absorbing properties [100].

The flow regimes in the channel are influenced by the fluid properties, superficial velocities, and support channel, while pressure drop and distribution (including mass, heat and species concentration) depend on the flow regimes [92]. Figure 2.11 illustrates the flow profile in the reaction cell. When fluid enters the cell, a paraboloid flow profile is developed. The flow velocity is the highest at the central line and decreases near the wall. The decrease in the flow near the wall is caused by shear stress. The boundary layer is formed near the wall. This is the layer where all the diffusion of the adsorption and desorption takes place and could be the rate-limiting mechanism for the reaction. Since catalytic conversion efficiency is highly dependent

on this surface diffusion step, it is vital to design a washcoat layer with a minimum boundary layer. Moreover, the washcoat layer also affects the pressure drop in the system.

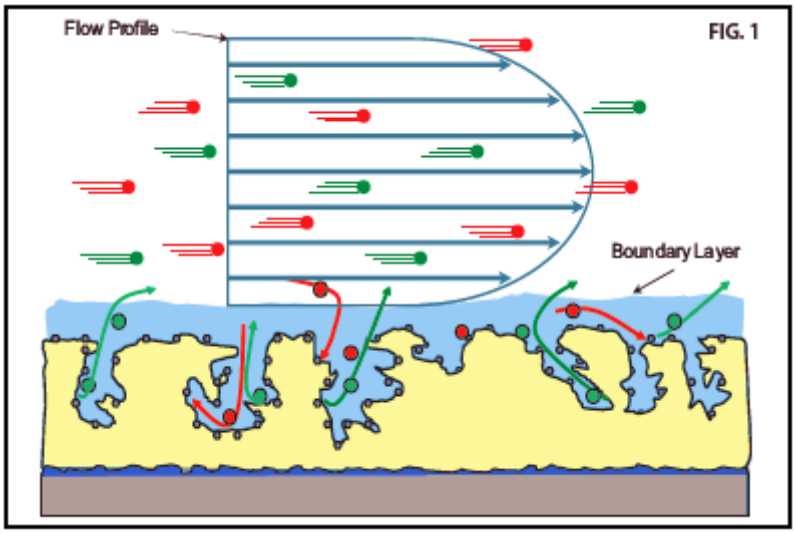

Figure 2.11 Flow profile inside the catalytic converter system [101]

The pressure drop in the system is caused by the energy dissipated across the surface of the fluid flow. The friction that occurs between the channel surface (surface roughness) and the working fluid contributes to the dissipation of energy. In general, the pressure drop across the monolith system can be calculated using an equation (2.9). As can be seen from the equation, it depends linearly on the flow velocity and length of the support [102].

$$\Delta p = f\left(\frac{L}{D_h}\right)\left(\frac{\rho v^2}{2}\right) \qquad [2.9]$$

Δp: pressure drop (N.m^{-2}); f: friction factor dimensionless; D_h: hydraulic diameter (m); L: monolith length (m); v: velocity in channel (m.s^{-1}); ρ: gas density (kg.m^{-3})

The standard geometry for a monolith square channel is defined by the following expressions.

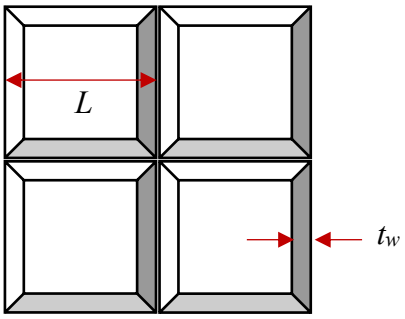

Figure 2.12 Monolith channel geometry

Cell density: $n = \frac{1}{L^2}$ [2.10]

Open Frontal Area (OFA): $OFA = n(L - t_w{}^2) = \frac{(L - t_w)^2}{L^2}$ [2.11]

Geometric Surface Area (GSA): $4n = (L - t_w) = 4\frac{(L - t_w)}{L^2}$ [2.12]

Hydraulic Diameter: $d = 4\left(\frac{OFA}{GFA}\right) = \frac{(L - t_w)}{4}$ [2.13]

t_w : Wall thickness, L: Channel length,

When it is required to increase the surface area for reaction, a monolith with a high cell density is used. However, higher cell density correlates to a smaller hydraulic diameter. For this reason, more energy is needed to force the fluid to enter the cell through a small open frontal area. Consequently, the pressure drop becomes higher in the system. Not only does the system suffer from high back pressure, but the engines also have to burn more fuel so that the energy is sufficient to flow through the catalytic converter. Proper understanding of the correlation

between each of the geometry parameters is crucial to design a monolith with optimized performance. Maximising the design and production by means of manual experiments, however, can be time-consuming and costly. For these reasons, the techniques aided by computational fluid dynamic (CFD) have gained attention in accelerating the process.

2.5 Ceramic Hollow Fibre Micro Reactor

The utilisation of ceramic hollow fibre as a substrate in the heterogeneous microreactor has been demonstrated by some researchers. One of the earliest introductions of hollow fibre substrate for automotive applications were presented by A. Rahman et al. and García-García et al., known as catalytic hollow fibre microreactor (CHFMR) for fuel micro-reformer. They have demonstrated that over the conventional reactors, the new design offers advantages of high surface area to volume ratios, high heat and/or mass transfer rates, low pressure drops, good phase contacting, and instant mixing of reactants [24,103]. As shown in Figure 2.13, the open microchannel with a finger-like structure can be used as the support for catalyst deposition in the gas phase reactions. This unique microchannel structure enhanced the surface area of the reactor with a much larger hydraulic diameter [104].

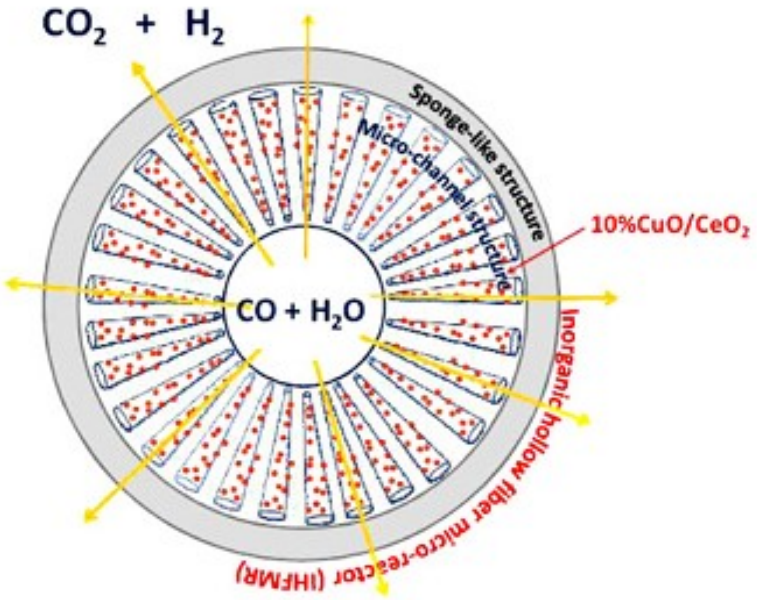

Figure 2.13 Schematic representation of the catalytic hollow fibre microreactor [104]

Furthermore, Kingsbury et al. demonstrated that the use of ceramic hollow fibre as a catalytic converter substrate fabricated through extrusion assisted phase inversion produced highly ordered microchannels with high GSA value. The new design is claimed to be able to increase reaction performance with reduced backpressure [105]. The overall improvement of the microreactor design relies on the advanced manufacturing process where the flexibility to produce a symmetrical or asymmetrical structure of microreactor substrate is useful for satisfying different applications according to their unique needs. The fabrication process of the substrate using ceramic material is done through the extrusion process. The symmetrical or unsymmetrical structure is formed as a result of the phase inversion process. Details of the manufacture of ceramic hollow fibre are discussed in detail in the following sections.

2.5.1 Ceramic Hollow Fibre Fabrication

2.5.1.1 Spinning Suspension

A viscous mixture of ceramic powder, binder, solvent and additives is known as the spinning suspension or dope solution. Depending on the composition of each component in the rotating suspension, a different final product is created. There are several factors that need to be considered when choosing the material for suspensions such as particle size, shapes and its rheology since these properties can significantly affect the formation process. Typically, long-chain polymers dissolved in a solvent are used as a ceramic binder. At the later sintering stage, this binder and other organic additives need to be entirely removed, since impurities reduce its strength and/or cause defects in the structure. In addition, the polymer-solvent pair also affects the densification of fibre during sintering. The main component in the suspension is the ceramic powder. Selection of ceramic material is subject to the properties of the final product. As the overall structure is dependent upon the spinning composition and spinning parameters, one detail to consider with ceramic powder is its particle size. This ceramic undergoes particle rearrangement and packing during the fabrication process. Thus, the selection of a suitable particle size is vital for tailoring the density of the fabricated hollow fibre.

The solvent selection in the phase inversion process, on the other hand, relies on two significant properties. The first one is the strength of the solvent to dissolve the polymer, as it is essential in producing a homogeneous solution. The second criterion is the exchange rate property of the solvents with the non-solvents. As the formation of the microchannel structure in the hollow fibre is due to the phase exchange process, the use of a solvent with the capability for high exchange rate is paramount. Lastly, additives may be added to change or enhance specific properties of the suspension. Such additives include dispersant, anti-foaming agents, pore

former, chelating agents, etc. Among these, a dispersant is essential in order to deagglomerate ceramic particles to ensure homogeneity of the dope solution. A non-homogeneous solution may cause several defects on the hollow fibre product. Examples of the defects may include the formation of unwanted porosity, pinholes, or even reduced density of the hollow fibre. A dispersant works by breaking the surface bonding between particles and keeps them separated by ionic repulsion or steric hindrance. The ionic repulsion is the process of charging particles in order to repel each other, while steric hindrance involves coating of particles with a layer that prevents them from attaching to one another. Even though there are general rules for each composition, the ceramic suspension is mostly altered by experience to achieve the desired structure.

Common steps for preparation of a ceramic suspension are as follows: (i) dissolve additives in solvent in a suitable container; (ii) add an appropriate amount of sieved ceramic powder to the additive solution; (iii) roll the mixture on the roller milling system using the ball milling technique for 48 hours; (iv) add polymer binders and continue rolling until the solution becomes homogenous, and (v) vacuum degassing of dope solution before the spinning process. Since the preparation process of a spinning suspension involves a lot of stirring, air bubbles are normally trapped in the suspension. The trapped bubbles can also create pinholes in the hollow fibre that reduce their mechanical strength. A common degassing method is by partial vacuum-assisted by gentle stirring. Before the fabrication starts, it is vital to ensure that the suspension solution is mixed well to prevent clogging in the spinneret.

2.5.1.2 Extrusion of Ceramic Hollow Fibre

Spinning is the process of fabricating a hollow fibre through the extrusion of a dope suspension. The tube-in-orifice called spinneret is used to mould the hollow fibre structure when the predetermined suspension solution is extruded through its orifice. The essential components needed for fabrication are the spinning suspension, internal coagulant and external coagulant. These are the main parameters of the controlled induced phase inversion process. Extrusion of the ceramic hollow fibre can be carried out by a spinning system, as shown in Figure 2.14.

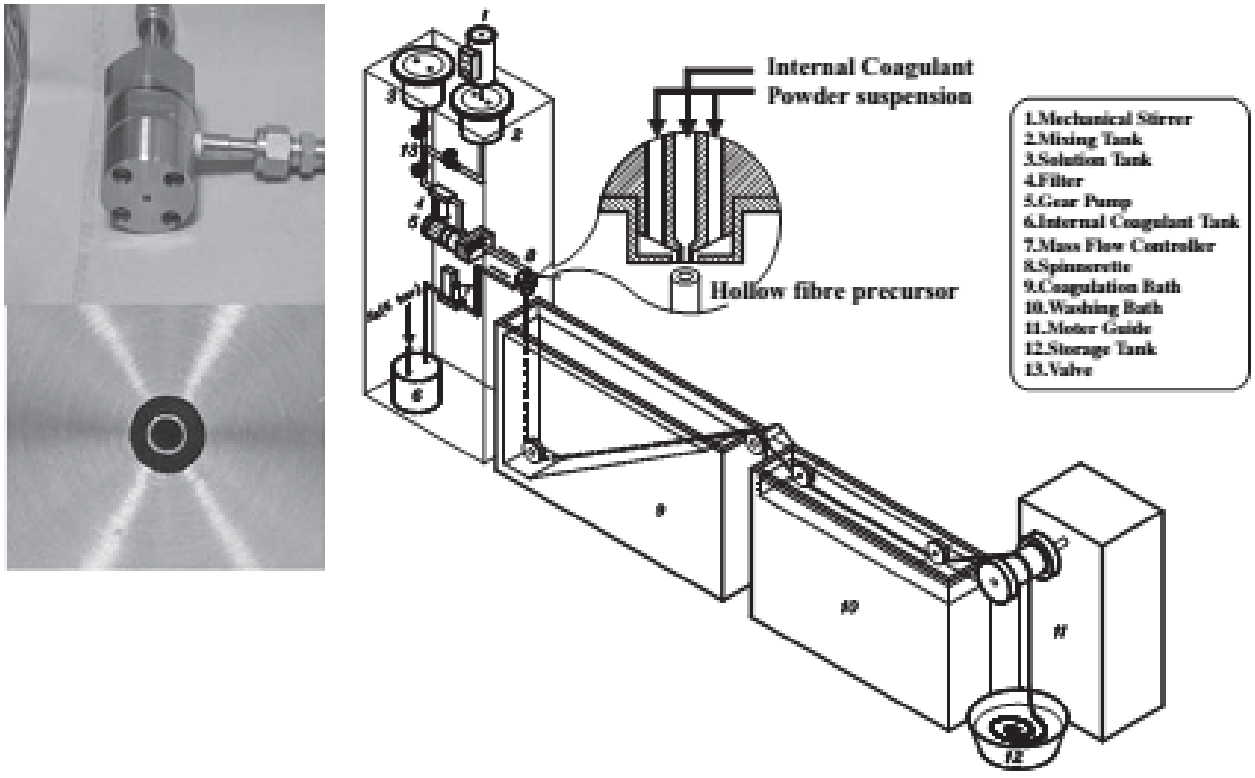

Figure 2.14 Schematic diagram of hollow fibre spinning setup [106]

The phase inversion process is a process of fabricating membranes by exploiting the chemical state of the precursor solution containing a liquid-polymer by removing the solvent from its composition during the solidification phase and creating a porous membrane. Loeb and

Sourirajan were the pioneers of this process and the initial intention of this innovation was to make cellulose acetate membranes [107]. Until now, this is the only known process capable of producing thin and large surface area membrane for commercial applications. A schematic ternary phase diagram for polymer/solvent/non-solvent for polymeric membrane formation is shown in Figure 2.15. Path A to D represents the coagulation path, where the solidification of the polymer membrane takes place. In this region, a two-phase separation occurs [108,109]. At the moment when the polymeric solution touches the non-solvent coagulation bath, solvent – non-solvent diffusion starts and creates a polymer concentration gradient at the interphase [110]. This diffusing phenomenon stops once the two phases reach an equilibrium state and the solid membrane structure is formed. The precipitation mechanism relies heavily on the selection of solvent, polymer binder, and non-solvent.

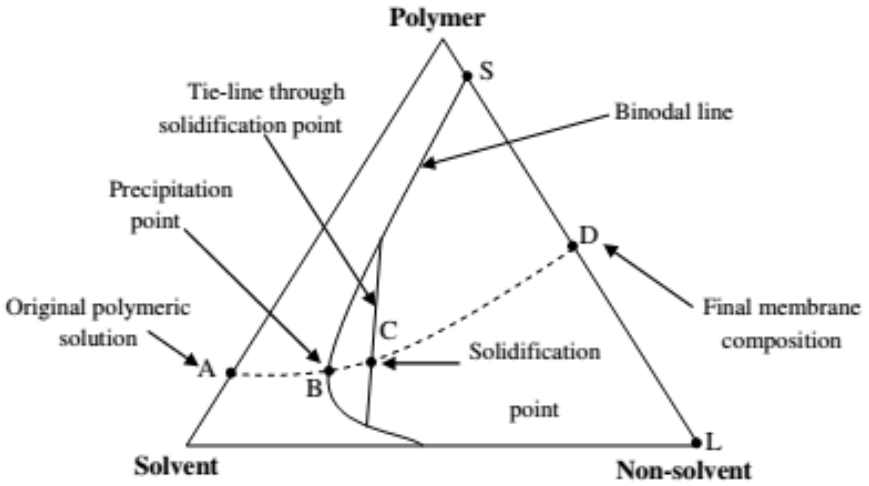

Figure 2.15 Schematic ternary phase diagram of polymer/solvent/non-solvent for polymeric membrane formation [111]

Furthermore, the extrusion of suspension and internal coagulant is controlled by a gear pump. The extruded nascent fibre through the vertically aligned spinneret is collected in the water bath where the phase inversion process takes place. The resulted nascent fibre which is very flexible in its structure at this stage due to the addition of polymeric binder is usually left overnight in the water tank to ensure the completion of phase inversion before being dried and sintered.

Great efforts have been made to better understand the phase inversion mechanism during the fabrication process. Discussions mainly try to decode the driving force that leads to the structural formation that is affected by the thermodynamics and kinetics of polymer precipitation. The universally accepted mechanism theory for microchannel formation is due to the concentration gradient between the suspension and the precipitant. Strathmann et al, however, argued that the gradient in the chemical potential is the driving force for any mass flux [111]. They believed that the derived diffusion coefficient shows that the phase separation flows from the lower concentration to the higher concentration. This movement is against the concentration gradient, but it follows the chemical potential gradient.

For the concentration gradient mechanism, the formation can be explained by the Rayleigh-Taylor Instability theory. Microchannel formation through this theory was discussed by Melanie et al, where five different solvents were used to fabricate alumina membranes. With DMSO as the solvent, microchannel has a long, straight, cylindrical and densely packed structure. The NMP and DMAc resulted in pear-shaped microchannels, while DMF and TEP solvents formed symmetric membranes with sponge-like structures [112]. Although in the study, they have claimed that the R-T stability is the primary mechanism which induces the fingering effects, other mechanisms such as the Marangoni effect and Kelvin-Helmholtz

instability theory should not be excluded. The Marangoni effect explains the mass transfer due to the surface tension gradient along two-fluid interphases, while the Kelvin-Helmholtz instability theory discusses shear velocity that may occur due to velocity differences between two fluid interphases**.** Figure 2.16 represents a ceramic hollow fibre structure having sponge-like regions and finger-like regions or microchannel regions as a result of the phase inversion process.

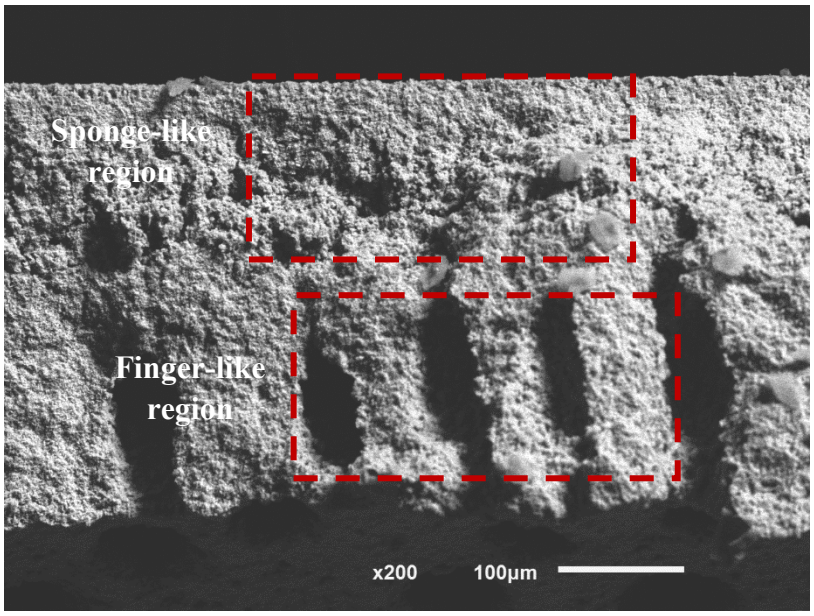

Figure 2.16 Example of ceramic hollow fibre structure

2.5.1.3 Thermal Treatment (Sintering Process)

The final treatment in the ceramic hollow fibre fabrication is known as the sintering process. The process involves firing the precursor hollow fibre at a high temperature to densify the fibre, to change its properties from the precursor product and to improve their mechanical strength. Variables such as temperature, particle size, pressure, packing condition, composition and sintering atmosphere influences the morphology of the end product [113]. There are two

ongoing mechanisms in the sintering process, which are evaporation and combustion of any additives and secondly, surface oxide reduction of the compact particles. Solid-state sintering for ceramic hollow fibre is generally driven by the decrease in the surface free energy thus creating cohesion between the compact ceramic powder. In some conditions, temperature itself is not sufficient to induce this effect. In this case, applying external pressure during heating is needed, and it is call pressure sintering. For conventional sintering without the need for pressure, there are three primary stages at play;

i) Initial stage: particle rearrangement, atomic mobility (plastic flow), neck growth.
ii) Intermediate stage: Significant coarsening of the grain, grain growth forming channel-like pores, solution-precipitation.
iii) Final stage: removal of the remaining porosity, densification.

When the temperature reaches one half of the ceramic melting temperature, the polymer binder and other additives such as the dispersant and water is removed from the precursor fibres. This initial stage leads to a more compact ceramic particles arrangement. Removal of organic additives needs to be controlled appropriately in the initial step. As combustion of this component produces volatile decomposition by-products, excessive accumulation of by-products in the ceramic hollow fibre precursor may lead to cracking. The cracking is caused by the internal pressure gradient. The best practice in this initial stage is to slow down the decomposition kinetics, by introducing heat in stages at a temperature between 300-700 ^{o}C [114]. The technique, on the other hand, may assist the rebinding process in reducing defects formation on the product. Generations of neck growth will later occur as an effect of further increase in temperature caused by an atomic diffusion of solid-state sintering or diffusion from viscous flow if the liquid phase is present. At the neck part, where the vapour pressure is lower,

particles diffusion happens through its lattice, which leads to the production of bigger particles and grain growth. A solid solution strengthening effect occurs with the densification of the solid packed regions, and hollow fibre shrinkage is visible due to the reduction in pore size and volume.

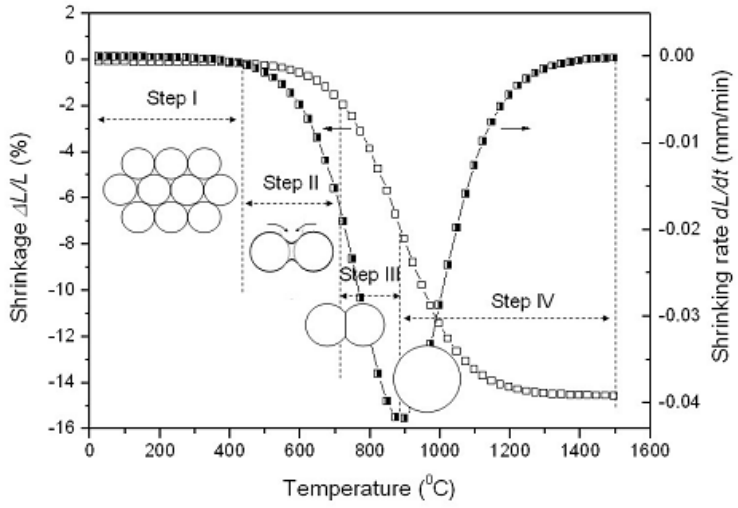

Figure 2.17 Schematic diagram of sintering profile for ceramic hollow fibre membranes [115]

The schematic diagram in Figure 2.17 shows the grain growth and hollow shrinkage profile in the sintering phase. Neck formation starts to occur in Step II, and further grain growth can be seen in Step III and Step IV, and here, available grain boundaries also decrease. Further increments of temperature show an inversely proportional effect on the hollow fibre size. As the grain size gets bigger, the rate of shrinkage reduces dramatically throughout the process. Here, another two mechanisms have been discovered. The growth of the grain size may either cause densification or coarsening and these two produce different porosity profiles. If denser ceramics are favoured, the conditions of the sintering temperature need to be tailored so that the coarsening mechanism does not dominate the grain growth. And so, if hollow fibre with high porosity is favoured, temperature control is critical in suppressing the densification

mechanism from dominating. Various sintering conditions for ceramic hollow fibre have been intensively researched. The main reported effect is on the changes in morphology, structure and mechanical strength [116–118]. Therefore, optimum control in the sintering profile such as heating rates, dwelling time and sintering temperature is critical in order to avoid an over-sintered product which can cause a loss of mechanical properties and undesired microstructure.

2.6 Summary

It is true that the current design of the catalytic converter can comply with current emissions regulations. But in the near future, as the law gets more stringent, the advancement of a better system will be required. One option is through the development of the catalyst support. Although extensive efforts have been made to design a monolithic substrate with higher GSA, the conventional method of reducing the wall thickness and increasing the CPSI are limited by the mechanical strength and backpressure constraints. For these reasons, the introduction of a new substrate design is critical.

The second issue regarding the depletion of PGM resources and price volatility calls for steps to be taken to reduce reliance on this metal. However, with the constraints of the converter to achieve high conversion efficiency, PGM is still the best catalyst so far. While it is still not possible to completely discard PGM from the system, reducing the amount of PGM can be a practical solution to the depletion problem. Design of the new catalyst configuration then requires that the catalytic performance is optimised with a lesser amount of catalyst used.

The third issue in the development of a catalytic converter is related to the catalyst formulation and the ageing profile. The harsh operating environments in the exhaust stream leads to deterioration of the catalytic performance and can shorten the life expectancy of the catalytic converter. The primary cause of immature ageing is originated from the washcoat layer phase transformation, causing the loss of surface area in the system. The common solution for the problem is through addition of a stabilising material to the washcoat layer. While addition of a stabilising material increases the thermal stability of the washcoat to a certain extent, the phase transformation is inevitable. Removal of the washcoat layer would remove the necessity of controlling the thermal stability of this layer. However, with the current monolithic support structure, elimination of the washcoat layer is not worth considering, given that the surface area would be insufficient for catalyst deposition in the system.

To fill the gap in the catalytic converter research development, a few ideas were proposed. Firstly, hollow ceramic fibre with asymmetric structure and microchannels in the lumen side can be seen as an attractive option of the new substrate for a catalytic converter. The single-step extrusion assisted by phase inversion fabrication process is simple, and geometry enhancement can be expected. The presence of microchannels can be tailored through the fabrication process and the structure is beneficial in increasing the surface area for deposition of the active catalyst. Design of the substrate must comply with several critical characteristics such as low thermal expansion to prevent thermal shock, suitable porosity and pore size distribution to limit mass transfer resistance, melting point beyond 1450 ^{o}C because of high combustion temperature of the ICE, sufficient strength to survive the robust condition in the exhaust environment and a compatible washcoat and catalyst layer to ensure excellent adhesion between each layer [119,120]. Alumina is seen as the best candidate for ceramic support.

Microchannel structures in the new substrate are expected to allow better catalyst distribution in the system. As heterogeneous catalysis is based on the surface reaction, better catalyst distribution can optimise the use of active sites during reaction. The new support template would make it possible to reduce the amount of catalyst deposited in the system, in order to tackle the PGM scarcity issue. For this hypothesis, a low amount of palladium only catalyst was deposited on the microchannel to see the possibility of reducing catalyst content in the new substrate design. In addition, while it is impractical to remove the washcoat layer in the current catalytic converter design, an attempt was made to directly deposit catalyst on the substrate without the washcot layer. Since PGM only catalyst will not survive for long in this condition due to sintering problem, a new catalyst formulation based on palladium doped perovskite catalysts were synthesised. Lastly, taking into account all the necessary requirements and development gaps in catalytic converter research, the use of ceramic hollow fibre substrate catalytic converter for automotive emissions control is thoroughly evaluated in this study.

Chapter 3

Experimental Procedures

This chapter listed all materials used in the study and experimental procedures which have been taken place to achieve the listed objectives of the thesis in Chapter 1

3.1 Materials

3.1.1 Alumina Hollow Fibre Substrate

α-alumina (Al_2O_3) powder (1 μm, 99.9 % metal basis, surface area 6 – 8 $m^2 g^{-1}$, Inframat Corporation) was used as supplied. N-Methyl-2-pyrrolidone (NMP, synthesis grade, Merck) and Arlacel P135 (Polyethyleneglycol 30-dipolyhydroxystearate, Uniqema) were used as the solvent and dispersant, respectively. Polyethersulfone (PESf) (Radel A-300, Ameco Performance, USA) and Poly(methyl methacrylate) (PMMA) (Radel A-300, Ameco Performance, Greenville, SC) were used as polymer binders. A mixture of NMP/ethanol (HPLC grade, VWR), and distilled water were used as the internal and external coagulants, respectively.

3.1.2 Pd/Al_2O_3 Catalyst

γ-Alumina (Al_2O_3) powder (99.995%, surface area 100 ± 30 m^2 g^{-1}, 35 – 45 μm, Inframat Advanced Materials) was used for the washcoating layer without further purification. hydrochloric acid (HCl) and palladium (II) chloride ($PdCl_2$) (99.9% metal basis, min 59.0% Pd, Alfa Aesar) were used to prepare a metal salt precursor solution.

3.1.3 Perovskite Catalyst

Lanthanum (III) nitrate hydrate 99.9% trace metals basis, iron (III) nitrate nonahydrate, ≥ 99.95% trace metals basis, manganese (II) nitrate hydrate 98%, cobalt (III) nitrate hexahydrate, and palladium (II) chloride 99.999% were purchased from Sigma-Aldrich. Hydrochloric acid 37% vol%, ethanol absolute, AnalaR Normapur, Assay (V/V) 99.95%, and ethylene glycol (Assay on anhydrous substance min. 98% and citric acid anhydrous (ACS Reagent ≥ 99.5%) were purchased from VWR. γ-Alumina powder (Al_2O_3) with a surface area of 100 ± 30 m^2 g^{-1} and α-alumina (Al_2O_3) powder (1 μm, 99.9% metal basis, surface area 6 –8 m^2 g^{-1}) purchased from Inframat Advance Materials. All chemicals were used as supplied.

3.2 Preparation of Ceramic Hollow Fibre Substrate

The spinning suspension was prepared by dissolving a small amount of Arcalel P135 dispersant in the NMP solvent for 30 minutes. α-Alumina powder was then added to the solution and rolled with 20 mm agate milling balls for 72 hours. Polymer binder was added to the suspension, and the milling was continued for another two days. The suspension was degassed

before the spinning process to remove air bubbles trapped before being transferred into a stainless-steel syringe container. The fabrication process was carried out with a single layer orifice spinneret. Details regarding the introduction of the spinning process have been reported elsewhere [121]. Distilled water was used as the external coagulant, while a mixture of solvents was used as the bore coagulant. Suspension extrusion rate and bore fluid flow rate was controlled by syringe pumps (PHD 2000 Programmable, Harvard Apparatus). No air gap was introduced, and the process was carried out at room temperature. Figure 3.1 shows the spinning system set up and spinneret used.

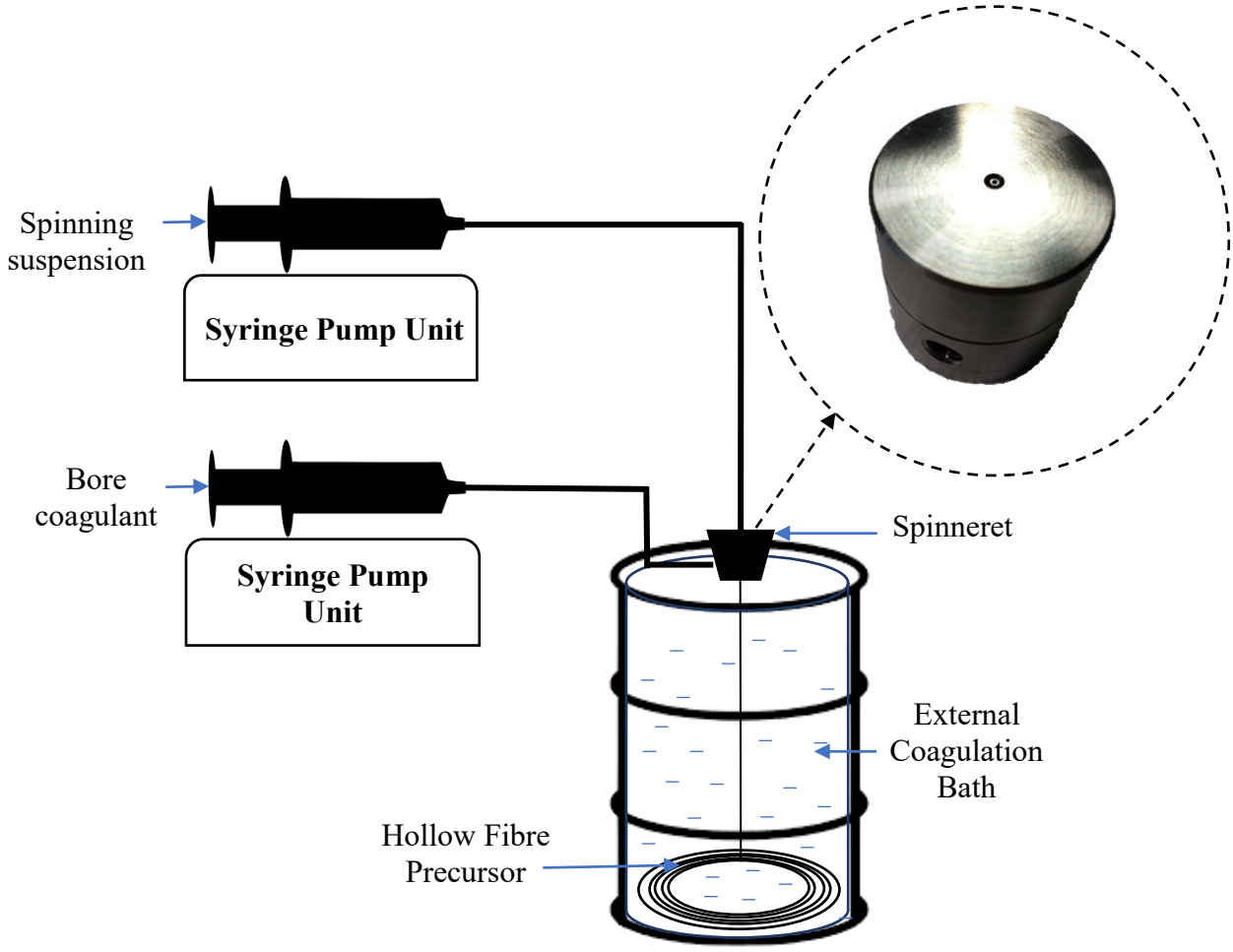

Figure 3.1 Schematic diagram of the extrusion spinning process and the single-layer orifice spinneret

The spinning parameters are presented in Table 3.1. Subsequently, the hollow fibres produced were immersed in distilled water overnight for completion of the phase-inversion and solidification process before cutting, straightening and drying at room temperature. The dried hollow fibres were thermally sintered from room temperature to 600ºC for 3 hours to remove organic binders with a ramping rate of 1 ºC.min^{-1}. Then the temperature was increased at a rate of 2 ºC.min^{-1} to 1500 ºC and dwelled for an additional 4 hours. To avoid thermal shock, the cooling down process was taking place at a ramping rate of 2 ºC.min^{-1} to the room temperature.

Table 3.1 Spinning suspension compositions and fabrication parameters

Materials	**Compositions (%)**	
	PESf based powder suspension	**PMMA based powder suspension**
Alumina	57.0	54.11
PESf	5.7	-
PMMA	-	8.73
NMP	36.80	36.68
A135	0.5	0.48
Spinning Parameters		
Bore Fluid composition	NMP/Ethanol (70:30)	NMP/Ethanol (60:40)
Air gap (cm)	0	0
Suspension extrusion rate (ml min^{-1})	9	8
Bore fluid extrusion rate (ml min^{-1})	8	10
Spinneret dimensions, outer/inner (mm)	3.0/1.2	3.0/1.2

3.3 Catalyst Preparation

3.3.1 Palladium Supported Alumina Preparation

0.075 wt.% palladium supported on the γ-Al_2O_3 catalyst was prepared by a standard wet incipient impregnation. The dissolved palladium chloride solution was mixed with γ-Al_2O_3 powder, stirred for one hour, dried overnight, and the catalyst was calcined for one hour at 500 ^oC. Another set of Pd supported on γ-Al_2O_3 was calcinated at 700^oC for four hours to study the effects of high temperature on Pd catalyst.

3.3.2 Perovskite Catalyst Preparation

Two different types of perovskite oxide catalysts, $LaFe_{0.7}Mn_{0.225}Pd_{0.075}O_3$ and $LaFe_{0.7}Co_{0.225}Pd_{0.075}O_3$, were synthesised via the citrate sol-gel method. Aqueous mixed metal nitrate solutions were prepared composed of stoichiometric amounts of lanthanum, iron, manganese or cobalt nitrate dissolved in 5 mL de-ionised water and 15 mL of ethanol absolute. The stoichiometric ratio was calculated on the basis of 4 mmol of lanthanum. The mixture was sonicated for 15 minutes to ensure uniform mixing of the mixed metal solution.

Palladium (II) chloride was dissolved in 0.05 M hydrochloric acid solution with a molar ratio of 1:1.5 respectively and was heated at 80 ^oC for 30 minutes until a clear solution was obtained. The mixed metal nitrate solution and the palladium chloride solution were mixed and further sonicated for 30 minutes. Subsequently, the mixture was prepared with an aqueous solution of citric acid, with a molar ratio of 15% excess citric acid with respect to the sum of metal salts. The mixture was stirred for an hour and allows for complexation of the metal cations. The

solution was continuously stirred and dried overnight in a water bath at 80ºC for the elimination of liquid. After obtaining a dry powder, the mixture was further dried in an oven at 80 ºC for eight hours, to remove any remaining moisture. To form crystal perovskite, the powder was calcined at 700 ºC for four hours. The catalyst obtained was mechanically ground using pastel and mortar to form a fine particle. $LaFe_{0.7}Mn_{0.225}Pd_{0.075}O_3$ and $LaFe_{0.7}Co_{0.225}Pd_{0.075}O_3$ are denoted as LFMPO and LFCPO respectively. The full preparation technique is presented in Figure 3.2.

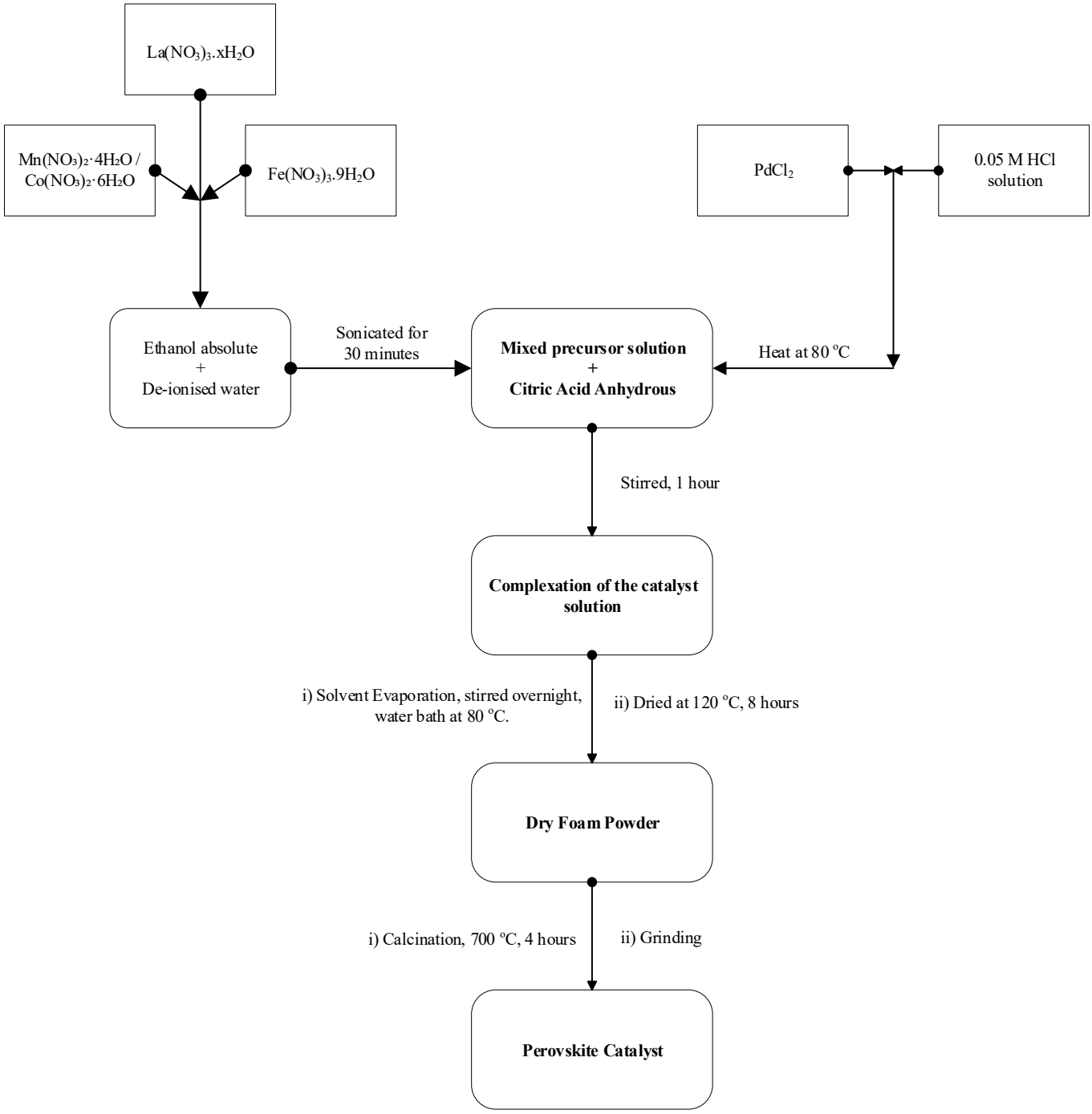

Figure 3.2 Flow steps for the synthesis of the perovskite catalysts

3.4 Washcoating

3.4.1 Alumina Washcoating Process and Incipient Wetness Impregnation

The washcoating process was initiated with 50 mg of γ-Al_2O_3 powder dispersed in 250 ml of distilled water and ultrasonicated for one hour. This was done to minimise the agglomeration of particles. The suspension was continuously pumped into the hollow fibre for fifteen minutes at a flow rate of 50 $ml.min^{-1}$ of solution flow rate and then dried for one hour in the oven at 150 ºC. The weight increment was recorded, and the washcoating process was repeated until the target loadings of 3, 5, 8 and 10 wt% were achieved. The samples were assigned as W0, W3, W5, W8 and W10 which represents each of the washcoat loadings in the hollow fibre. For the catalyst impregnation, an aqueous metal salt precursor was prepared by dissolving $PdCl_2$ in HCl solution at a concentration of 5 x 10^{-2} M [122]. A metal solution of 0.4 ml was injected into 100 mm of washcoated hollow fibre sample, and subsequently, dried in an oven for 1 hour at 150 ºC. The process was repeated until the desired catalyst weight loading of 1.0 wt% Pd was achieved. All the hollow fibre catalytic converters were calcined in the air at 500 ºC for one hour.

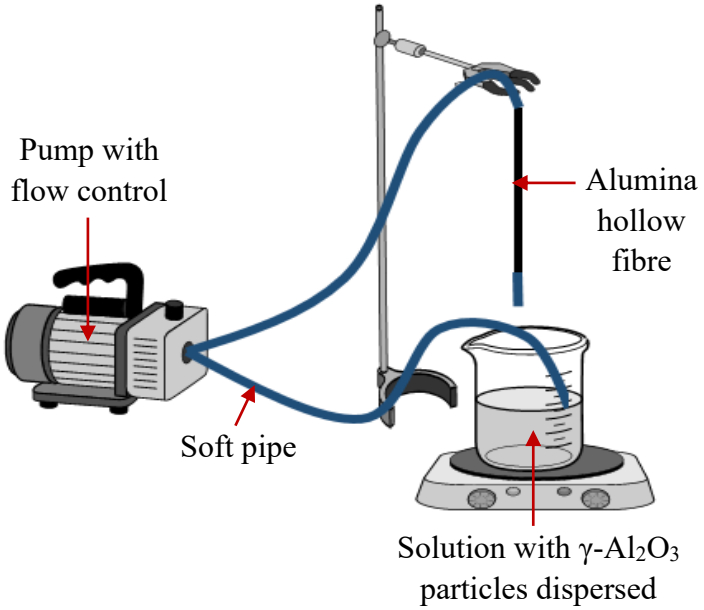

Figure 3.3 Washcoating controlled amounts of γ-Al_2O_3 into alumina hollow fibre

3.4.2 Perovskite Catalyst Washcoating

A specific amount of catalyst was washcoated on the ceramic hollow fibre substrate. 50 mg of the perovskite catalyst was dispersed in 500 ml of distilled water and was sonicated for an hour prior to washcoating, to avoid particles agglomerations. The washcoating cycle was repeated until the target amount of catalyst deposited was achieved. A set of 5 mg and 10 mg of each perovskite catalyst were deposited directly onto the hollow fibre substrate without any additional secondary oxide / washcoat layer.

3.5 Characterisations

3.5.1 Scanning Electron Microscopy (SEM)

JEOL JSM-5610 scanning electron microscopy (SEM) was used for the morphology investigation at different magnifications. Samples were carefully broken into suitable size and mounted onto the sample holder. Before imaging characterisation was being carried out, samples were sputtered with gold coating.

3.5.2 Transmission Electron Microscopy (TEM) and Energy Dispersive X-ray (EDX)

Transmission electron microscopy (TEM) and Energy Dispersive X-ray (EDX) observations were conducted using the JEOL EM-2100F TEM and Oxford Instruments INCA EDS 80 mm X-Max detector system, respectively. EDX mapping was performed on an alumina substrate after a successful impregnation cycle was completed

3.5.3 Brunauer-Emmett-Teller Surface Area (BET)

Brunauer-Emmett-Teller (BET) surface area analysis was carried out using a Micrometrics TRISTAR Surface area analyser. Multilayer adsorption of non-corrosive N_2 gas was measured as a function of relative pressure. The samples were dried at 110 ^oC under vacuum overnight prior to the analysis. The measurement was done on both the particle form, as per synthesised catalyst and the impregnated hollow fibre sample. Prior to analysis, the samples were dried overnight at 110^oC.

3.5.4 Porosity Test

To investigate the porosity profile of the hollow fibre, bubble point measurements were carried out using a porometer, Porolux 1000. 25 mm of the hollow fibre sample was mounted into a stainless-steel sample holder exposing only one end, and another end was sealed with epoxy resin. The adhesive was left to dry overnight before the test was carried out. N_2 gas feed was introduced from the lumen side, and samples were tested under the dry and wet conditions.

3.5.5 X-Ray Diffraction (XRD)

The structural characterisation, of the catalyst, including the crystallite size, their structure and phases, was performed on a PANalytical X-ray diffractometer for X-ray diffraction (XRD) with CuKα radiation in the range from 0 to 90^o.

3.5.6 Crystallite Size Calculation

Based on the XRD graph, the crystallite size is calculated by using the Scherrer equation as below;

$$D = \frac{K\lambda}{\beta \cos \theta} \qquad [3.1]$$

Where D = the average thickness in a vertical direction of the crystal face, K is Scherrer constant, λ is the wavelength of X-ray, β is the half high width of the diffraction peak of the sample, θ is the Bragg diffraction angle.

3.6 Catalytic Testing

3.6.1 CO Oxidation of Pd/Al_2O_3

The reaction was performed under atmospheric pressure. Prior to the test, the hollow fibre catalytic converter was pre-treated with a mixture of 5 ml min^{-1} H_2 and 30 ml min^{-1} argon to reduce the metal oxide surface at 450ºC for one hour. Further, 50 mm of hollow fibre catalytic converter sample was mounted into the cylindrical quartz tube, with a space velocity GHSV of ~ 59, 000 h^{-1}. Mass flow controllers (Model 0154, Brooks Instrument) were used to maintain a total gas flow rate of 100 ml min^{-1}**.** A gas mixture of 50 ml min^{-1} air and 50 ml min^{-1} (10% CO in 90% Argon) was fed into the reactor system. The gas mixture in the reactor system represents the lean-burn condition. The flow of the gas mixtures was pre-heated to the reaction temperature and placed in an upstream motion through the hollow fibre catalytic converter. An on-line gas chromatograph (Varian 3900) equipped with a thermal conductivity detector (TCD) was connected to the reaction outlet via gas sampling tubing. The TCD detects the changes in the thermal conductivity between the effluent column and compares it to a reference flow of the carrier gas. In addition, a bubble flow meter was used to measure the outlet flow rate. Sampling for analysis was recorded every thirty minutes, after stabilisation of each temperature intervals. A series of light-off temperature performance tests were carried out at room temperature until 100% conversion was achieved. CO conversion was calculated from pre-plotted calibration curves based on the peak areas formed. The percentage conversion of CO oxidation is defined as follows;

$$\% \text{ conversion of CO} = \frac{C_{CO\ inlet} - C_{CO\ outlet}}{C_{CO\ inlet}} \times 100\ \% \qquad [3.2]$$

Where $C_{CO\ inlet}$ and $C_{CO\ outlet}$ are the CO concentrations in the inlet and outlet of the system, respectively.

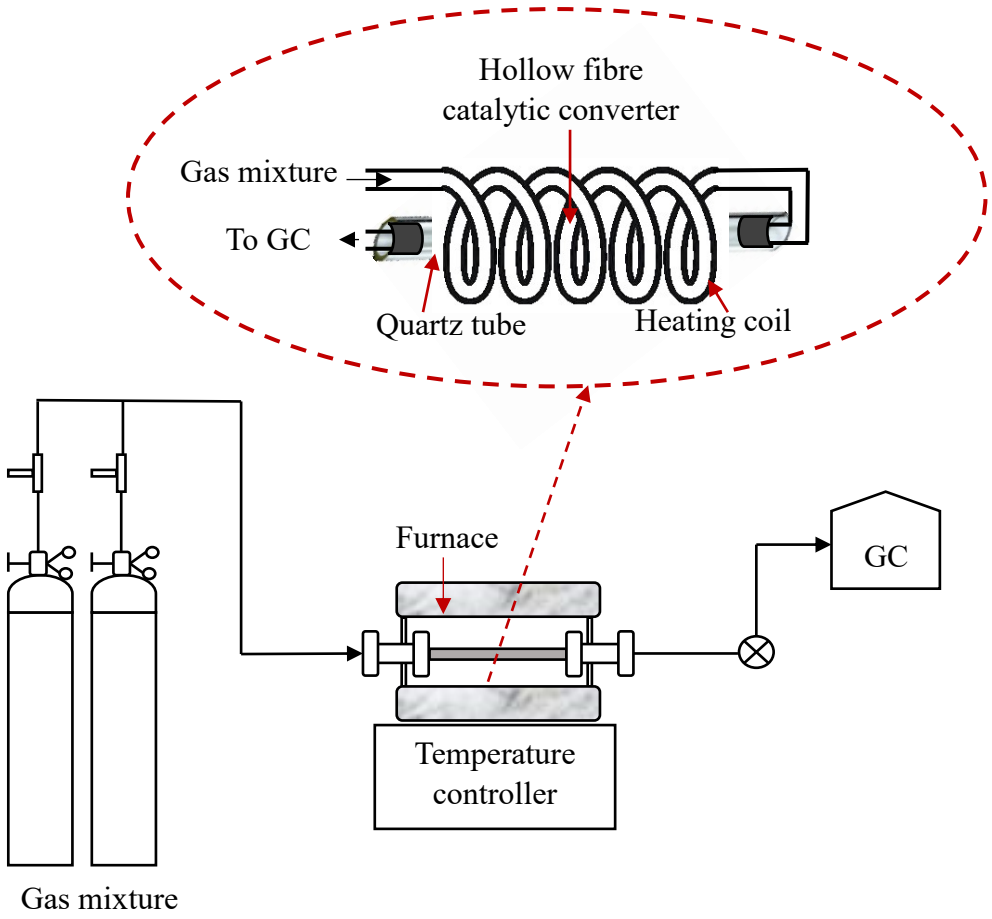

Figure 3.4 Schematic diagram of the system for catalytic reaction tests

3.6.2 CO Oxidation of Perovskite Catalyst

CO oxidation was used to evaluate catalytic performance of perovskite catalyst and perovskite/hollow fibre structured composite, which also facilitated the comparison with our earlier work which involved Pd/γ-alumina as the catalyst. Two different catalyst packing configurations were chosen as shown in Figure 3.5. For the packed-bed configuration, 5 mg of perovskite catalyst (average particle size of 5 μm) was mixed with 200 mg of α-Al_2O_3 powder (particle size of ~ 1 μm), before being loaded into a 5 mm I.D. quartz tube and secured by quartz wool at both ends of the catalyst bed. The catalyst bed was approximately 20 mm in length. For the structured configuration, 5 ± 0.5 mg of catalyst was washcoated into alumina hollow fibre of 50 mm long, which weight at approximately 200 ± 10 mg. The hollow fibre sample was mounted into the quartz tube connected to a metal coil to pre-heat gaseous reactants to the reaction temperature. The quartz tube was placed horizontally in a furnace (Vecstar Furnace, VCTF/SP). Mass flow controllers (Model 0154, Brooks Instrument) were used to control the gas flow into the system. A mixture of air and CO (10% CO in 90% Argon) at a ratio of 1:1 was fed into the reactor system, which represents the lean-burn condition with an excess of oxygen (. The flow rate of feed gas was calculated to achieve a space velocity GHSV of ~ 5300 h^{-1}. An on-line gas chromatograph (Varian 3900) was connected to the outlet stream to analyse the effluent. The reaction temperature was gradually increased, and the sampling was taken after thirty minutes of temperature stabilisation intervals. A series of reaction temperature was used, from room temperature until 100% of the CO conversion. The conversion of CO was calculated based on the equation 3.2.

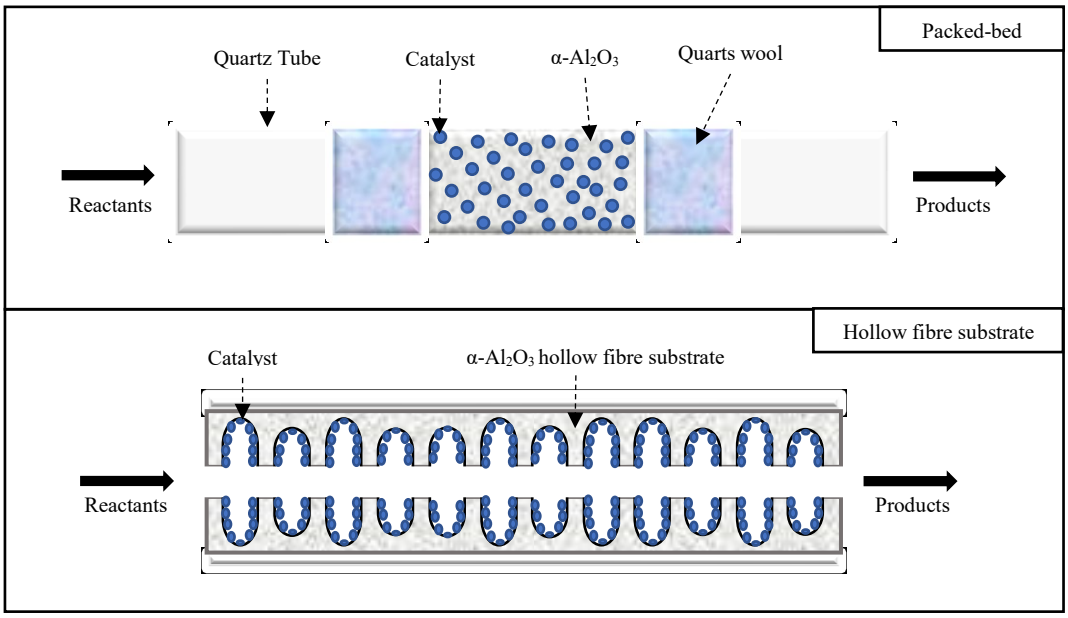

Figure 3.5 Variation of packing configuration

3.7 Pressure Drop in Substrates

Table 3.2 listed monolith channel geometry of the commercial cordierite catalytic converter and the hollow fibre substrate, while Table 3.3 listed air properties at 20 ºC, 1 atm. These dimensions and parameters were used to calculate pressure drop in the substrates.

Table 3.2 Monolith channel geometry and dimensions

	Commercial Catalytic Converter	Hollow Fibre Catalytic Converter
	Scale 10 mm = 66.7 mm 0 120 	Scale 10 mm = 21.8 mm 0 43.64 
Channel dimensions		
Diameter (mm)	0.85	2.4
Length (mm)	120	120
Surface roughness	0.75 [123]	

Table 3.3 Air properties at 20 ºC, 1 atm

Thermodynamic Properties	**Value**
Molar mass ($kg.mol^{-1}$)	28.96
Density ($kg.m^{-3}$)	1.225
Dynamic Viscosity ($kg.m^{-1}s^{-1}$)	1.7894×10^{-5}

Chapter 4

A Study on the Extrusion of Ceramic Hollow Fibre for the Fabrication of Ceramic Hollow Fibre Substrates for Catalytic Converters

This chapter discusses the development of ceramic hollow fibre as a new substrate for automotive catalytic converters

Abstract

Ceramic hollow fibres were fabricated through a single step spinning assisted by the phase inversion and sintering process. Two types of polymeric binders, polyethersulfone (PESf) and poly(methyl methacrylate) (PMMA) were used for fabrication. In the early stages, several spinning sessions were carried out with different sets of spinning parameters. In this chapter, only the best hollow fibres produced from these two polymers are presented and discussed. Tailoring the spinning parameters may well affect the formation of the fibres. With the phase inversion assisted spinning process, hollow fibres with a matrix of self-oriented microchannels protruding from the outer surface to the lumen side were produced. But in comparison, hollow fibres made with PMMA resulted in a finer microchannel homogeneity and the reproducibility using this formulation was also high. Ceramic hollow fibres with such morphology can

function as a substrate for heterogeneous catalytic applications. Geometric evaluations show that the ceramic hollow fibre substrate results in a geometric surface area (GSA) of 40.7 $cm^2.cm^{-3}$, which is comparable to the honeycomb monolith with 750 cells per inch square (CPSI), but with the additional advantage of a larger frontal diameter opening. With an inner diameter of approximately 1.6 mm, the hydraulic channel diameter is 60% and 170% larger than the 400 and 900 CPSI respectively. This is beneficial in reducing the pressure drop in the system, further enhancing engine performance. The simplicity and flexibility of the spinning technique in combination with structural advancements make this new structure more attractive over the conventional substrate used in automotive emissions abatement technology.

4.1 Introduction

The introduction of emission regulations in 1970 has brought a new narrative to the automotive industry. The regulations have enforced that every automotive manufactured since 1975 has to be equipped with a catalytic converter. From a very basic catalytic converter made from the supported platinum catalyst in the pallet, packed in metal canisters as shown in Figure 4.1, it has now evolved into a structured catalyst, comprised of a monolithic substrate, a secondary washcoat layer and a metal catalyst which are capable of simultaneously converting carbon monoxide (CO), hydrocarbons (HCs) and nitrous oxide (NOx) into innocuous substances. The shift from a packed-bed catalyst to a structured catalyst was due to the drawback of pressure drop and non-ideal flow with the packed-bed configuration. Since exhaust emits a large volume of gas during operations, any restriction in the outlet path raises the pressure-drop causes the internal combustion engine (ICE) to burn more fuel; this reduces the power needed to operate the car. As compared to the packed-bed configuration, the pressure drop in the monolithic

catalyst is up to two orders of magnitude lower [90]. The reason for the lower pressure drop is the absence of the eddy diffusion phenomenon in the structured catalyst, leading to less resistance to the mass transfer.

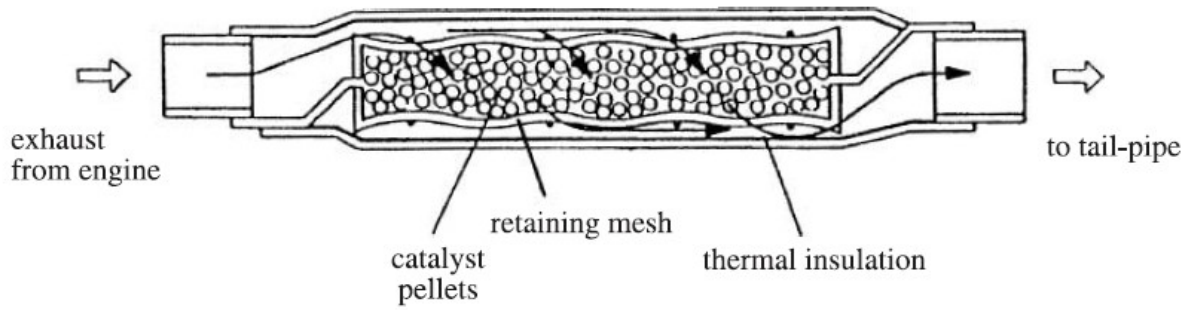

Figure 4.1 Diagram of the early invention of catalytic converter with pellet catalysts [4]

A conventional monolith is made up of either metal or ceramic materials. Although metal foils possess advantages of robustness and superior thermal conductivity over ceramic materials, the non-porous nature, high thermal expansion coefficient and adhesion problems with the washcoat layer have led to restrictions in advancing the usage of this material any further [93,94]. Hence, the ceramic monolith has been extensively researched as the most favourable option with the most common ceramic material used being cordierite ($(Mg,Fe)_2Al_4Si_5O_{18}$). The cell density of a ceramic monolith is defined by its cells per inch square (CPSI) number that ranges from 100 to 1200 [92]. A bigger CPSI number represents a ceramic monolith with a higher geometric surface area (GSA). On the other hand, the bigger the CPSI number, the smaller the diameter of each cell. These properties induce different effects on the catalytic converter. A high GSA means a huge surface area availability, especially for the deposition of the active catalyst which is known to affect the conversion efficiency of the catalytic converter. But a smaller entrance diameter causes higher backpressure. Both will eventually affect either the emission treatment or the engine performance; but from the perspective of the automotive

industry, these two cannot be compromised. Attempts have been made to further increase the GSA, without inducing further pressure-drop. One of the common approaches is by reducing the wall thickness since the open frontal area (OPA), the wall thickness and the cell density are dependent on each other. But an improvement of the GSA through an adjustment of the wall thickness is limited. Beyond a certain extent, it may impose problems upon the mechanical strength of the ceramic monolith. With such limitations, a new design is needed to enhance the GSA value.

Membrane technology has evolved from the initial invention made mainly for filtration systems into other applications in micro-reactor technology. In recent years, the use of ceramic hollow fibre as the support in heterogeneous catalysis, known as a microreactor has become a topic of discussion. Given the features of this unique support such as a high surface area to volume ratio, low pressure drop, high mass transfer rate and the ability to provide good contacts and mix of reactants, this type of support is highly favourable in catalytic reactions. For some applications where the volume of the flow of reactants is high, hollow fibre microreactors can be a better substitute for current conventional monolith support. Rahman et al. and García-García et al. have introduced the use of hollow fibre for heterogeneous catalytic gas reactions through a series of published research work [24,103]. The asymmetric structure of hollow fibres consisting of a sponge-like region and finger-like microchannels can serve the purpose of providing mechanical integrity for the former, while the latter structure allows for additional surface area for the catalyst deposition. Furthermore, the use of hollow fibre in catalytic converter applications was briefly demonstrated by Kingsbury et al. from the same group [105]. Comparisons were made with conventional monolith structures and results showed that with a 79% reduction of metal content in the system, the light-off temperature of CO oxidation was

only 15 ºC higher. Overall, they concluded that the hollow fibre substrate could offer catalytic improvements at low catalyst loading, with reduced a backpressure profile.

Interestingly, the hollow fibre microreactor design is not limited to catalytic reactions only, but demonstrates multifunctional behaviours as a heat exchanger, a reactant mixer and a particulate filter [104]. With the aforementioned success of utilising the hollow fibre substrate in different catalytic applications, it has opened the possibility of using this support design for catalytic converters, since the reaction process in catalytic converters is comparative to the microreactor system. The primary key in bringing this new substrate design to the application is to understand the manufacturing process and any other complexity that may exist.

Ceramic hollow fibre is commonly fabricated through an extrusion called a spinning technique, which is straightforward. It is relatively cheap, simple to scale-up, and with a high reproducibility [124,125]. While the normal extrusion method only produces a symmetric product, the extrusion assisted by the phase-inversion technique produces an asymmetrical structure, which is beneficial as a catalytic support. For purpose of catalytic converters, the aim is to have an open microchannel in the lumen side of the hollow fibre substrate so that this area can be used to deposit the washcoat and the catalysts. The fabrication of ceramic hollow fibre substrate through a spinning technique assisted by the phase-inversion process was chosen considering the process advantages. The ceramic suspension is usually prepared from a combination of ceramic powder, a polymeric binder, a dispersant, and a solvent. This solution is then brought to the fabrication process. The produced hollow fibre is later sintered to remove organic compounds to consolidate their mechanical properties and structure [118]. Through this technique, hollow fibres with a wide range of ceramic materials are spinnable, giving room

to experimentation with versatile materials. It also gives the flexibility to control the morphologies and microstructures depending on the target application.

For this study, a ceramic hollow fibre as a new substrate for automotive catalytic converters was prepared. Al_2O_3 was used as the main ceramic material, and the hollow fibres were fabricated through a single phase-inversion process followed by a sintering step. The effects of different suspension formulations on the fibre morphology and the improvement brought by the new substrate design were investigated. The advantages of the ceramic hollow fibre substrate over the conventional honeycomb substrate are discussed further in this chapter.

4.2 Experimental

All materials and experimental procedures can be extracted from Chapter 3. Materials are listed in subsection 3.11, while the ceramic hollow fibre fabrication technique is discussed in subsection 3.2. Parameters for pressure drop in hollow fibre substrate calculation are listed in subsection 3.7.

4.2.1 Selection of Ceramic Material

The material α-alumina has been chosen as the building block of the hollow fibre substrate being used in the catalytic converters for automotive emissions control. Materials selected as substrates must comply with a strict requirement regarding their physical and chemical properties with a guarantee that these properties would not pose any significant hindrance to their performance. Since catalytic converters are used in an area where thermal fluctuations are a norm during operation, the ceramic used needs to have a high thermal shock resistance with low thermal expansion. This is crucial in order to avoid cracking and to ensure that the adhesion of the catalytic materials on the support does not suffer prematurely. With such requirements, alumina is seen as a good starting material which satisfies most of the properties mentioned, in addition to being inert and available in abundant quantity.

4.3 Results and Discussion

4.3.1 SEM

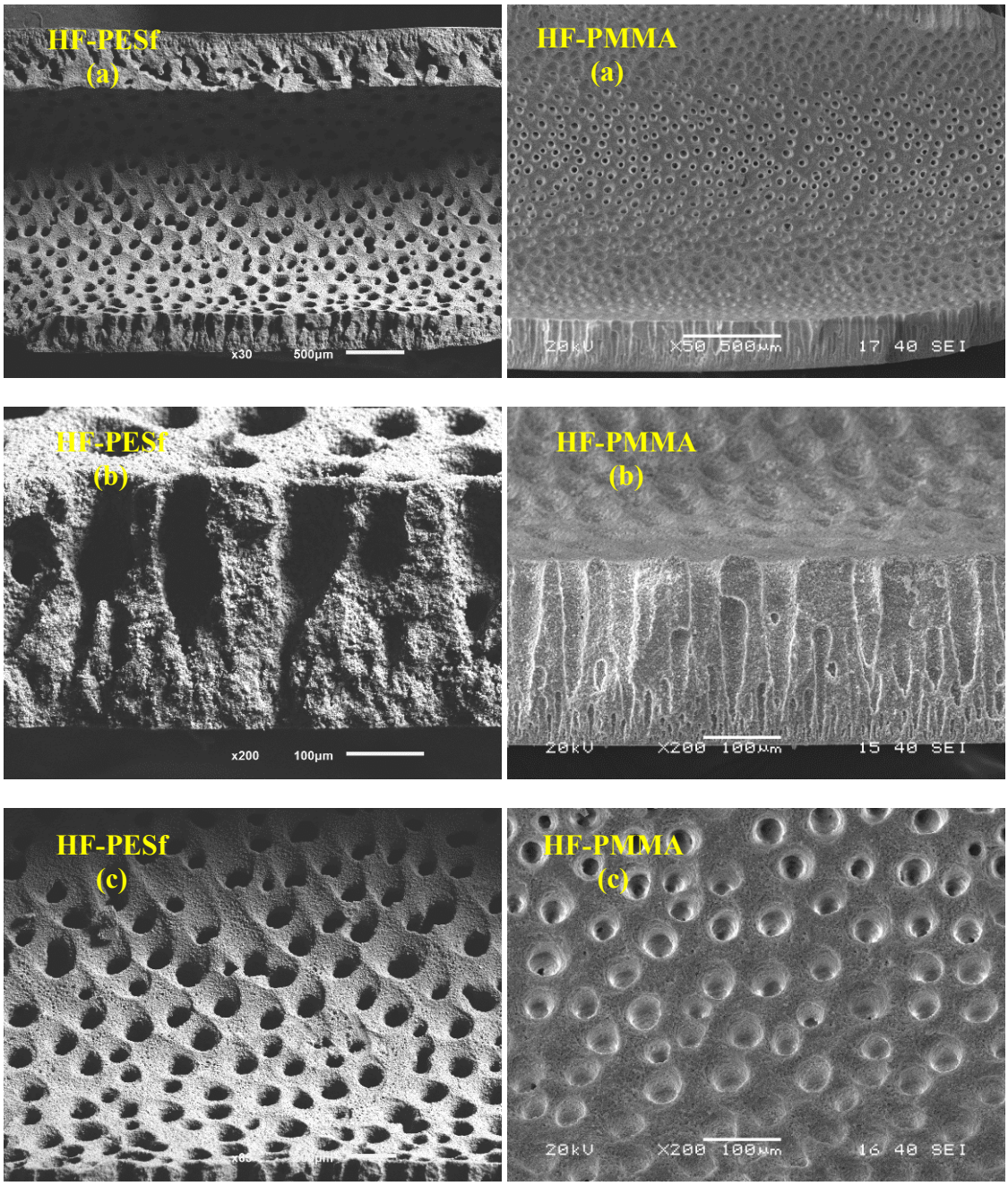

Figure 4.2 SEM images of the ceramic hollow fibre made with PESf binder (HF-PESf) and PMMA binder (HF-PPMA)

Observation of the fabricated hollow fibres indicates that the phase inversion-assisted extrusion process resulted in a hierarchical structure, composed of self-organised microchannels and a thin sponge. Figure 4.2 represents the morphology evaluation carried out by SEM for both hollow fibres fabricated with PESf and PMMA polymeric binders, with the best compatible spinning parameters to produce an open microchannel in the lumen of the hollow fibre. As can be seen, both hollow fibres resulted in about the same morphology having extensive arrays of microchannels. The hollow fibres show an asymmetric structure with approximately 20% of the total cross-section as a sponge-like layer near the outer surface, which is responsible for providing additional mechanical support for the hollow fibre. The dimensions of the fibre are approximately 2.4 mm of the outer diameter and 1.6 mm of the inner diameter after sintering at 1500 ^{o}C. In Figure 4.2, the structure of the microchannel with an opening of 40 μm is formed as a result of the penetration of the external coagulant during the phase-inversion spinning process, and detailed discussions on the micro-channel formation can be found elsewhere [111,112,126].

The overall structural evaluation showed that the hollow fibres made from PMMA resulted in a more regular microchannel geometry. It can be seen from Figure 4.2 (HF-PESf (b)), that some microchannels penetrated from the inner lumen up to the outer layer. Microchannels with a larger open entrance can be considered more attractive as a washcoat deposition process is easier in this structure. However, the open microchannel from the inside to the outside creates problems such as i) the mechanical strength with this structure is very low and ii) the structure is not suitable for catalytic converter configuration since the reactants flow through in axial directions. Another issue related to the formulation with PESf binder is that the dope stability is sensitive to any minor variations in conditions during preparation. A second attempt to fabricate the hollow fibre with the same conditions resulted in fibres as shown in Figure 4.3**,**

with an irregular microchannel geometry. The ceramic hollow fibre with a PMMA binder, on the other hand, is proven to have high stability and repeatability where each fabrication set produces similar morphology each time.

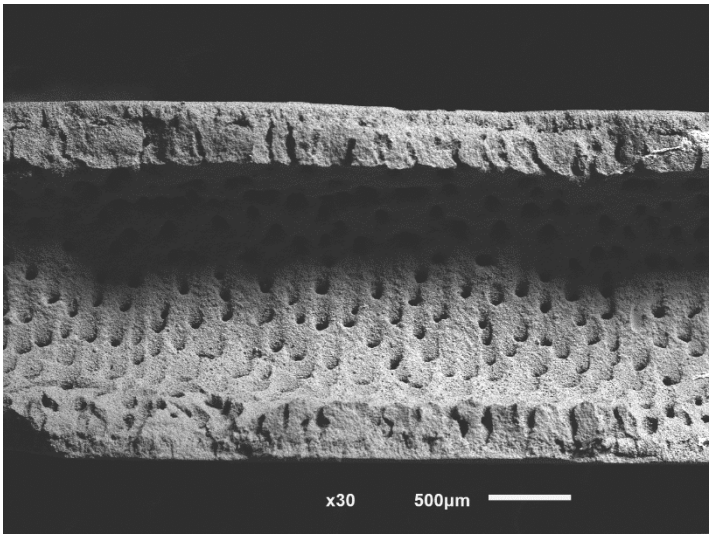

Figure 4.3 Ceramic hollow fibre made with PESf formulation - second repetition

With the limitations above, the following section will focus on the characterisations of the hollow fibre made with PMMA binder only.

The fabrication of alumina hollow fibre assisted by the phase inversion process offers flexibility in tailoring the morphology of the substrate. The porosity and the formation of the microchannels are dependent on the spinning parameters chosen. In the case of alumina hollow fibre as the catalytic converter substrate, the hollow fibre should have microchannels sufficient in size so that the catalytically active washcoat can be deposited along the channel opening. If the channel is too narrow or smaller than the washcoat material, the washcoat layer will settle on the inner surface layer of the hollow fibre.

4.3.2 Porosity, Specific Surface Area, and Geometric Surface Area (GSA)

Further structural evaluations of the hollow fibre were carried out to measure the specific surface area and their porosity profile. All measurement values are as presented in Table 4.1. An additional evaluation of the morphology can be seen in Figure 4.4, where scanning at higher magnification shows that the ceramic hollow fibre has a highly porous surface.

Table 4.1 Dimension and specific surface area of the ceramic hollow fibre

Dimensions (measured by SEM)	**BET Surface Area (m^2g^{-1})**
Outer Diameter: 2.5 mm	1.61 ± 0.0196
Inner Diameter: 1.61 mm	
Average microchannel opening: ~ 40 μm	

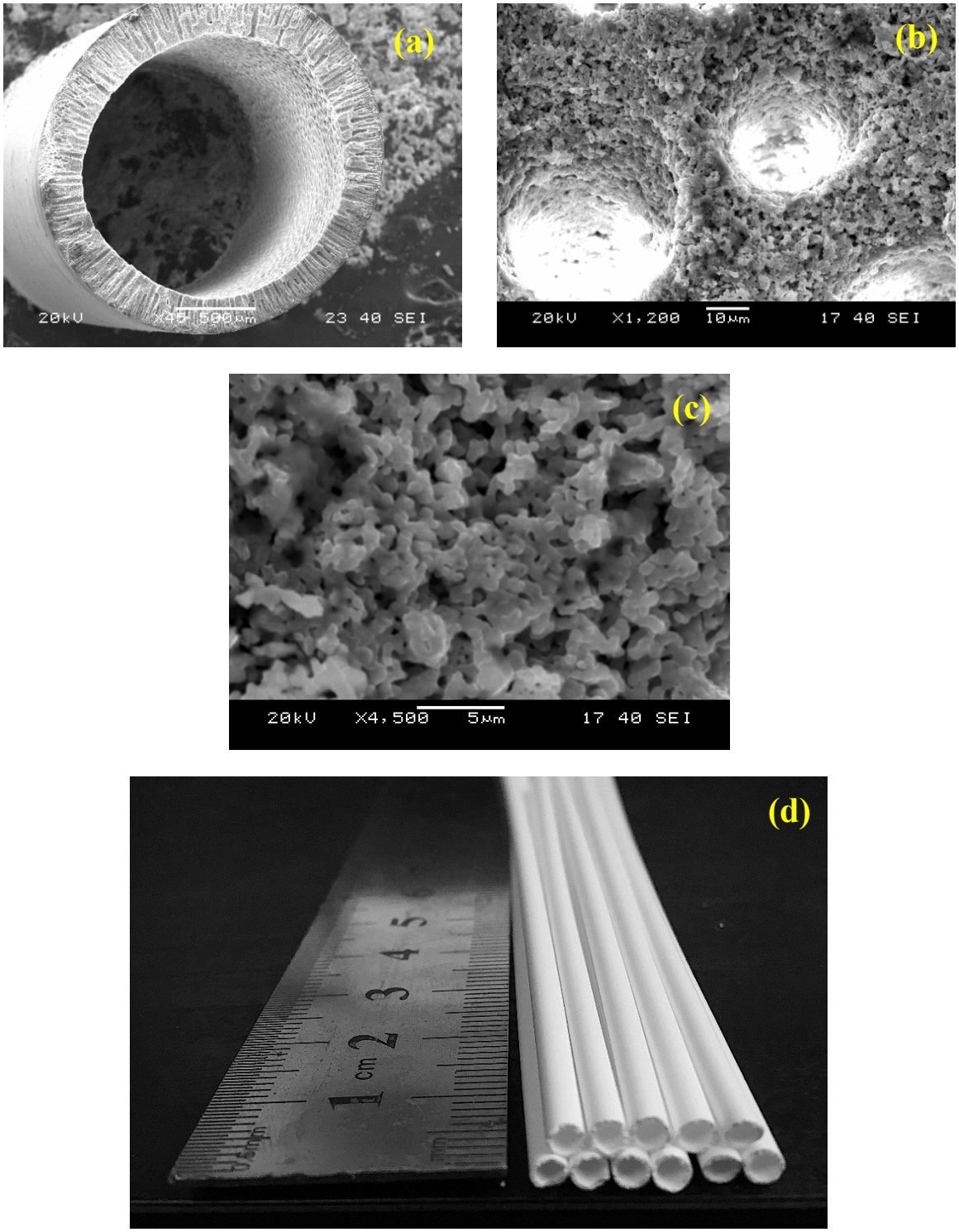

Figure 4.4 (a-c) SEM cross-section pictures of the fabricated alumina hollow fibre sintered at 1450 ^{o}C at different magnifications (d) Photographic image of the alumina hollow fibre substrates fabricated by a single spinning phase-inversion process followed by the sintering step

Table 4.2 presents comparisons between the GSA value of the hollow fibre substrate and a commercial honeycomb monolith. Assuming that the hollow fibre has an ideal packing of 91 hollow fibres in a bundle, the GSA value has been calculated to compare with the commercial honeycomb monolith (Appendix A). Based on the calculation, the GSA value of the ceramic hollow fibre is comparable to the 750 CPSI monolith, but with double the hydraulic diameter. This feature highlights the advantage that can be brought about by the hollow fibre substrate, which induces lower back pressure on the system. Manual calculation of pressure drop value in a single commercial catalytic converter substrate, at fluid velocity 10 $m.s^{-1}$ resulted in a value of about 100 $N.m^{-2}$. While for a single channel of a hollow fibre substrate, 7 % of lower pressure loss value is recorded, from 100 $N.m^{-2}$ in the conventional design to 93 $N.m^{-2}$ in the hollow fibre substrate. Details calculation is presented in Appendix B. A correlation between the pressure drop and the hydraulic diameter is well understood. Not only is the large open frontal area attractive, but such a circular shape of the hollow fibre is also preferable for conversion efficiency in the reactor, as suggested by a previous study [13].

Table 4.2 Design improvement on the GSA value

Conventional monolith (CPSI)	**Geometric Surface Area (GSA)* $cm^2\ cm^{-3}$**	**Hydraulic Diameter (mm)**	**Reference**
400	29.3	11.18	[127]
600	36.2	0.97	
750	40.2	0.86	
900	43.7	0.78	
Ceramic hollow fibre	40.7		This study

*detailed calculation is given in appendix A

An improvement in the GSA value can lead to a substantial reduction in the dimensions of the catalytic converter, which subsequently allows the device to be located closer to the engine manifold. Therefore, the heat transfer between the internal combustion and catalytic converter can be made more efficient for the catalyst activation. In addition, the larger surface area enables a more uniform dispersion and significantly improved accessibility for the catalyst, thereby lowering the total catalyst loading required. This in parallel can solve a problem related to the typical monolith reactor where only 10% of the catalyst impregnated is involved in the reaction, while the remaining catalyst acts as the monolith support and void channels [15,16].

4.3.3 Ceramic Hollow Fibre as New Substrate for Catalytic Converter

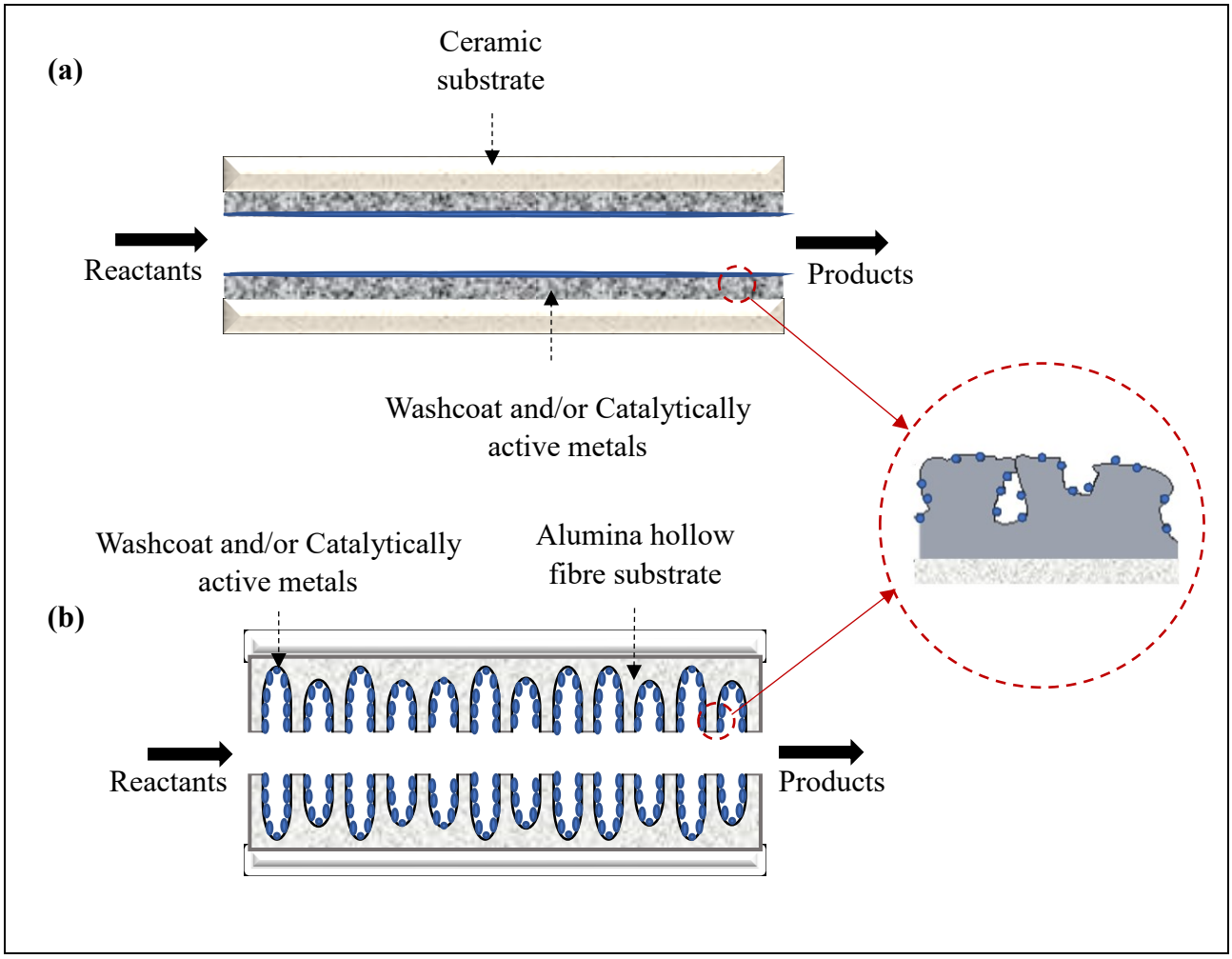

Figure 4.5 Differences of reactor configuration between (a) a conventional catalytic converter and (b) a ceramic hollow fibre catalytic converter

The difference between the catalyst configuration in the conventional substrate and the hollow fibre substrate for the catalytic converters is illustrated in Figure 4.5. As can be seen, a catalytic converter is comprised of a substrate, the washcoat and the catalyst. The washcoat layer has been added to the system since the surface area available in the conventional substrate is limited. But the washcoat layer contributes to additional restrictions to the mass transfer in the

system if it is not properly designed. Too little of the washcoat may cause an insufficient surface area for the catalyst deposition while an excessive washcoat causes mass transfer diffusion issues. Not only does the amount of washcoat matters, but the uniformity of distribution is critical too.

In the conventional system where the geometry of the cell is simple, the washcoat and the catalyst incorporation into the support is less challenging and different incorporation methods have been developed for this structure. But the hollow fibre support has a unique structure and requires a different procedure. For example, the deposition of the washcoat on the support wall in the conventional system is quite straightforward since most of the particles are embedded on the straight surface. But with the hollow fibre, the process is tricky and require modification from the common technique, since now the washcoat material needs to be embedded into the small microchannel surface. For this reason, the effects of the washcoat layer packing in the new hollow fibre substrate will be discussed in Chapter 5.

4.4 Conclusions

In this chapter, the new porous hollow fibre substrate using α-alumina has been successfully fabricated. Assisted by the induced phase inversion process, the new hollow fibre structure possessed a high-density of self-organised microchannels. Two different polymers were used as binders for the ceramic powders, namely PESf and PMMA. Out of these two, PMMA binder paired with compatible spinning parameters resulted in a hollow fibre having a morphology suitable to be used as a substrate in catalytic converter applications. The conical microchannels formed in the lumen side of the hollow fibre with an opening of 40 μm diameter on average can provide an increased surface area for deposition of catalytic materials. The controlled sintering profile used is compatible with the hollow fibre formulation. The final sintering product with a highly porous surface enables lesser mass transfer resistance for diffusivity of reactants to reach active sites in catalytic converter operations. The new design possesses a geometric surface area of 40.7 cm^2cm^{-3}, which is comparable to the commercial 750 CPSI honeycomb monolith at 40.2 cm^2cm^{-3} of GSA but with almost double the hydraulic diameter. Structural evaluations of the hollow fibre demonstrated that the new ceramic hollow fibre design is suitable to be used as a substrate in tailpipe technology to treat automotive exhaust emissions.

Chapter 5

Microchannel Washcoat Packing Effects on CO Oxidation Activity

This chapter discusses the effects of the washcoat packing inside the microchannel on CO oxidation activity by using palladium catalyst only and the work has been published in Catalysis Communications, N.I. Mahyon, T. Li, R. Martinez-Botas, Z. Wu, K. Li, A new hollow fibre catalytic converter design for sustainable automotive emissions control, 120 (2019), 86-90 [128].

Abstract

A porous ceramic hollow fibre substrate consisted of high-density self-organised microchannels was fabricated by the phase inversion-assisted extrusion process. The new substrate structure offers surface area comparable to the 750 CPSI monolith with almost double their surface diameter opening. The hollow fibre substrate was loaded with a washcoat layer and catalytically active metals. With the addition of a high specific surface area γ-Al_2O_3 washcoat, total CO oxidation conversion was achieved at temperatures lower than 200 ^oC with only 0.7 wt.% of palladium content in the system. The γ-Al_2O_3 washcoat was embedded into the microchannels of the hollow fibre followed by incipient wetness impregnation of palladium chloride solution. Different γ-Al_2O_3 loadings in the range of 3 – 10 wt.% created a variation in

washcoat packings with 5 wt.% of loosely packed washcoat in the microchannels that best serve with a CO oxidation light-off temperature of 187^{o}C. Even though specific surface area for the reaction is directly proportional to the washcoat loadings, hindrance effects were present when it exceeds a certain amount. The effects of washcoat packings on the light-off behaviour of Pd/Al_2O_3 catalyst were investigated. This study provides an insight into the transport effects on the reactivity of the Pd/Al_2O_3 catalyst impregnated onto the porous ceramic hollow fibre.

5.1 Introduction

Reliance on the catalytic converter to reduce a significant amount of exhaust pollutants resulted from incomplete combustion is of high importance. For decades, intensive research has been carried out to enhance catalytic converter efficiencies in converting noxious gases of carbon monoxide (CO), nitrogen oxides (NOx), and hydrocarbons into less harmful gases. The progression of research in this area is driven by stringent emissions regulations set by the government. To ensure a new standard is established, improvements are necessary for the research and development stages of catalytic converters. The new set of regulations that is revised frequently every few years has led to catalytic converter evolvement, from the simple pallet catalyst packed in stainless steel casing to the monolithic catalyst configuration. Since the catalytic converters are made up of three basic components, namely: i) substrate, ii) washcoat and iii) catalytic active metals, development of each component affects their performance differently. Substrate development is usually related to the surface area and back-pressure reduction, the washcoat research mainly involved the formulation of better substrate-metal interaction and the creation of an additional surface area, while catalyst studies focus on

the catalyst that can be light up at the lowest possible temperature and reaction performance in general.

The biggest contributor to the effectiveness of the catalytic converter originated mainly from their catalyst formulation. Latest trend tries to shift the dependency on platinum group metals (PGM) catalyst to the non-PGM catalyst. This is caused by the price volatility of the PGMs and their limited availability. Although different types of non-PGM catalyst have been proposed, most of them are still in the experimental stage. Vanadium-based, copper and iron zeolites and perovskites-based catalyst have been claimed as a better option, each with its exclusive advantages, such as higher thermal resistance, cost-effectiveness, and availability [25,43,129]. However, a highly valuable platinum group metal (PGM) catalyst remains favoured. It is suggested that PGM catalysts have high stability and are less prone to deactivation by fuel sulfur [4]. Due to those reasons, methods are currently being developed to address the aforementioned issues. One solution is to reduce the catalyst loading in the catalytic converters. This can be achieved by increasing the geometric surface area (GSA) of the monolith on which the catalytic washcoat will be deposited [130]. Increasing the support surface area will further enhance the contact size for reactants. Therefore, having a higher cell per square inch (CPSI) value is viewed as the simplest solution, owing to the proportional relationship with GSA. In addition, advancement in manufacturing technologies has made it possible to produce a honeycomb of up to 1600 cpsi [25,46]. However, as the exhaust flows at a high velocity, introducing this type of cells to the tailpipe may cause the internal combustion engine to suffer from a backpressure related problem. Thus increasing the cell densities is impractical for the application.

A ceramic hollow fibre consisting of high-density self-organised microchannels fabricated by extrusion, which are induced by the phase inversion process is proposed as the new monolith for catalytic converter systems. It has been reported that ceramic hollow fibre catalytic converters have exhibited the potential to become a substitute of the commercial honeycomb monolith, mainly due to the reduced substrate volume, precious metal loading, pressure drop and beneficial structured flow of hydrodynamics [130]. Presently, Kingsbury et al are the only group of researchers, who have reported a study on the feasibility and emissions conversion efficiency by using the ceramic hollow fibre as a new monolith design in catalytic converters. With moderate available information of the ceramic hollow fibre for catalytic converter, more studies are required to close the information gap, to make this invention feasible for commercialisation.

With limited surface area available for reaction, layering the substrate with secondary material is required in order to prepare the system for a finer catalyst distribution. The refractory oxide layer or washcoat in catalytic converters play a critical role in assisting the reactivity of the catalyst. The washcoat layer also provides additional advantages of surface area, a barrier to contamination, and the metal-oxide interactions can either facilitate or suppress the reaction. In spite of the fact that the washcoat could provide a large surface area which is beneficial for the reaction process, diffusion resistances that occurs in this layer have been shown to reduce reaction rates [131]. Studies to optimise this layer have been intensely carried out to overcome the mass transfer limitation in the system, where for conventional honeycomb monolith, washcoat thickness is recommended to be in the range of 10-100 μm [132].

In addition, various procedures can be applied to deposit washcoat substance onto monolith walls, which would produce different distribution profiles. Such a method includes sol-gel

coating, slurry coating, and colloidal solutions coating. But to date, a structured study has not yet been carried out that can demonstrate the technique to incorporate washcoat into the ceramic hollow fibre. Since ceramic hollow fibre substrate contains arrays of microchannels with around 40 μm of channel opening, a new washcoating technique is required. The loading of washcoat is believed to cause different packing configurations and the unique transport conditions of reactants through the microchannel structure could create several challenges

Further insight into understanding the transport mechanism in this new system is crucial. The present report studied a palladium catalyst supported on various loadings of the washcoated γ-Al_2O_3 substrate (0, 3, 5, 8 and 10 wt.%). The report investigated the effects of washcoat packing inside microchannels on the CO oxidation performances. The discussion on the results obtained could provide additional understanding of the transport phenomena in the new system, which affects reaction performance.

5.2 Experimental

Details concerning the preparation procedure of the suspension and spinning process have been reported in detail in Chapter 4. The best suspension compositions with the PMMA based powder suspension, and operating conditions found in Chapter 4 are adopted here. All experimental procedures for this chapter are as presented under subsections 3.1.1 and 3.2 for hollow fibre preparation, subsections 3.3.1 and 3.4.1 for supported catalyst preparation and washcoating procedure, respectively. Characterisations are as described in 3.5.1, 3.5.2, 3.5.3 and 3.5.4. CO oxidation performance evaluation is described in 3.6.1.

5.3 Results and Discussion

5.3.1 SEM

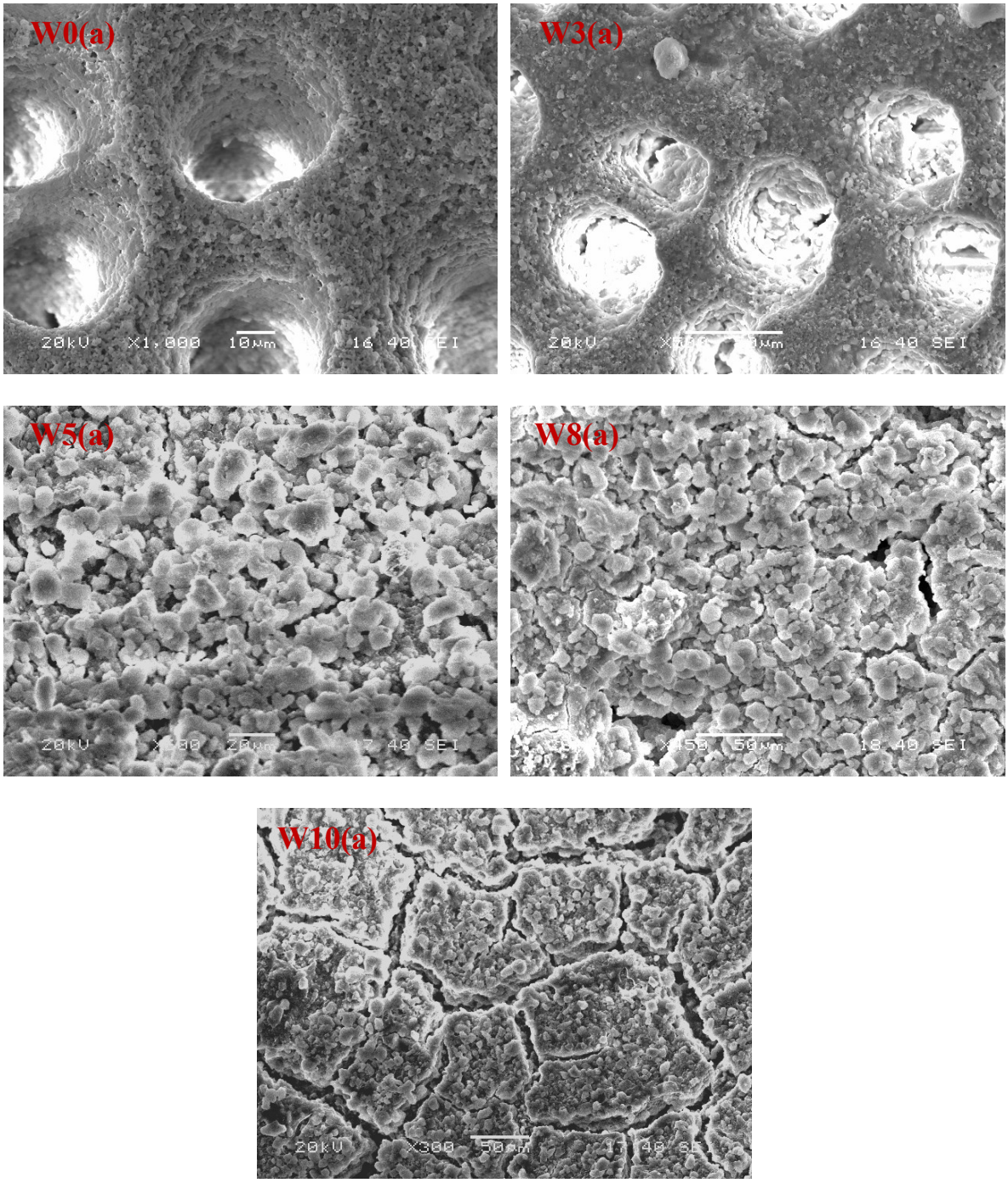

Figure 5.1 SEM inner surface (a) images of ceramic hollow fibre catalytic converter at 0 wt.% (W0), 3 wt.% (W3), 5 wt.% (W5), 8 wt.% (W8) and 10 wt.% (W10) washcoat loadings, respectively

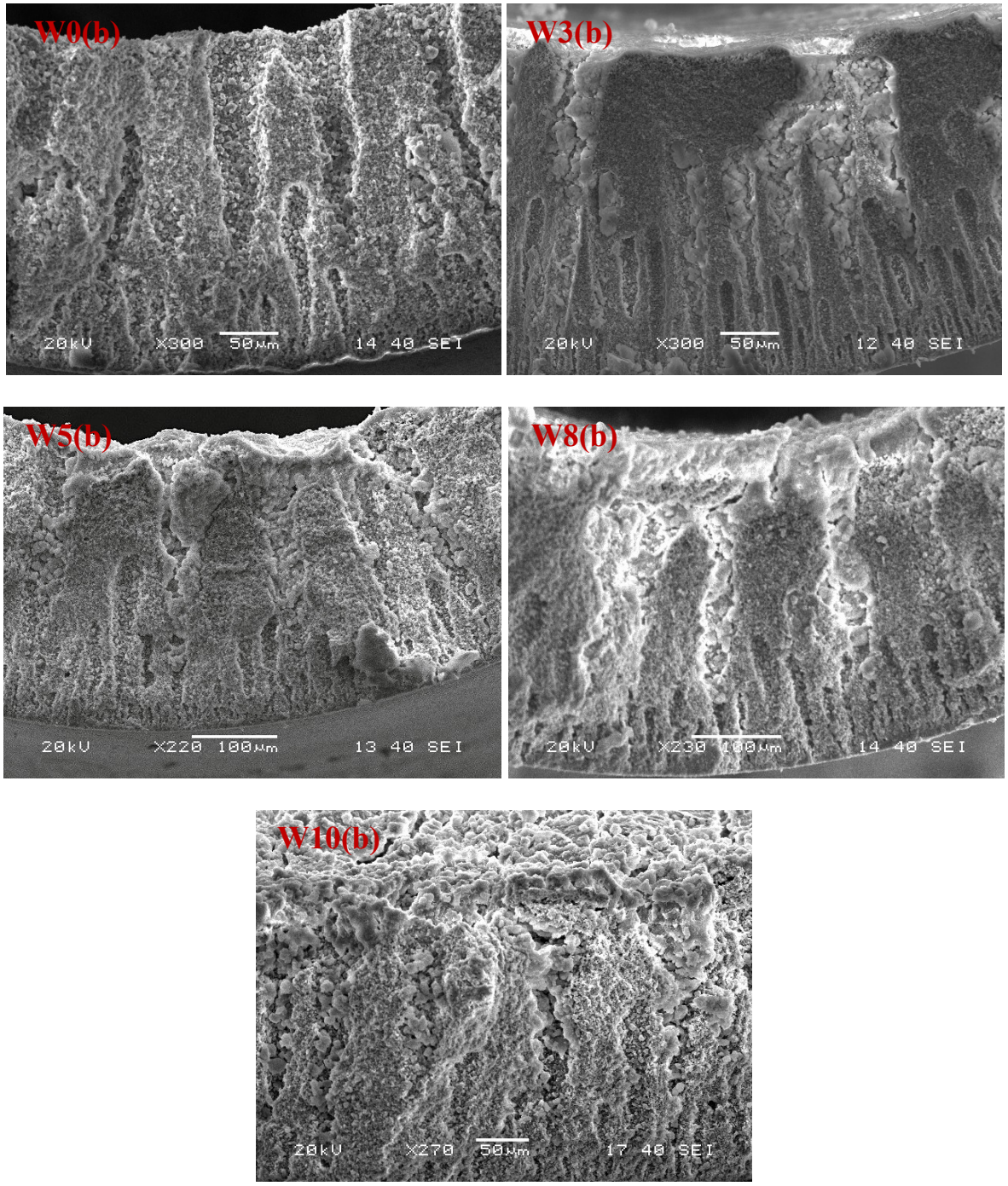

Figure.5.2 SEM cross-section (b) images of ceramic hollow fibre catalytic converter at 0 wt.% (W0), 3 wt.% (W3), 5 wt.% (W5), 8 wt.% (W8) and 10 wt.% (W10) washcoat loadings, respectively

The noble metal distribution, and overall catalytic converter performance is affected by the shape and packing configuration of the washcoat [133]. Hence, a new structure design and the washcoat layer are vital areas of research in the field of catalytic converters. Also, it is known that the washcoat acts as a refractory oxide layer, which can provide a high specific surface area for deposition of active catalyst, and a secondary physical barrier from contamination of masking agents and other undesired reactions [101]. However, the thickness of the washcoated substrate needs to be carefully controlled, especially to limit the intra-phase transport resistance. This is required so that the reactant gases can reach the active sites more efficiently. Thus, it is crucial to find an acceptable trade-off between its role and its performance efficiency. The reported commercial washcoat loadings are at about 10 wt.% or 20 – 60 μm in thickness. But as the hollow fibre has already given an additional surface area, it would be possible to reduce the amount of washcoat required in the system.

Figure 5.1 and Figure 5.2 shows a different loading of γ-Al_2O_3 washcoated into the microchannels of the hollow fibre substrate. Each increase in the content of the washcoat resulted in a different packing distribution. For 3 wt.%, the washcoat is distributed evenly along the channels, allowing the microchannel to remain open for gas to flow. At 5 wt.% loading, the microchannels are filled with γ-Al_2O_3 particles and served as individual packed bed micro-reactors. Further increase in the loading of up to 8 wt.% and 10 wt.% shows a total blockage of the channel openings. The washcoat is tightly packed and starts to accumulate and embed on the inner surface of the hollow fibre. This accumulation of the washcoat on the surface could reduce the gas entrance opening, further making the frontal opening of the hollow fibre smaller than its initial diameter. This could induce an increase in the backpressure to the system.

5.3.2 The Specific Surface Area

The general correlation between catalytic activity and its surface area is greatly studied and understood in the catalytic research field. The reaction will only take place when there is a collision between the gas or liquid particles with the solid particles. Higher surface area increases the chances for reactants to collide, therefore, significantly increasing the rate of reaction and the number of collisions. Thus, providing a large specific surface area for catalyst deposition is of high importance. Table 5.1 shows the specific surface area values with the addition of a washcoat layer at different loadings. It is evident that an increase in loadings leads to a linear improvement of the specific surface area available for impregnation of the catalyst.

Table 5.1 BET surface area with an addition of the washcoat to the hollow fibre at different loadings

Washcoat loading (wt. %)	BET surface area (m^2/g)	BET improvement
Honeycomb monolith (400 cpsi)	0.3	
0	1.75	5.83
3	5.55	18.50
5	7.47	24.90
8	10.66	35.53
10	12.85	42.83

γ-Al_2O_3 is widely used, as a support for catalytic reaction, due to its Lewis acid sites containing fractions of cation vacancies, which can facilitate the electron-deficiency of active components. Thus, this process enhances the activity of noble metals with support [134].

5.3.3 Catalyst Distribution

Catalyst distribution on the washcoat is influenced by a few factors. For monolithic catalysts, where the catalyst content is relatively low per size of reactor volume, obtaining an even distribution of catalyst along the geometric surface of the monolith has become a significant challenge in the industry. Due to the catalyst content over the reactor volume ratio in this system, as compared to the packed bed column, the dispersion and metal loading play a pivotal role in generating highly active sites. Different techniques and metal precursor used will affect the distribution differently, as the process involves an ion exchange process of the metal complex with the support. In the case of palladium impregnated onto the surface of γ-Al_2O_3, the concentration of metal precursors needs to be considered. Such a consideration exists for two different reasons. First, the metal precursor concentration has to be below its supersaturation point. This is important as it prevents premature particles from bulk deposition. Further, the point of zero charge (PZC) of alumina is approximately around 8, the metal solution is most efficient when in the range of $4 < pH < 13$ for a homogeneous distribution [47,90]. In addition, the catalyst's particle size significantly influences its catalytic performance, since the electronic properties and surface structure is dependent on the particle size range [135].

To study the suitability of the impregnation method used, TEM and EDX characterisations were carried out. Figure 5.3 shows the TEM images of palladium catalysts impregnated on the γ-Al_2O_3 washcoat. TEM micrographs provide evidence that the palladium nucleation process has taken place in the desirable condition, with an average of 10 nm particle size produced on the surface of the support. The metal palladium grew into a small particle without any apparent clusters. This evenly distributed particle growth could also be attributed to the properties of γ-Al_2O_3, which can help stabilise the Pd metal and increase the dispersion of the noble metal.

Therefore, improving the catalyst resistance to unwanted side reactions or contamination. These properties are caused by allowing a part of the Pd to exhibit facile redox behaviour at low temperatures [136,137]. A good dispersion of metal catalysts can prolong the active sites activity. Substantial inter-particle distance makes the catalyst less susceptible to thermal sintering, which is caused by agglomeration, as opposed to when the arrangement is in a bulk cluster.

In general, the challenges of the monolithic catalyst impregnation process occurs due to the non-uniform distribution of the active phase. The catalysts were observed and exhibited a tendency to concentrate at the edges of the monolith. Further, these particles grew on the outer surface of the monolithic structure [48]. To ensure that the catalyst is distributed uniformly in the hollow fibre catalytic converter, an EDX analysis was carried out as presented in Figure 5.3**.** As it can be observed, region E is much darker than regions D and F. The darker area could be attributed to the height differences of the sample during analysis. This is confirmed by the EDX analysis. The results illustrate that the corresponding palladium contents' intensity is similar at different location. Pd was found uniformly dispersed in the system with a particle size of around 10 nm.

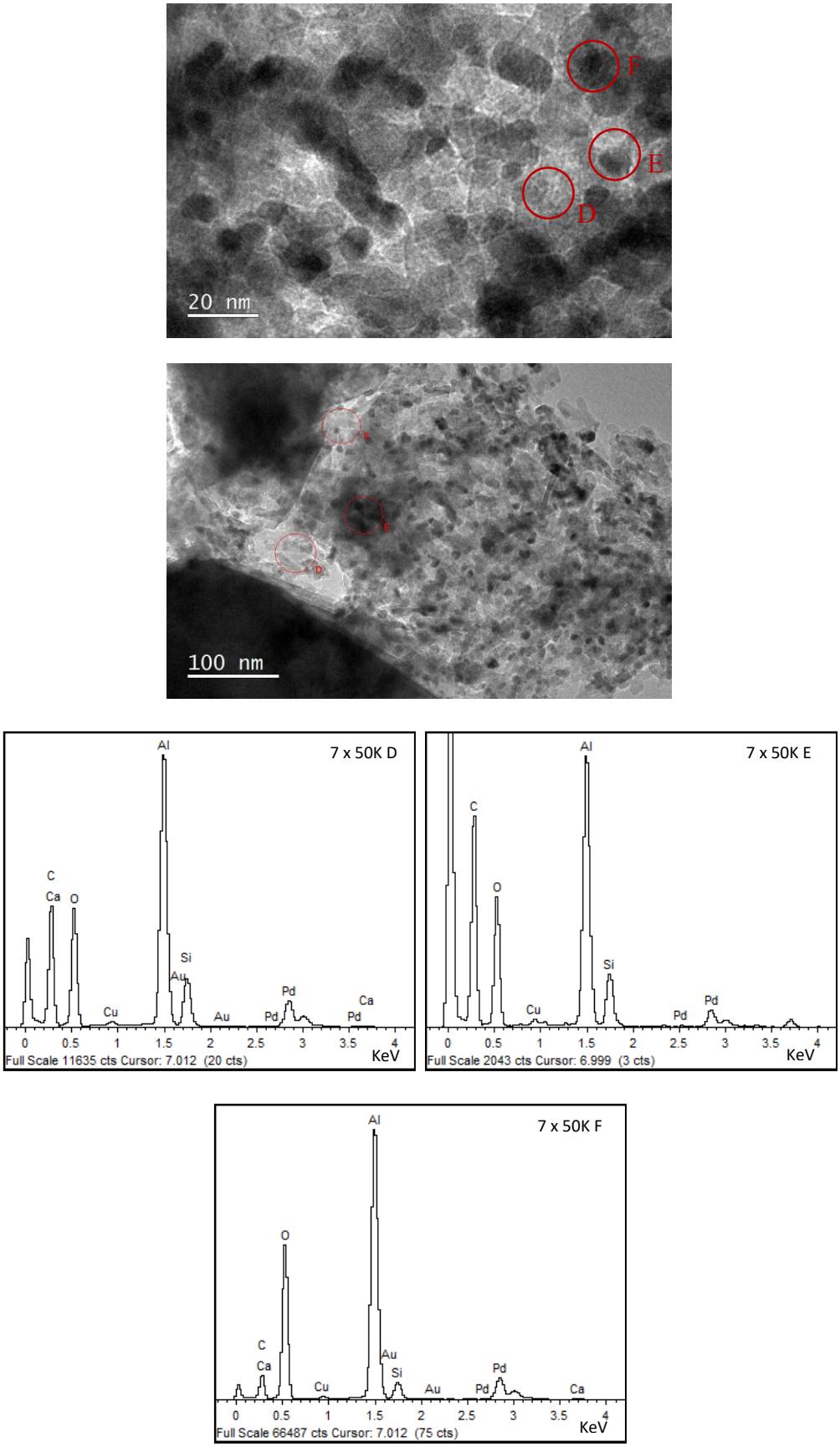

Figure 5.3 TEM images and energy-dispersive X-ray spectroscopy for palladium catalyst distribution on the hollow fibre surface

5.3.4 Catalytic Activity

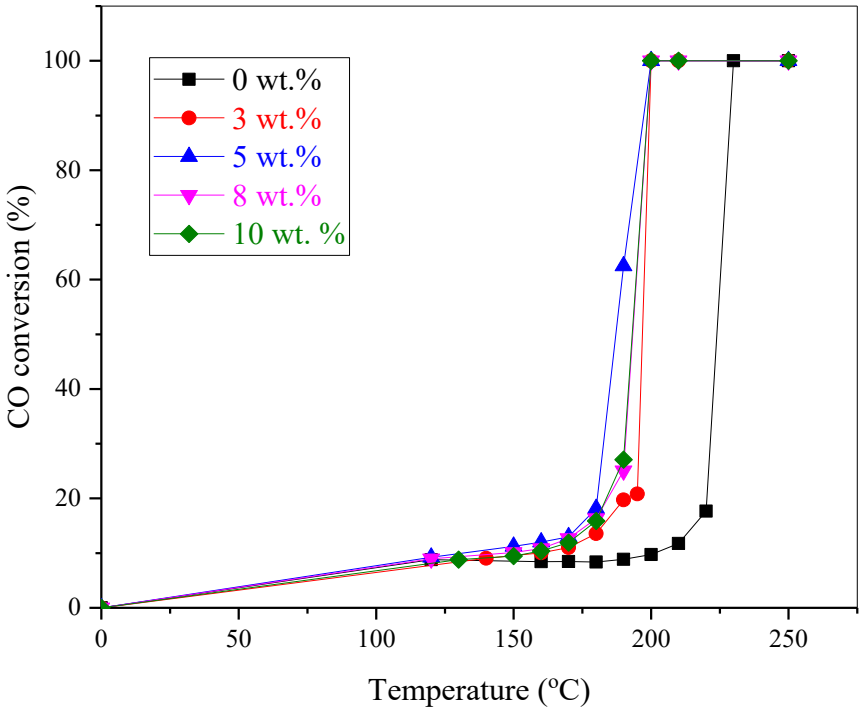

Figure 5.4 CO to CO_2 conversion as a function of temperature at different γ-Al_2O_3 washcoat loadings of 0,3,5,8, and 10 wt.%

Figure 5.4 shows the CO oxidation light-off curves of the ceramic hollow fibre catalytic converter, which are tested at different washcoat loadings. The hollow fibre catalytic converters show an excellent activity for CO oxidation. Full conversion was achieved at a temperature lower than 200°C for all samples loaded with a washcoat layer. In the sample, with the exemption without the washcoat, CO was only fully oxidised at 230°C. With nearly 30 °C observed decrease in the light-off temperature, as compared to the sample without the washcoat, provides evidence of the importance of this secondary refractory layer in assisting with the reaction process. In comparisons with the best palladium-based catalytic converter supported on alumina, for CO oxidation from other studies as shown in Table 5.2, this hollow

fibre performance displays apparent advantages. Further, the reader should consider the high performance of this hollow fibre with a scant amount of catalyst in the system.

Table 5.2 Comparisons of CO oxidation light-off temperature of palladium-based catalysts supported on alumina

Sample	**Testing condition**	**Supported catalyst loadings (mg)**	**Flow rate / GSHV**	**Reported light-off temperature (ºC)**	**Reference**
2.5 wt% Pd/Al_2O_3	Fixed bed	20	76 ml min^{-1}	212 at T50	[136]
2 wt% Pd-Al_2O_3 /CeZr	Fixed bed	150	500 ml min^{-1}	270 at T50	[138]
1 wt.% Pd/Al_2O_3	Monolithic catalyst	3000	150,000 h^{-1}	216 at T50	[139]
0.7 g/L Pd/Al_2O_3	Monolithic catalyst	1300	98,000 h^{-1}	336 at T50	[140]
1.0 wt.% Pd/Al_2O_3	Monolithic catalyst	2000	30,000 h^{-1}	410 at T90	[141]
2 wt.% Pd/Al_2O_3	Fixed bed	50.0	200 ml min^{-1}	153 at T50	[142]
1.0 wt.% Pd/0 Al_2O_3	Monolithic catalyst	2.0	100 ml min^{-1} / 59, 000 h^{-1}	224 at T50	This study

1.0 wt.% Pd/3 Al_2O_3	Monolithic catalyst	8.1	100 ml min^{-1} / 59, 000 h^{-1}	195 at T50	This study
1.0 wt.% Pd/5 Al_2O_3	Monolithic catalyst	12.1	100 ml min^{-1} / 59, 000 h^{-1}	187 at T50	This study
8 wt.% Pd/8 Al_2O_3	Monolithic catalyst	18.2	100 ml min^{-1} / 59, 000 h^{-1}	193 at T50	This study
10 wt.% Pd/10 Al_2O_3	Monolithic catalyst	22.2	100 ml min^{-1} / 59, 000 h^{-1}	193 at T50	This study

T50 = at 50ºC temperature

T90 = at 90ºC temperature

The ratio of catalyst to the support consisted of the hollow fibre, while the washcoat remained constant at 1 wt.% for all samples. This means that higher washcoat loading should contain more catalyst and higher active metals in general. Shown in Figure 5.5, the catalyst deposited on the surface is visually darker, and visible at greater γ-Al_2O_3 content. However, surprisingly the conversion rate agrees with the concept of higher catalyst content, better performance, only up to the 5 wt.% of washcoat. Beyond the 5 wt.% loading, the conversion light-off temperature decreases 5ºC from the optimum light-off temperature of 187ºC. Further, the loading increments did not contribute towards any significant improvements in performance.

The scenario could be explained by the involvement of mass transfer and diffusion resistance in the hollow fibre. This correlates to the washcoat packing effects. Greater washcoat loading would induce a higher resistance for reactants to reach the active sites. Thus, designing a washcoat of optimum thickness is necessary.

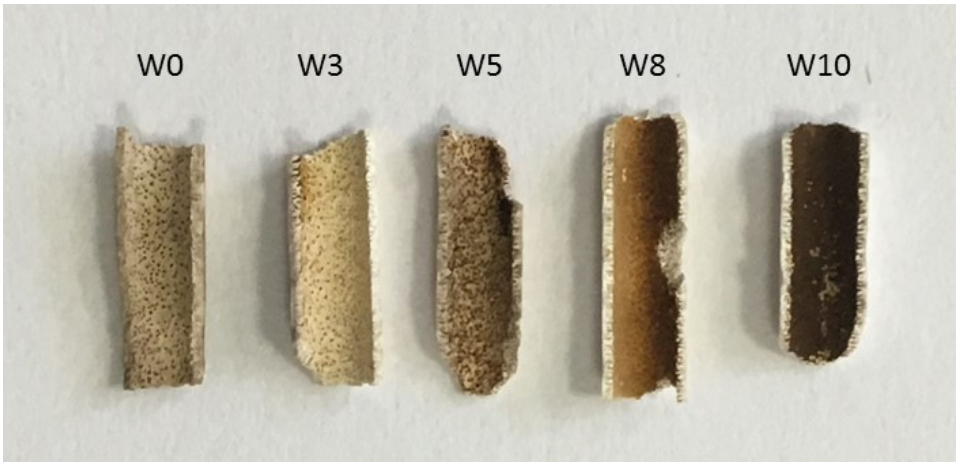

Figure 5.5 Hollow fibre catalytic converter cross-section at different washcoat loadings W = 0, 3, 5 ,8 and 10 wt.%

5.3.5 Effects of Varying Washcoat Packing on Gas Transport

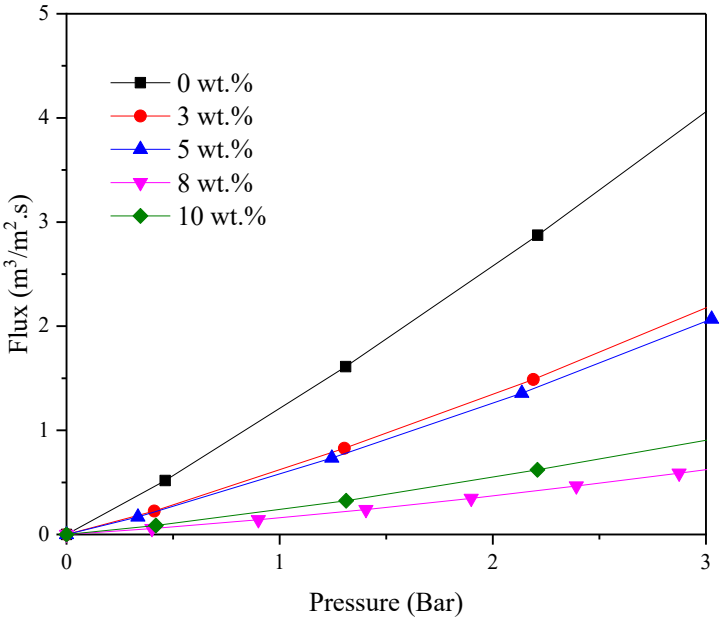

Figure 5.6 N_2 permeation flux of the ceramic hollow fibre catalytic converter at different washcoat loadings

Further, an N_2 permeation test was carried out to study the transport of gas flow inside the hollow fibre. It can be observed in Figure 5.6 that the highest flux was achieved in the sample without any washcoat. Increased washcoat loadings resulted in a reduction in the gas permeation flux through the hollow fibre. This primarily occurred due to resistance to mass transfer, which was caused by the washcoat layer's blocking effects. But at 10 wt.% loading, a slight increase in flux was noticed. This increment can be explained by the packings conditions. As shown in Figure 5.1, W8(a) and W10(a), the 8 wt.% particles are tightly packed with a minor observable crack on the surface. In the case of the 10 wt.%, the cracks are evident everywhere, which gives an additional advantage for the gas to permeate through the defects. Therefore, a higher flux is gained.

For 3 wt.% and 5 wt.% there is no significant reduction in the permeation rate. Loosely packed particles in the microchannels did not show evidence of distinguishable hindrance effects on the gas transport in the hollow fibre, when compared to the coat on the surface washcoat layer. In this case, a better performance of the CO catalytic oxidation could be induced by the higher active sites and a larger specific surface area available. At 8 wt.% and 10 wt.% loading, the thickness of the washcoat and the smaller interparticle gaps may exhibit additional resistance to the transport and diffusivity of the reactants.

The monolithic catalyst is notorious for its complexity, primarily due to the catalytic performance that heavily relies on factors other than the number of active sites. Gas phase convective, diffusivity of the mass, energy, and momentum take place in radial and axial directions, which produces a unique mechanism that is exclusive to its particular design [88]. Therefore, further studies are essential to understand the transport mechanism and feasibility of making practical commercial hollow fibre catalytic converters.

5.4 Conclusion

The new porous hollow fibre monolith design proposed in this chapter replaces the honeycomb structure fabricated in a single extrusion process. Assisted by the induced phase inversion process, the new hollow fibre possessed high-density self-organised microchannels. At 0.7 wt.% of a palladium catalyst, the hollow fibre catalytic converter light-off temperature was attained at a temperature under 200ºC for all tested samples, at different washcoat loadings. The observations found the best result at 187ºC with 5 wt.% of γ-Al_2O_3. Different washcoat content in the system produced different packing conditions, which affect the diffusivity of the gas transported. The loosely packed washcoat in the microchannels offers the best packing configuration for consideration in further research. This study takes into account the beneficial features of the new design, which requires a very low PGM content in the system. The experiment proves that the hollow fibre catalytic converter can be a potential alternative, and an innovative monolith, for the device. Future work should focus on exploring the catalytic activity through a three-way catalytic converter, with the possibility of further reducing reliance on PGM catalysts. This would also require a study on the long-term performance of the ageing catalyst.

Chapter 6

Integrating Pd-Doped Perovskite Catalysts with Ceramic Hollow Fibre Substrate for Efficient CO Oxidation

This chapter discusses the palladium doped perovskite synthesis process, its structural evaluation, and the packing effects on CO oxidation activity. The work has been submitted for publication in the Journal of Environmental Chemical Engineering.

Abstract

Two perovskite catalysts, i.e. $LaFe_{0.7}Mn_{0.225}Pd_{0.075}O_3$ (LFMPO) and $LaFe_{0.7}Co_{0.225}Pd_{0.075}O_3$ (LFCPO), were synthesised, characterized and evaluated in this study for CO oxidation. Doping Palladium (Pd) reduces light-off temperatures of perovskite catalysts, and improves the thermal-chemical stability of catalysts due to less sintering problems. This also reduces the catalyst cost by decreasing the use of PGMs and extends the life of catalytic converters. Light-off temperatures of CO oxidation are used to investigate the advantages of incorporating the perovskite catalysts inside a micro-structured ceramic hollow fibre support, which is further compared with a packed bed configuration. Evaluations suggest that LFMPO deposited inside

the hollow fibre substrate could be light up at a temperature of 232 ºC, which is 10 ºC lower than that of a packed-bed counterpart with the same amount of catalyst (5 mg) and GHSV of ~ 5300 h^{-1}. Excessive incorporation of catalyst (10 mg) generates significantly higher transfer resistance, which in turn impairs the efficiency of a hollow fibre reactor, with CO conversion per gram of catalyst reduced from 0.01 mole g^{-1} to 0.0051 mole g^{-1}.

6.1 Introduction

Incomplete combustion in the internal combustion engine leads to the release of noxious gases, such as carbon monoxide (CO), nitrogen oxides (NOx), and hydrocarbons (HCs), which need to be treated before being exposed to the environment. These emissions should comply with the regulatory standards established. To ensure compliance, exhaust systems are equipped with catalytic converters. The technology concerning catalytic converters requires continuous research and development, considering the rapid advancement in emissions regulations and standards. Present generation catalytic converters are manufactured using three essential components. These components are the monolithic substrate, a high surface area washcoat, and an active metal, conventionally the Platinum Group Metals (PGM) catalyst. However, PGM price volatility and their scarcity is seen as the biggest challenge in the long term. Plus, the issue of the washcoat and PGM thermal stability have triggered various attempts to reduce the dependability on the PGM and to formulate a high thermal resistance supported PGM catalyst in three-way catalytic applications.

In a previous study, we introduced a new ceramic hollow fibre catalytic converter design. The new design offers a greater surface area for deposition of the active catalyst. Further, palladium

supported on γ-Al_2O_3 washcoat was used on the sample catalyst and studied for potential improvements for the new design [128]. The new substrate provides a huge geometric surface area (GSA) approaching 900 cells per inch square (CPSI) of the conventional honeycomb monolith without drawbacks of further pressure drop in the system. The high GSA substrate could enable a compact design of catalytic converter, and positioning of the device closer to engine manifold to utilise the heat from internal combustion which is needed for catalyst activation. This could shorten the time taken for catalyst light-off during the cold-start. However, exhaust gases in gasoline combustion engines can reach up to 1000 ºC, and the operating temperature window would induce sintering effects on the conventional oxide washcoat, γ-Al_2O_3 [97]. Due to phase transformation (i.e. from γ-Al_2O_3 to α-Al_2O_3), over a period of time, the washcoat layer used to increase surface area for deposition of the metal catalyst loses its properties. If such is the case, a better composition of washcoat and catalyst material is essential so that the catalyst could retain their performance at high internal combustion engine temperature, to increase the average lifespan.

Perovskite's attractive characteristics such of their flexibility, adaptability, thermal stability, abundant availability and most importantly, their low cost have attracted attention towards using this type of material for numerous applications [54,55]. There is evidence in the literature concerning the high thermal stability of perovskite oxide with an ABO_3 stoichiometry as a three-way catalyst [60,143–145]. It is seen as a better alternative that would scale down reliance upon the precious group metal (PGM) catalysts in the converters [146,147]. The attributes of perovskite that can be tailored for different applications make the material a widely researched catalyst. The flexibility of perovskite allows A-site and B-site substitutions allowing for several applications. The A-site cation is usually occupied by larger rare earth metals (La, Nd, Yb), while the B-site cations is occupied by smaller transition metals. Furthermore, research has

provided evidence that the B-site cation has a greater effect on the properties of the catalyst than the A-site cation [57,58]. Therefore, while tailoring specific characteristics of the perovskite, the selection of materials for the B-site is important.

Despite the aforementioned advantages of perovskite catalysts, their specific surface area is much smaller than the conventional PGM supported on secondary oxide washcoat layer, which challenges their application since a large amount of such catalyst has to be used. Here, the use of hollow fibre as support for perovskite catalysts could enables more significant utilisation of catalyst, which will address the limited specific surface area of the perovskite. By using this technology, two issues could be addressed; i) the limited surface area of perovskites by using the hollow fibre microreactor, and ii) the ageing problem of PGM supported on washcoat via more stable perovskites. Thus, a more durable catalytic converter based on perovskites is possible for future operation.

Till date, out of the many options of transition-based metal perovskites, Lanthanum based perovskites have been shown to produce the highest reactivity for an oxidation process, when coupled with Co, Mn, Fe, Cr or Ni in their B sites [68]. From that, in this study, two different types of perovskite, $LaFe_{0.7}Mn_{0.225}Pd_{0.075}O_3$ (LFMPO) and $LaFe_{0.7}Co_{0.225}Pd_{0.075}O_3$ (LFCPO) were synthesised using the citrate sol-gel method. The catalytic process can be altered by modifying the interactions between the B-site species and the oxygenated species in the perovskite lattice. Substitution of the B-site with a different material changes the oxidation state and generates an oxygen vacancy in the lattice, where it is beneficial to provide vacancy for the adsorption and activation of the reactant species [60,146]. On the other hand, the high thermal stability of lanthanum-based perovskite as has been demonstrated by previous research is attractive for catalytic converter application. This study presents research, conducted for the

first time, which incorporates perovskite catalyst without any washcoat layer, into a hollow fibre substrate for catalytic converters application. A traditional packed bed reactor was tested in this study, which is further used for comparison with hollow fibre reactors using the same perovskite catalysts. The effects of catalyst packing and their reaction to CO oxidation were evaluated and discussed as a sample reaction.

6.2 Experimental

Experimental procedures for this study are as described in Chapter 3, subsection 3.1.3 and 3.3.2 for catalyst preparation, washcoating procedure in 3.4.2, while 3.5.1, 3.5.3, 3.5.4 and 3.5.5 for characterisations and 3.6.2 for performance evaluation through CO oxidation reaction.

6.3 Results and Discussion

6.3.1 Phase Composition of Perovskite Catalysts

Figure 6.1 shows the XRD pattern of the LFMPO and LFCPO, which were calcined at 700ºC for four hours and have an orthorhombic crystal structure. The XRD patterns also indicate that calcination temperature of 700ºC can enable good transformation of the synthesised perovskites [148]. Further reducing calcination temperature to 660 ºC will yield significant oxide phases for perovskites with Pd doping [149], which will impair catalytic performance as a consequence.

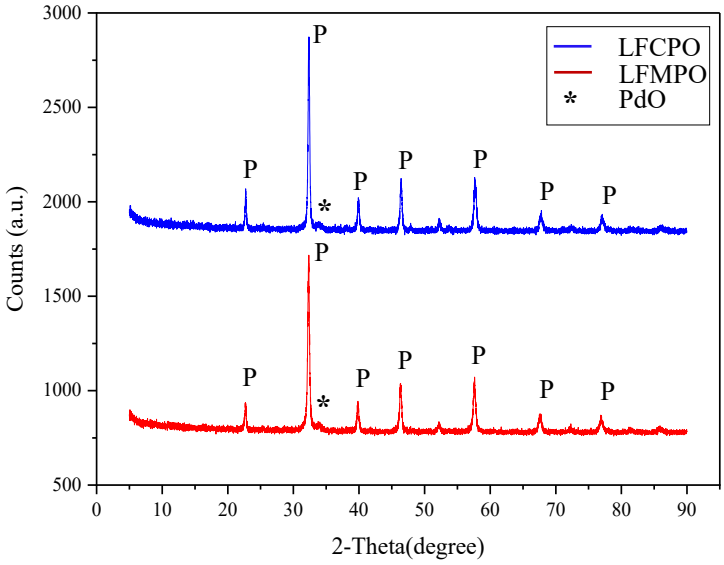

Figure 6.1 XRD diagram of $LaFe_{0.7}Mn_{0.225}Pd_{0.075}O_3$ and $LaFe_{0.7}Co_{0.225}Pd_{0.075}O_3$ calcined at 700ºC for four hours

The XRD patterns in Figure 6.1 indicate that there is a small peak at the 2θ value of 33°, which is next to the main perovskite peak of LFMPO and LFCPO. This small peak indicates the presence of PdO [150], as a result of incomplete integration of Pd into perovskite oxides. If a calcination temperature higher than 700 °C was used, a full integration of Pd is possible [150]. However, it should be noted that full integration of Pd into perovskite lattices may retard catalytic performance, compared to Pd supported on perovskites which is more active due to easier interactions with reactants [53]. On the other hand, Pd integrated into perovskite is thermally more stable and has less sintering problems, which will enable longer catalyst life span.

As a common washcoat material with high a surface area, γ-Al_2O_3 is well-known for its microstructural evolution when exposed to high temperatures. This is due to the transition of the phase from γ to the metastable δ-θ and finally the thermodynamically stable α phase, which results in the densification of the washcoat layers, leading to a reduction in specific surface area and consequently deteriorating catalytic performance. As shown in Table 6.1, the Pd supported on γ-Al_2O_3, which was prepared at 500 °C, has a reduction of 12.3 % in specific surface area after being treated at 700 °C. In contrast, perovskite catalysts with fully developed phase structure (Figure 6.1) have no such problems. But due to the low specific surface area (Table 6.1) and potential reactions between perovskites and γ-Al_2O_3 that impairs catalytic performance [147,151], the perovskite catalysts free from washcoat layer were deposited inside hollow fibre substrates with a unique bi-modal pore structure in this study.

Table 6.1 Structural and chemical properties of the synthesised catalysts

Sample	S_{BET} (m^2g^{-1})	Average Crystallite Size (nm)	XRD Crystal Structure
$LaFe_{0.7}Mn_{0.225}Pd_{0.075}O_3$	20.69 ± 0.09	24.01	Orthorhombic
$LaFe_{0.7}Co_{0.225}Pd_{0.075}O_3$	10.73 ± 0.05	27.88	Orthorhombic
Alumina Hollow Fibre Substrate	1.42 ± 0.01	-	-
5mg 0.075 Pd/Al supported on hollow fibre, Calcination at 500 ºC	4.55 ± 0.01	-	-
5mg 0.075 Pd/Al supported on hollow fibre, Calcination at 700 ºC	3.99 ± 0.01	-	-

6.3.2 Micro-structure of Perovskite / Hollow Fibre Substrate

Figure 6.2 (a) presents a cross-section of the hollow fibre substrate with a bi-modal pore structure [125], which consists of packed-pores of approximately 40 μm and many oriented microchannels for which perovskite catalysts were deposited. LFMPO (Figure 6.2 (b)) and LFCPO (Figure 6.2 (c)) catalysts were deposited on the microchannels and show an average particle size of approximately 5 μm, which is much larger than the α-alumina used for preparing hollow fibre substrates.

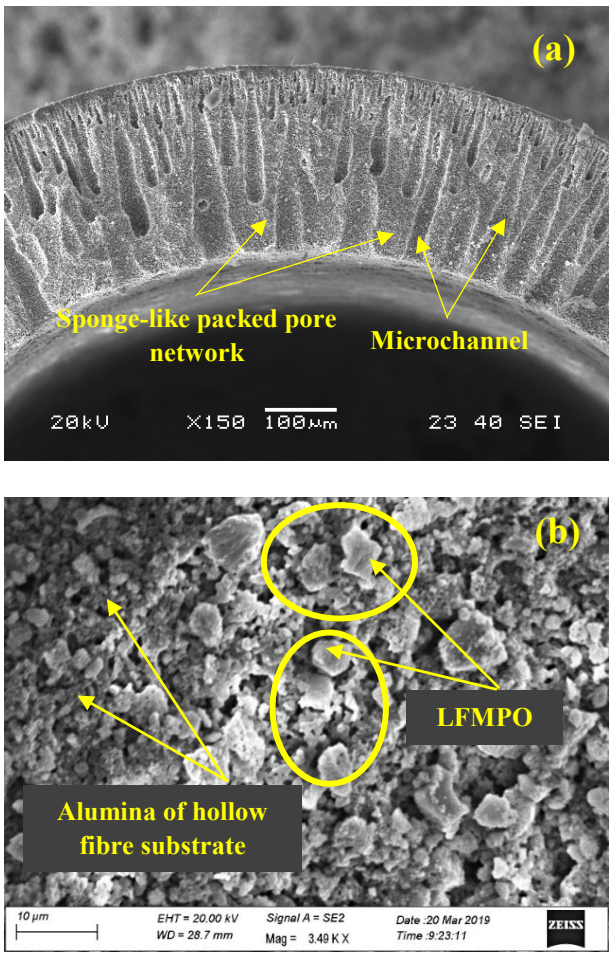

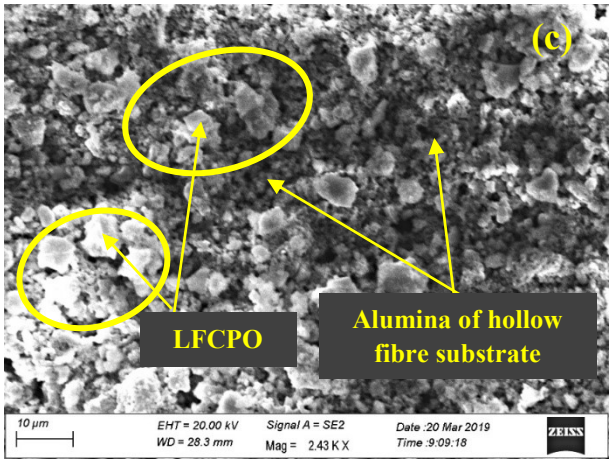

Figure 6.2 SEM images of a) cross-section of hollow fibre substrate, b) $LaFe_{0.7}Mn_{0.225}Pd_{0.075}O_3$ and c) $LaFe_{0.7}Co_{0.225}Pd_{0.075}O_3$ catalyst deposited inside hollow fibre substrate

Morphologies of hollow fibre substrates deposited with 5 ± 0.5 mg of perovskite catalysts are displayed in Figure 6.3. As seen in a(i) and a(ii), hollow fibre substrates have open microchannel ends at the inner surface of approximately 40 µm in diameter. Substrates of this type could provide a GSA value of approximately 40.7 cm^2cm^{-3}, which is the same as that of a conventional monolith of 750 CPSI (GSA of 40.2 cm^2cm^{-3}) [128]. Deposition of 5 ± 0.5 mg of perovskite catalysts maintains good microchannel opens at both the inner surface and cross-section, as shown in Figure 6.4 (b(i), b(ii), c(i) and c(ii)), by forming a thin catalyst layer along the surface of the microchannels. This is critical to the efficient interaction between the gaseous reactants and catalysts deposited inside the hollow fibre substrate [104].

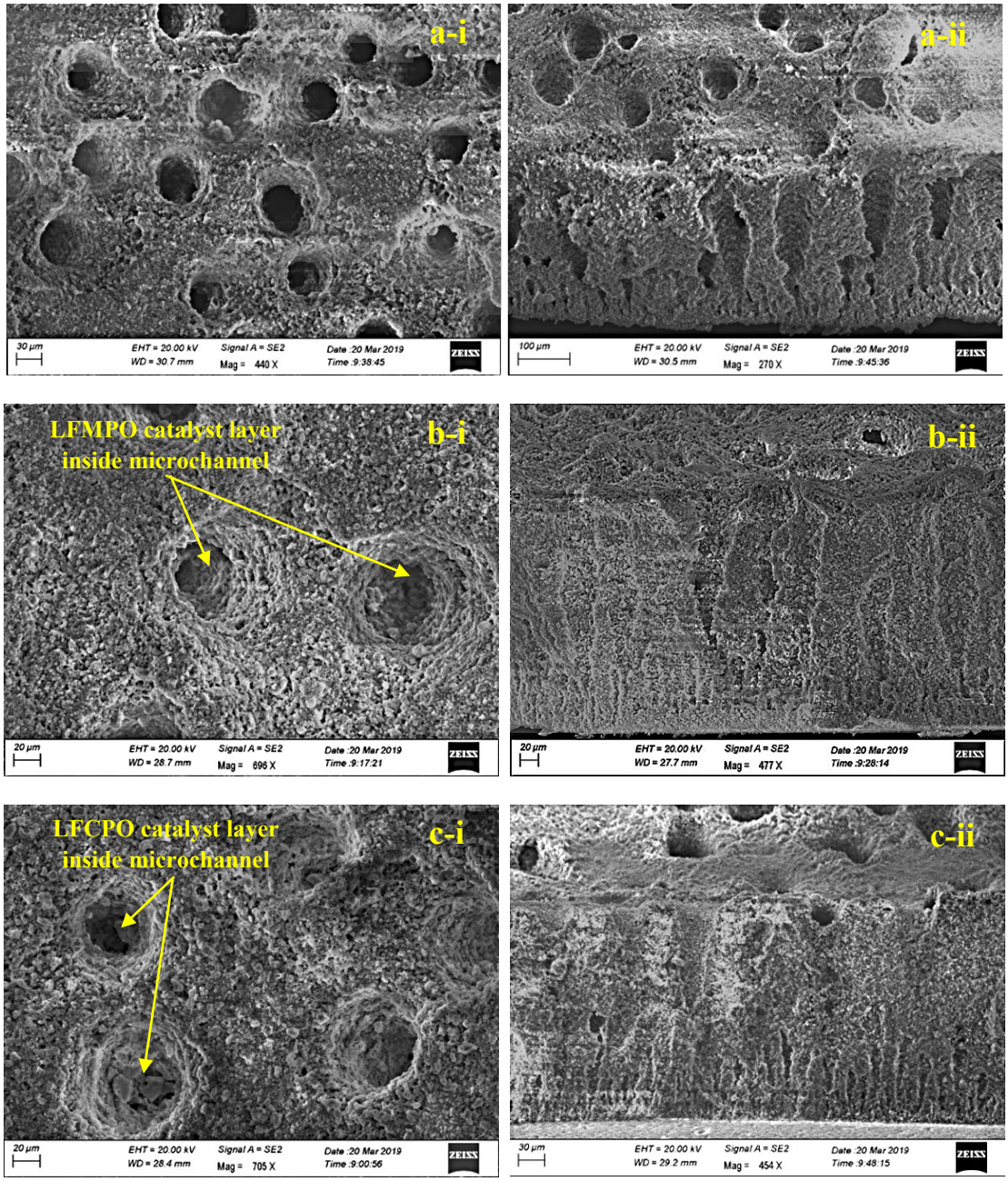

Figure 6.3 SEM images of (a) substrate without catalyst; (b) substrate with 5mg LFMPO catalyst; (c) substrate with 5mg of LFCPO catalyst. (i) top-view of substrate inner surface and (ii) side-view of substrate cross-section

By increasing the amount of perovskite catalysts to approximately 10 mg, catalyst particles start to form mini-packed-beds inside the microchannel of hollow fibre substrates. As can be seen in Figure 6.4, approximately 50% of the microchannel volume is filled by the LFMPO

catalyst, with the microchannel endings at the substrate inner surface remained open (a(i) and a(ii)). In contrast, the microchannel is largely filled with the LFCPO catalyst, which also blocks microchannel endings at the inner surface of the substrate (b(i) and b(ii)). An increasing amount of perovskite catalyst inside the hollow fibre substrates provides more active sites for the catalytic reaction to proceed, which benefits the conversion of CO in this study. Meanwhile, the formation of mini-packed-beds (Figure 6.4) indicates a higher transfer resistance compared to the catalyst layer in Figure 6.3, which retards the access of CO to the active sites of perovskite catalyst and consequently reduces efficiency of the reaction.

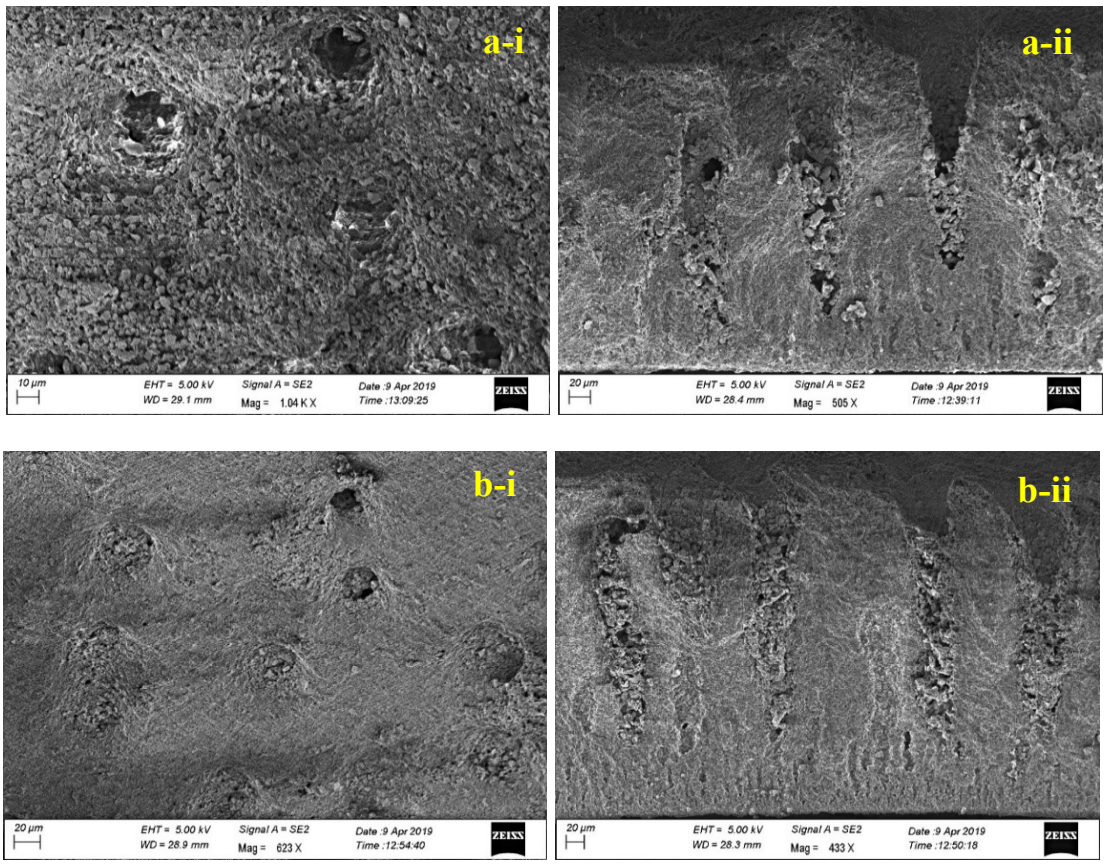

Figure 6.4 SEM images of (a) substrate with 10mg LFMPO catalyst; (b) substrate with 10mg of LFCPO catalyst. (i) top-view of substrate inner surface and (ii) side-view of substrate cross-section

The difference in the packing condition for all catalysts could be attributed to the difference in their crystal size. The LFMPO is 3.87 nm smaller than the LFCPO. Even though the difference in particle size in Figure 6.2 is not obviously visible, a smaller crystal would result in a more tightly packed agglomeration. With these values, the LFMPO could be packed in a denser packing thus creating many free spaces in the microchannel. On the contrary, the bigger LFCPO particles would occupy larger volume in the microchannel.

6.3.3 Evaluation of Catalytic Performance – CO Oxidation

Two reactor configurations were employed in this study (Figure 3.5) to investigate the catalytic performance of perovskite catalysts, which include a conventional packed-bed reactor as the benchmark of catalyst performance, and a second hollow fibre reactor which can potentially be developed into a new generation of catalytic converter for automotive emissions control, due to its structural advantages over ceramic monoliths reported in Chapter 4 [128].

6.3.3.1 Packed-bed Reactor

A packed-bed configuration is commonly used for investigating catalyst performance, due to an irregular flow through the voids of packing, where it creates a turbulent mixing at Reynolds numbers lower than conservative domains. This enhances the fluid transport through the braiding effect and increases contact with the catalyst through enhanced diffusion [152]. For the packed bed reactor in this study, 5 mg or 10 mg of perovskite catalysts were mixed with 200 mg of α-Al_2O_3 and packed inside a quartz tube reactor. Figure 6.5 presents the CO conversion as a function of operating temperatures, with the corresponding values of T_{50} (the light-off temperature at 50% of CO conversion) listed in Table 6.2. As can be seen, LFMPO shows a conversion of CO higher than LFCPO at temperatures over 200 ^oC, which is in line with the higher surface area of LFMPO (Table 6.1). In addition, since the catalytic process can be altered by modifying the interactions between the B-site species and the oxygenated species in the perovskite lattice, the change in oxygen vacancy concentration alters the catalytic activity. From a material point of view, Mn has a higher number of oxidation states than Co. This contributes to a higher synergistic activity brought by Mn substitution. By doubling the amount of catalyst inside the packed-bed reactor, T_{50} of LFMPO reduces from 242 ^oC to 213 ^oC, with LFCPO reduced from 252 ^oC to 235 ^oC (Table 6.2).

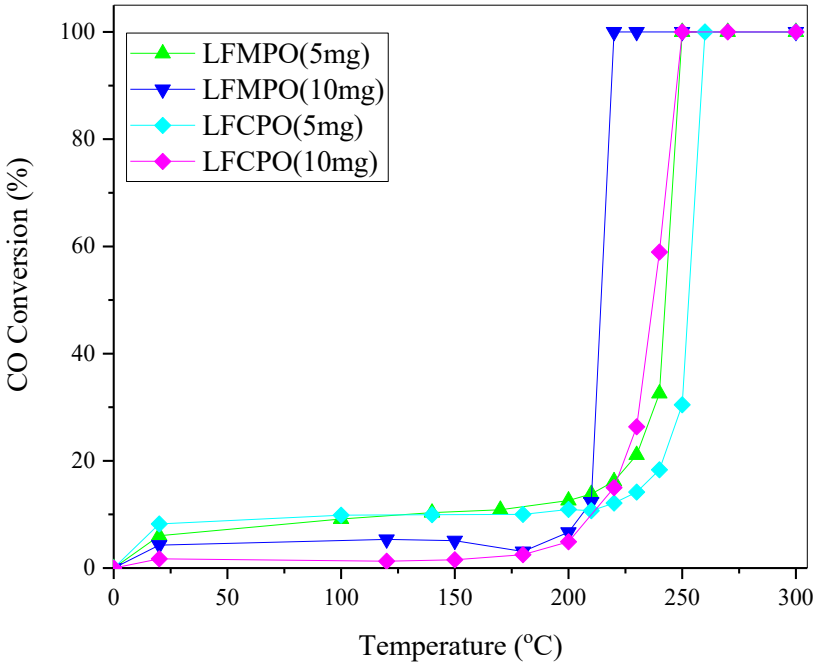

Figure 6.5 Light-off temperature of CO oxidation for packed bed reactors

Table 6.2 Light-off temperatures of CO oxidation for packed-bed reactors

Catalyst	**Condition**	**T_{50} (°C)**
$LaFe_{0.7}Mn_{0.225}Pd_{0.075}O_3$	5 mg	242 ± 2
$LaFe_{0.7}Mn_{0.225}Pd_{0.075}O_3$	10 mg	213 ± 2
$LaFe_{0.7}Co_{0.225}Pd_{0.075}O_3$	5 mg	252 ± 2
$LaFe_{0.7}Co_{0.225}Pd_{0.075}O_3$	10 mg	235 ± 2

6.3.3.2 Packed-bed Reactor vs Hollow Fibre Reactor

For hollow fibre reactors, the CO oxidation reaction was performed by maintaining the same conditions as the packed bed reactors, in terms of the amount of perovskite catalyst and the space velocity (GHSV of ~ 5300 h^{-1}). For hollow fibre reactors with 5 mg of perovskite catalysts (Figure 6.6 and Table 6.3), LFMPO shows better conversion of CO than LFCPO, which is in line with packed bed reactor (Figure 6.5). Moreover, the hollow fibre reactor shows a light-off temperature lower than that of its packed bed counterpart. For instance, the light-off temperature of LFMPO shifted from 242^{o}C in packed-bed to 232^{o}C in the hollow fibre reactor (Table 6.3).

In contrast to a packed-bed reactor, in which reactants "flow-through" the porous bed, a hollow fibre reactor has a very different flow pattern. Instead of "flowing-through", bulk phase of reactants flow along the length direction of the hollow fibre substrate, relying on a much slower diffusion process in the radial direction for accessing the catalyst deposited. As a result, the reduction in light-off temperature is mainly due to the structural advantages of hollow fibre substrates, together with the formation of a thin catalyst layer along the microchannels inside the substrate (Figure 6.3). This enables better and more uniform access of reactants to the perovskite catalysts deposited, with less transfer resistance and as established in the previous studies in Chapter 5 [128].

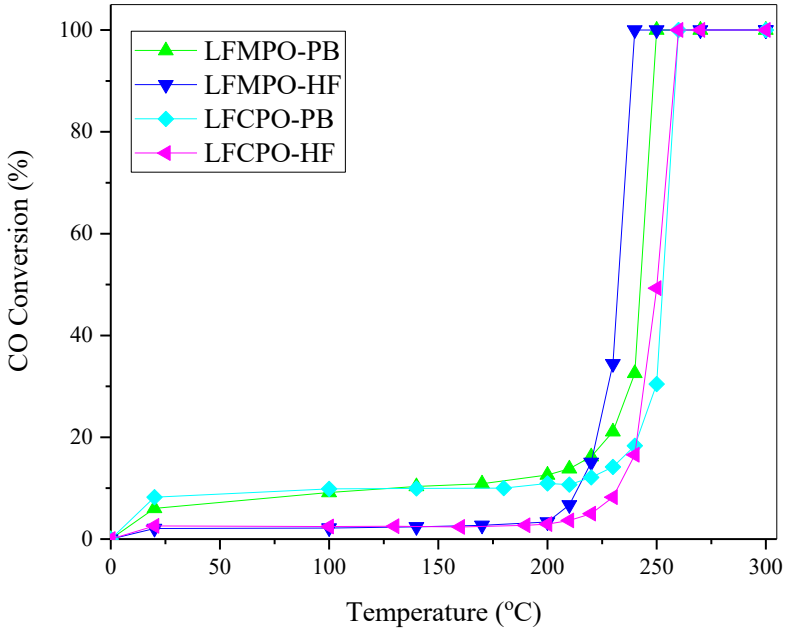

Figure 6.6 Light-off temperature of CO oxidation for packed-bed (5mg of catalyst mixed with 200mg of α-alumina) and hollow fibre reactor (5mg of catalyst washcoated in 50mm of hollow fibre)

Table 6.3 Light-off temperature of CO oxidation for packed-bed (5mg of catalyst mixed with 200mg of α-alumina) and hollow fibre reactor (5mg of catalyst deposited in 50mm of hollow fibre)

Catalyst	**Condition**	**T_{50} (°C)**
$LaFe_{0.7}Mn_{0.225}Pd_{0.075}O_3$	Packed-bed	242 ± 2
$LaFe_{0.7}Mn_{0.225}Pd_{0.075}O_3$	Hollow Fibre	232 ± 2
$LaFe_{0.7}Co_{0.225}Pd_{0.075}O_3$	Packed-bed	252 ± 2
$LaFe_{0.7}Co_{0.225}Pd_{0.075}O_3$	Hollow Fibre	248 ± 2

By increasing the amount of catalyst to 10 mg, mini-packed-beds are formed inside the microchannel (Figure 6.4), it is interesting to see that hollow fibre reactors performed worse than packed bed counterparts (Figure 6.7 and Table 6.4). With the same amount of catalysts involved, light-off temperatures increases from 215°C in packed-bed to 222°C in hollow fibre reactor for LFMPO, with the one for LFCPO increased from 237°C to 245°C (Table 6.4).

By comparing CO oxidation results in Figures 6.5-6.7, it is quite obvious that, the formation of mini-packed-bed inside the microchannel significantly increases diffusion resistance in the radial direction of hollow fibre substrates, which reduces the efficiency of catalyst utilization and consequently increases the light-off temperature.

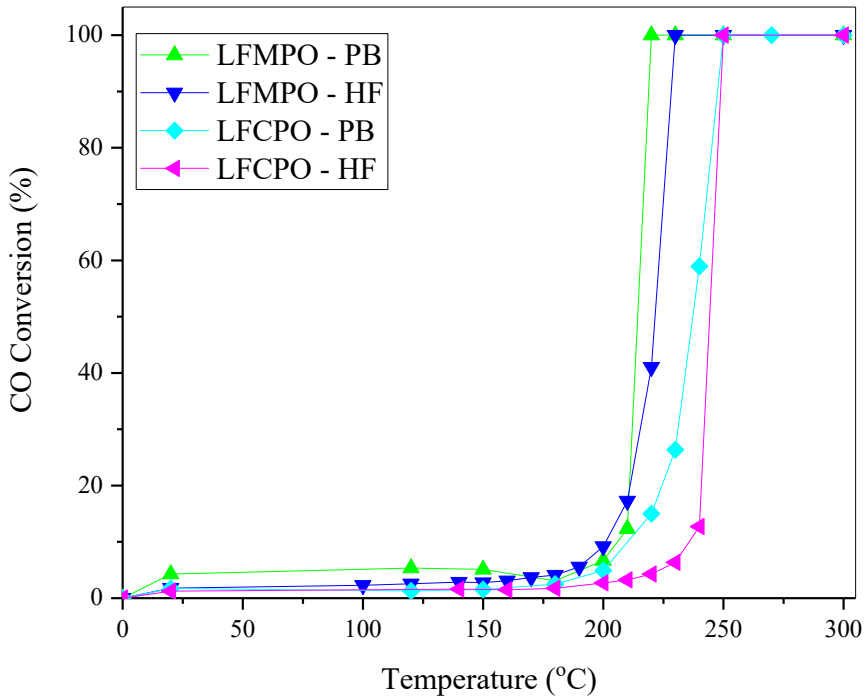

Figure 6.7 Light-off temperature of CO oxidation for packed-bed (10mg of catalyst supported on 200mg of α-alumina) and hollow fibre (10mg washcoated on 50mm of hollow fibre)

Table 6.4 Light-off temperature of CO oxidation for packed bed (10mg of catalyst mixed with 200mg of α-alumina) and hollow fibre reactor (10 mg of catalyst deposited in 50mm hollow fibre substrate)

Catalyst	Condition	T_{50} (°C)
$LaFe_{0.7}Mn_{0.225}Pd_{0.075}O_3$	Packed-bed	215 ± 2
$LaFe_{0.7}Mn_{0.225}Pd_{0.075}O_3$	Hollow Fibre	222 ± 2
$LaFe_{0.7}Co_{0.225}Pd_{0.075}O_3$	Packed-bed	237 ± 2
$LaFe_{0.7}Co_{0.225}Pd_{0.075}O_3$	Hollow Fibre	245 ± 2

The surface reaction adsorption and desorption of CO oxidation are so rapid that the overall rate of reaction is limited by the rate of reactants transfer from the bulk gas to the catalyst surface. As the velocity during the reaction test was low, the reaction fell into the diffusion limited region. In this region, the boundary layer thickness on the catalyst surface was large. Thus, having a denser packing will accentuate the mass transfer resistance. After the catalyst was packed into the micro-channels, the movement of the gas was no longer following the axial direction only, but additional flow in radial direction should be expected. This could add flow resistance caused by the momentum of the changed fluid direction. When the catalyst is deposited evenly on the surface without creating any additional packed-bed condition in the micro-channel, the flow in the radial movement would carry momentum and improve the mixing of gas in the channel. But, having a packed catalyst in this region adds resistance to fluid transport.

To further understand how transfer hindrance affects the conversion of CO, which relies on the format of perovskite catalyst packing inside microchannel of hollow fibre substrate, gas

permeation tests were performed and shown in Figure 6.8. As can be seen, permeation fluxes for hollow fibre reactors with 5 mg catalysts are significantly higher than the one with 10 mg of catalysts. Furthermore, the permeation flux of LFMPO-10mg is almost double the one of LFCPO-10mg, which agrees well with Figure 6.4 (a-ii) and (b-ii). This also indicates that, an excessive amount of catalyst does not work for the hollow fibre reactor design, since the actual catalyst involved in the reaction is reduced due to the significantly increased transfer resistance. In this study, 5 mg of perovskite catalysts were able to convert 0.01 mole of CO per gram of catalyst used. In contrast, 10 mg of the same catalyst converted CO at a rate of 0.0051 mole g^{-1} only, which is almost half the conversion capacity.

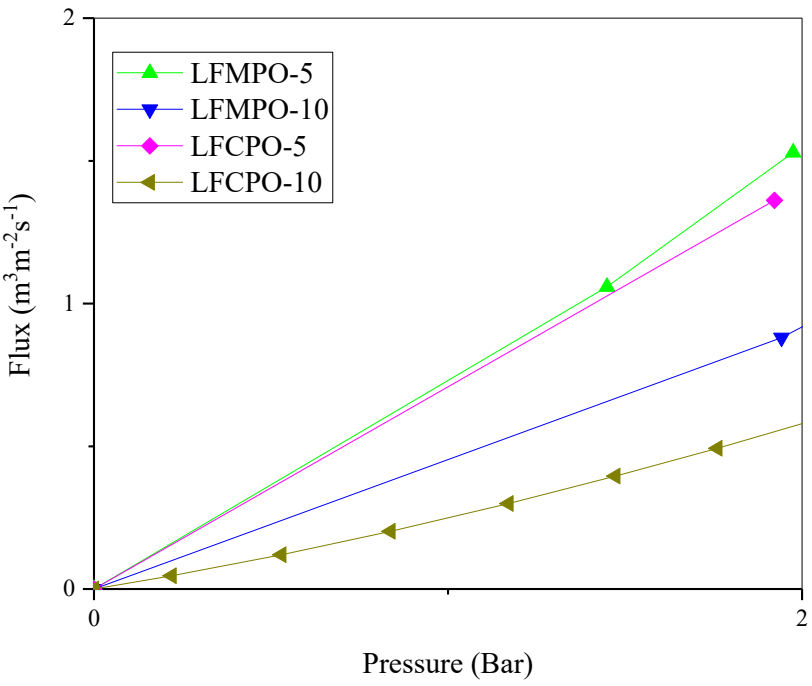

Figure 6.8 N_2 gas permeation tests of hollow fibre substrates deposited with different amount of catalysts

A comparison was made between the synthesised perovskite from literature. Although Pd-free perovskites have been proven by other researchers to have the ability to act as a three-way catalyst, the perovskite catalyst reactivity with Pd inclusion is much superior to the one without Pd. Table 6.5 shows the perovskite catalyst light-off temperature comparisons between Pd-free perovskite and their Pd-doped perovskite counterpart for CO oxidation reaction. The promoter effects from Pd insertion in the perovskite lattice is believed due to the increased oxygen vacancy concentration, which facilitates the diffusion of oxygen transport from the bulk to the catalyst surface [153–155].

Table 6.5 Comparison of light-off temperature for CO oxidation with different perovskite catalyst

Catalyst	Catalyst amount (mg)	Reactor configuration	T_{50} (^oC)	Reference
LaFe	75	Packed-bed	270	[156]
$LaFe_{0.94}Pd_{0.06}O_3$			240	
$LaFe_{0.74}Cu_{0.2}Pd_{0.06}O_3$			240	
$LaSrCuO_4$	250	Packed-bed	220	[153]
$LaSrCu_{0.9}Pd_{0.1}O_4$			200	
$LaFe_{0.6}Co_{0.4}O_3$	100	Packed-bed	285	[157]
$LaFe_{0.57}Co_{0.38}Pd_{0.05}O3$			142	
$LaFeO_3$	100	Packed-bed	535	[158]
$LaFe_{0.9}Pd_{0.1}O_3$			495	
$LaMnO_3$			485	
$LaMn_{0.9}Pd_{0.1}O_3$			425	

$LaFeO_3$	100	Packed-bed	330	[159]
$LaFe_{0.97}Pd_{0.03}O_3$			230	
$LaFeO_3$	100	Packed-bed	249	[68]
$LaFePd_{0.05}O_3$			150	
$LaMnO_3$			249	
$LaFePd_{0.05}O_3$			170	
$LaCoO_3$			190	
$LaCoPd_{0.05}O_3$			155	
$LaFe_{0.7}Mg_{0.225}Pd_{0.075}O_3$	5	Hollow fibre	232	This study
$LaFe_{0.7}Co_{0.225}Pd_{0.075}O_3$			248	
$LaFe_{0.7}Mg_{0.225}Pd_{0.075}O_3$	10	Hollow fibre	222	This study
$LaFe_{0.7}Co_{0.225}Pd_{0.075}O_3$			245	

Furthermore, a perovskite is prone to sulphur poisoning. Exposure to SO_2 originated in the fuel creates chemically bonded compounds such as sulphates, sulphites and/or sulphides depending on the condition of the environment it is exposed to [66]. The reaction is irreversible and may deactivate a perovskite catalyst. Nonetheless, it is reported that PGM can be added to the perovskite lattice not only to increase their catalytic reaction but also to delay the catalyst deactivation process. By incorporating Pd into the perovskite lattice, the Pd surface is hindered; thus, lanthanum sulphates are formed instead of the $PdSO_4$ [72].

Although in general, the light-off temperature of perovskite is not as low as of the PGM only catalyst as presented in Chapter 5, but the thermal stability of perovskite catalyst could make positioning of catalytic converter closer to the engine manifold possible, to optimise utilization of heat from the internal combustion.

6.4 Conclusion

Two perovskite catalysts doped with palladium, $LaFe_{0.7}Mg_{0.225}Pd_{0.075}O_3$ and $LaFe_{0.7}Co_{0.225}Pd_{0.075}O_3$, were synthesised by the sol-gel citrate method. The perovskite catalyst was successfully made with a crystalline structure of orthorhombic perovskite crystal having a specific surface area of between 10 to 20 m^2g^{-1}. A series of CO oxidation conversion tests were performed on the catalyst mixed with α-Al_2O_3 in the packed-bed configuration and, subsequently, deposited onto the ceramic hollow fibre substrate with a high geometric surface area. CO oxidation evaluation suggests that incorporation of 5 mg LFMPO and LFCPO catalyst into the hollow fibre could be light-up at 232 ^oC and 248 ^oC, respectively, which is 3% lower than the packed-bed counterpart with the same amount of catalyst at GHSV of ~ 5300 h^{-1}. Further incorporation of a 10 mg catalyst inside the hollow fibre resulted in a lowered catalyst activity where the CO moles converted reduced from 0.01 mole g^{-1} for 5mg catalyst to almost half, 0.0051 g^{-1} for the 10 mg catalyst. Excessive incorporation of catalyst impairs the utilisation of the catalyst active sites due to higher transfer resistance generated by the packing condition inside the microchannel. On the other hand, perovskite doped with palladium offers greater reactivity than the perovskite-free palladium with an additional advantage of improved thermal-chemical stability, while the incorporation of perovskite catalyst into the hollow fibre substrate tremendously reduced the amount of catalyst needed in the system compared to the conventional packed-bed configuration. With additional advantages of lower pressure drop due to bigger hydraulic diameter, the deposited perovskite on the hollow fibre appears to be a promising candidate for new catalytic converter systems.

Chapter 7

Conclusions and Recommendations for Future Work

This chapter concludes all findings from studies that were carried out in accordance with the objectives stated in Chapter 1. Recommendations for future studies in the subject area are also presented.

7.1 General Conclusions

This thesis focuses on introducing a ceramic hollow fibre as a new design of the substrate for catalytic converters. Studies on the fabrication of such ceramic hollow fibre have become the core content of this research. A single-step extrusion assisted by a phase inversion has been applied in order to fabricate the substrate with open microchannels in the lumen side. A series of characterisations were made to evaluate the hollow fibre structure and its suitability for catalytic converter application. Subsequently, a γ-Al_2O_3 washcoat was deposited on the hollow fibre support followed by a wet-incipient impregnation of a palladium catalyst. Further advancement was made by depositing a perovskite catalyst on the system without an additional secondary oxide layer, and the CO oxidation light-off temperature tests were carried out to

evaluate conversion efficiency. It has been discussed in the relevant chapter that the packing conditions and the configuration in the ceramic hollow fibre induced different effects on the system. The results show that a loosely packed washcoat is favourable for a ceramic hollow fibre catalytic converter. In this study, the possibility of employing a ceramic hollow fibre substrate in a catalytic converter has been demonstrated.

7.1.1 A Study on the Extrusion of Ceramic Hollow Fibre for the Fabrication of Ceramic Hollow Fibre Substrates for Catalytic Converters

Objective 1.2 (i)

A porous ceramic hollow fibre with arrays of microchannels was successfully fabricated. Two different polymers, PSEF and PMMA, were used as binders. The ceramic hollow fibre fabricated is intended to be used in catalytic converter applications for automotive emissions control. For such applications, the substrate should provide high surface area sufficient for catalytic active materials deposition. Due to this reason, the hollow fibre support should have microchannels wide enough to support any secondary oxide or washcoat layer. Assisted by the phase inversion technique, extrusion of the ceramic hollow fibre is capable of producing open microchannels from the lumen side. After many experiments with different suspension composition pairs with compatible spinning parameters, a suspension with PMMA produced a ceramic hollow fibre with the best structure for heterogeneous catalytic support. With the combination of the suspension composition and spinning parameters used, the resulting fabricated ceramic hollow fibre possessed a geometric surface area of 40.7 cm^2 cm^{-3}, comparable to the 750 CPSI honeycomb monolith substrate, but with almost double the hydraulic diameter. The microchannel opening of on average 40 nm provides easy access for

the washcoat layer deposition. Morphology evaluations also showed that the ceramic hollow fibre has a porous wall. This is important and beneficial for catalytic reactions in minimising mass transfer resistance of the reactants to reach the active sites for operation. With such a structure, a ceramic hollow fibre fabricated through extrusion, and assisted by the phase inversion process is seen as a suitable substrate for application in catalytic converters.

7.1.2 Microchannel Washcoat Packing Effects on CO Oxidation Activity

Objective 1.2 (ii) and (iii)

γ-Al_2O_3 was successfully washcoated into a micro-structured ceramic hollow fibre substrate with a varied amount of 0 – 10 wt.%. The continuous washcoating technique was used to deposit the secondary oxide layer. An SEM evaluation shows that the secondary oxide layer is distributed evenly in the microchannel by using this technique. The process was followed by impregnating 0.7 wt.% of Pd catalyst. Catalyst deposition in this study used the wet-impregnation technique with palladium salt as a precursor solution. The use of this technique resulted in an even deposition of the catalyst with an average particle size of 10 nm. With such a low active catalyst available in the system, CO oxidation measurement resulted in a conversion level which is same as that found in its commercial counterparts. 5 wt% of washcoat produced the best light-off temperature of 187 ^{o}C. Among the results of the different washcoat packings in the microchannels, the best configuration is the loosely packed washcoat. This configuration is believed to provide the maximum surface area for the catalyst deposition without causing any additional mass transfer resistance during operation. This study serves as ground research for using ceramic hollow fibre in catalytic converter applications.

7.1.3 Integrating Pd-Doped Perovskite Catalysts with Ceramic Hollow Fibre Substrate for Efficient CO Oxidation

Objective 1.2 (iv)

Two palladium doped perovskite catalysts, $LaFe_{0.7}Mg_{0.225}Pd_{0.075}O_3$ (LFMPO) and $LaFe_{0.7}Co_{0.225}Pd_{0.075}O_3$ (LFCPO) were successfully synthesised by using sol-gel citrate method. The produced perovskite catalysts have a specific surface area of 20 m^2g^{-1} for LFMPO and 10 m^2g^{-1} for LFCPO with orthorhombic crystal structures found in both catalysts. The catalysts were packed in two different configurations, namely, a packed-bed configuration as well as deposited in a ceramic hollow fibre and performance evaluations were carried out with CO oxidation reaction measurements. All catalysts tested could light up at temperatures lower than 250 ºC.When compared to the packed-bed configuration, 5 mg of perovskite deposited on the hollow fibre samples exhibited lower light-off temperatures, each from 242 to 232 ºC for LFMPO and from 252 to 248 ºC for LFCPO. Perovskite catalysts are demonstrated to have higher thermal stability than the conventional Pd supported γ-Al_2O_3, and claimed to have regeneration properties, which is beneficial in a redox reaction environment [64]. This study demonstrated that perovskite deposited on a ceramic hollow fibre substrate without any washcoat layer appears to be promising candidates for new catalytic converter systems.

7.2 Recommendations for Future Work

The proposed ceramic hollow fibre as a substrate for catalytic converters is rather new in the field of substrate development. A lot of unknowns need to be uncovered and research gaps need to be filled before a feasible claim for applying this new design to commercial applications can be made. Although the single hollow fibre studies have offered a lot of promising

advantages, from an engineering perspective, plenty of more studies are required in order to refine this knowledge further.

7.2.1 Adhesion and Long-term Ageing Test

In order to integrate the ceramic hollow fibre catalytic converter into practice, a long-term stability test has to be carried out. The long-term is especially important for catalyst stability in terms of their sintering behaviour in the harsh exhaust environment. As the catalyst will be exposed to rigorous redox reactions, any fluctuations in the temperature in the system will accentuate the thermal ageing of the catalyst. As a result, the sintered active sites will lose their effective surface area and lead to a reduction in performance. With a better understanding of the long-term ageing profile, modifications to the catalyst formulations can be made to enhance their thermal strength, to prolong the window of efficiency. In addition, the adhesion test should also be added. Catalytic converter operations involve a lot of vibrations. Poor active material adhesion will cause a loss of material, blockage on the channel, and increase of particulate pollutants in the environment. The results from catalyst adhesion studies can help in finding a better washcoating technique in the future.

7.2.2 Application of the System for Diesel Engine

Petrol is considered relatively cleaner as compared to diesel. It contains less sulphur, which is known as the most significant contributor to the cause of catalyst poisoning and deactivation of the active sites [160]. Latest studies conducted by the International Council on Clean Transportation revealed challenges faced by diesel engines. They require more complex

technologies to comply with the regulatory emission limits, with CO_2 emission of diesel engines exceeding those of petrol engines by 13% [161]. The gap in emissions between diesel and petrol engines mostly comes from the differences in their operations and the nature of the oil itself. Diesel combustion produces a higher concentration of NOx. With the different composition of exhaust emissions, integration of a new catalyst formulation is needed for diesel engine catalytic converter systems. Morever, each catalyst formulation produces their unique crystal and particle size. With such conditions, packing requirement of the new catalyst in the hollow fibre would be different, thus, a comprehensive study is needed to tackle this issue.

7.2.3 Diesel Particulate Filter (DPF)

The petrol engine exhaust treatment is straightforward while with the diesel engine, additional carbonaceous particulate matter (PM) substance is present and need to be sorted out simultaneously. Due to concerns related to health hazards by PM pollutant, a filter system has been introduced in the emission control system [4]. Conventional filtration for DPF uses extruded cordierite or silicon carbide (SiC) monolith, and alternate channels are blocked forcing the gas to permeate through the wall while the PM is trapped in the pores of the wall. The trapped PM is continuously removed by the regeneration process, either active or passive, in order to ensure the back-pressure of the engine is within the acceptable limits. Since the ceramic hollow fibre substrate contains arrays of microchannels, this empty volume is used to trap the PM. With a significant empty volume available in the hollow fibre, more PM could be filtered, and the regeneration interval is increased. The hollow fibre DPF having ample ash storage may offer benefits to improve the fuel economy of the engines.

7.2.4 Optimisation of the Hollow Fibre Packing

When comparing different geometries, a honeycomb packing is known to provide the best packing density with minimal weight and material. In order to be used in the catalytic converter, the ceramic hollow fibre must be made into a monolithic structure. A single fibre has low mechanical strength and is prone to breakage. Thus, the hollow fibre needs to be bundled into a module. In this case, a packing optimisation study is required to reduce as much of unwanted void space in between the hollow fibre of the sphere geometry. Apart from the optimisation of the packing geometry, a consideration for an adhesive material that can withstand high operating temperatures, with thermal expansion similar to the substrate material is critical. This is to avoid adverse effects caused by a mismatch in thermal properties that may reduce the mechanical strength of the support.

7.2.5 CFD Simulation Study for Mass Transfer Regime Coupled with Kinetic Data for Reaction Profile in the Hollow Fibre Substrate

The performance of a catalytic converter is affected by several crucial factors. One of them is the flow distribution in the system. Tailoring of the configuration of the catalytic layer may require a lot of trial and error to ensure the mass transfer in the system is optimised for better contact between the reactants and catalyst. As a ceramic hollow fibre substrate contains microchannels in their lumen and the washcoat layer is embedded into this void, an understanding of the mass transfer regime of this unique configuration is paramount. It can help in minimising the mass transfer resistance that may inhibit full utilisation of the active sites for reactions. However, optimisation of the catalytic converter through experimental pathways is time-consuming, expensive and furthermore labour extensive. A computational

fluid dynamics (CFD) package can be used to model mass, momentum, energy and species transport phenomena [162]. The first step is to understand the single-channel model; and then to extrapolate to a full-size reactor. With the use of appropriate methods and software, the experimentation time can be shortened, and various configurations can be tested at much less costs.

7.2.6 Impact of Backpressure on Engine Performance

Installation of catalytic converter reduces the brake thermal efficiency. This results in the increase of the brake specific fuel consumption, lead to high fuel flow pumping into the system to achieve a specific power output [163]. As claimed in Chapter 4, the new hollow fibre substrates could offer a significant backpressure reduction in the system, where it gives a better breathing capacity to the engine. Further, engine efficiency study through experimentation and engine simulation should be carried out to measure the effects of backpressure reduction on the internal combustion engine performance.

References

[1] World Energy Council, Global Transport Scenarios 2050 - Appendix, 2011. doi:10.1016/j.enpol.2011.05.049.

[2] R. Sims, R. Schaeffer, B. Soares Moreira Cesar Borba, R. Schaeffer, F. Creutzig, X. Cruz-Núñez, D. Dimitriu, M.J. Figueroa Meza, L. Fulton, S. Kobayashi, O. Lah, A. McKinnon, P. Newman, M. Ouyang, J.J. Schauer, D. Sperling, G. Tiwari, Y. Sokona, E. Farahani, S. Kadner, K. Seyboth, A. Adler, I. Baum, S. Brunner, P. Eickemeier, B. Kriemann, J. Savolainen, S. Schlömer, C. von Stechow, T. Zwickel, J. Minx, Assessment Report 5: 8 Transport, (2014) 599–671. https://www.ipcc.ch/pdf/assessment-report/ar5/wg3/ipcc_wg3_ar5_chapter8.pdf.

[3] R.M. Heck, R.J. Farrauto, Automobile exhaust catalysts, Appl. Catal. A Gen. 221 (2001) 443–457. doi:10.1016/S0926-860X(01)00818-3.

[4] M. V. Twigg, Controlling automotive exhaust emissions: Successes and underlying science, Philos. Trans. R. Soc. A Math. Phys. Eng. Sci. 363 (2005) 1013–1033. doi:10.1098/rsta.2005.1547.

[5] A.Y. Watson, R.R. Bates, D. Kennedy, Air Pollution, the Automobile, and Public Health, First, National Academy of Sciences, 1988.

[6] R. Carlisle, Scientific American Inventions and Discoveries, First, John Wiley & Sons Ltd, 2004.

[7] M. V. Twigg, Catalytic control of emissions from cars, Catal. Today. 163 (2011) 33–41. doi:10.1016/j.cattod.2010.12.044.

[8] I. Heo, M.H. Wiebenga, J.R. Gaudet, I.-S. Nam, W. Li, C.H. Kim, Ultra low temperature CO and HC oxidation over Cu-based mixed oxides for future automotive applications, Appl. Catal. B Environ. 160 (2014) 365–373. doi:10.1016/j.apcatb.2014.05.045.

[9] A. Glisenti, M. Pacella, M. Guiotto, M.M. Natile, P. Canu, Largely Cu-doped LaCo1-

xCuxO3 perovskites for TWC: Toward new PGM-free catalysts, Appl. Catal. B Environ. 180 (2016) 94–105. doi:10.1016/j.apcatb.2015.06.017.

[10] I.H. Kim, H.O. Seo, E.J. Park, S.W. Han, Y.D. Kim, Low Temperature CO oxidation over Iron Oxide Nanoparticles Decorating Internal Structures of a Mesoporous Alumina, Sci. Rep. 7 (2017) 40497. doi:10.1038/srep40497.

[11] S.P.S. Andrew, Development of a non-precious metal based catalyst for NOx removal from automobile exhausts, Chem. Eng. Res. Des. 75 (1997) 135–137. doi:10.1016/S0263-8762(97)80010-X.

[12] M. V. Twigg, Progress and future challenges in controlling automotive exhaust gas emissions, Appl. Catal. B Environ. 70 (2007) 2–15. doi:10.1016/j.apcatb.2006.02.029.

[13] U. Bardi, S. Caporali, Precious Metals in Automotive Technology: An Unsolvable Depletion Problem?, Minerals. 4 (2014) 388–398. doi:10.3390/min4020388.

[14] J.L. Williams, Monolith structures, materials, properties and uses, Catal. Today. 69 (2001) 3–9. doi:http://dx.doi.org/10.1016/S0920-5861(01)00348-0.

[15] G.E.B. Jr, J.H. Mack, R.W. Dibble, Homogeneous Charge Compression Ignition (HCCI) Engine, 2 (2014) 817–826.

[16] Y. Kim, K. Sartelet, C. Seigneur, A. Charron, J.L. Besombes, J.L. Jaffrezo, N. Marchand, L. Polo, Effect of measurement protocol on organic aerosol measurements of exhaust emissions from gasoline and diesel vehicles, Atmos. Environ. 140 (2016) 176–187. doi:10.1016/j.atmosenv.2016.05.045.

[17] M.L. Church, B.J. Cooper, P.J. Willson, No Title, SAE Pap. (1989) 1.

[18] C.L. Townsend, R. Maynard, Effects on health of prolonged exposure to low concentrations of carbon monoxide -- Townsend and Maynard 59 (10): 708 -- Occupational and Environmental Medicine, Occup. Environ. Med. 59 (2002) 708–711. http://oem.bmj.com/cgi/content/full/59/10/708%5Cnpapers2://publication/uuid/03E64

AEE-517C-4E8B-8964-30C527BCDB20.

[19] H. Iwakuni, Y. Shinmyou, H. Yano, H. Matsumoto, T. Ishihara, Direct decomposition of NO into N2 and O2 on BaMnO3-based perovskite oxides, Appl. Catal. B Environ. 74 (2007) 299–306. doi:10.1016/j.apcatb.2007.02.020.

[20] A. Sydbom, A. Blomberg, S. Parnia, N. Stenfors, T. Sandström, S.E. Dahlén, Health effects of diesel exhaust emissions, Eur. Respir. J. 17 (2001) 733–746. doi:10.1183/09031936.01.17407330.

[21] J. Lewtas, Air pollution combustion emissions: Characterization of causative agents and mechanisms associated with cancer, reproductive, and cardiovascular effects, Mutat. Res. - Rev. Mutat. Res. 636 (2007) 95–133. doi:10.1016/j.mrrev.2007.08.003.

[22] O. Raaschou-Nielsen, R. Beelen, M. Wang, G. Hoek, Z.J. Andersen, B. Hoffmann, M. Stafoggia, E. Samoli, G. Weinmayr, K. Dimakopoulou, M. Nieuwenhuijsen, W.W. Xun, P. Fischer, K.T. Eriksen, M. Sørensen, A. Tjønneland, F. Ricceri, K. de Hoogh, T. Key, M. Eeftens, P.H. Peeters, H.B. Bueno-de-Mesquita, K. Meliefste, B. Oftedal, P.E. Schwarze, P. Nafstad, C. Galassi, E. Migliore, A. Ranzi, G. Cesaroni, C. Badaloni, F. Forastiere, J. Penell, U. De Faire, M. Korek, N. Pedersen, C.G. Östenson, G. Pershagen, L. Fratiglioni, H. Concin, G. Nagel, A. Jaensch, A. Ineichen, A. Naccarati, M. Katsoulis, A. Trichpoulou, M. Keuken, A. Jedynska, I.M. Kooter, J. Kukkonen, B. Brunekreef, R.S. Sokhi, K. Katsouyanni, P. Vineis, Particulate matter air pollution components and risk for lung cancer, Environ. Int. 87 (2016) 66–73. doi:10.1016/j.envint.2015.11.007.

[23] Ambient air pollution: A global assessment of exposure and burden of disease, World Heal. Organ. (2016) 1–131. doi:9789241511353.

[24] F.R. García-García, B.F.K. Kingsbury, M.A. Rahman, K. Li, Asymmetric ceramic hollow fibres applied in heterogeneous catalytic gas phase reactions, Catal. Today. 193 (2012) 20–30. doi:10.1016/j.cattod.2012.01.006.

[25] C.K. Cavataio, G., Girard, J. J. E., Patterson, C., Montreuil, C., Cheng, Y., Lambert, Society of Automotive Engineering Technical Paper, SAE Int. 1 (2007) 1575.

[26] A.K. Ibrahim Aslan Resitoglu, Kemal Altinisik, The pollutant emissions from diesel-engine vehicles and exhaust aftertreatment systems, Clean Technol. Environ. Policy. 17 (2014) 15–27. doi:10.1007/s10098-014-0793-9.

[27] A. Joshi, Progress and Outlook on Gasoline Vehicle Aftertreatment Systems, Johnson Matthey Technol. Rev. 61 (2017) 311–325. doi:10.1595/205651317x696306.

[28] H. Uchida, Trend of Turbocharging Technologies, R&D Rev. Toyota CRDL. 41 (2006) 1–8.

[29] S. Bhattacharyya, R.K. Das, Catalytic Control of Automotive No : a Review, Int J Energy Res. 23 (1999) 351–369. doi:10.1002/(SICI)1099-114X(19990325)23:4<351::AID-ER497>3.0.CO;2-T.

[30] D.L. Davis, G.E. Onishi, Catalytic Converter Development Problems, (1962) 9. doi:10.4271/620398.

[31] J.R. Mellor, A.N. Palazov, B.S. Grigorova, J.F. Greyling, K. Reddy, M.P. Letsoalo, J.H. Marsh, The application of supported gold catalysts to automotive pollution abatement, Catal. Today. 72 (2002) 145–156. doi:http://dx.doi.org/10.1016/S0920-5861(01)00488-6.

[32] A.R. Ravishankara, J.S. Daniel, R.W. Portmann, Nitrous Oxide (N 2 O): The Dominant Ozone-Depleting Substance Emitted in the 21st Century, Science (80-.). 326 (2009) 123–125. doi:10.1126/science.1176985.

[33] Where Would You Find A Catalytic Converter? | MyCarNeedsA.com, (n.d.). https://mycarneedsa.com/blog/where-would-you-find-a-catalytic-converter- (accessed December 17, 2019).

[34] S. Bettuzzi, Catalysts: theory and experiment, Adv. Cancer Res. (2009).

doi:10.1016/S0065-230X(09)04001-9.

[35] H. Catalysis, Inorganic Solids as H e t e r o g e n e o u s Catalysts, (n.d.) 115–128.

[36] L. Liu, A. Corma, Metal Catalysts for Heterogeneous Catalysis: From Single Atoms to Nanoclusters and Nanoparticles, Chem. Rev. 118 (2018) 4981–5079. doi:10.1021/acs.chemrev.7b00776.

[37] S.M. Lang, I. Fleischer, T.M. Bernhardt, R.N. Barnett, U. Landman, Low-Temperature CO Oxidation Catalyzed by Free Palladium Clusters: Similarities and Differences to Pd Surfaces and Supported Particles, ACS Catal. 5 (2015) 2275–2289. doi:10.1021/cs5016222.

[38] F. Duprat, Light-off curve of catalytic reaction and kinetics, Chem. Eng. Sci. 57 (2002) 901–911. doi:10.1016/S0009-2509(01)00409-2.

[39] J.H. Lee, D.L. Trimm, Catalytic combustion of methane, Fuel Process. Technol. (1995) 339.

[40] K. Ravindra, L. Bencs, R. Van Grieken, Platinum group elements in the environment and their health risk, Sci. Total Environ. 318 (2004) 1–43. doi:10.1016/s0048-9697(03)00372-3.

[41] U.S.G. Survey, Rare Earth Elements — Critical Resources for High Technology, (2002) 1–11.

[42] J.S. Hepburn, K.S. Patel, M.G. Meneghel, H.S. Gandhi, Development of Pd-only three way catalyst technology, in: SAE Tech. Pap., 1994. doi:10.4271/941058.

[43] J. Wang, H. Chen, Z. Hu, M. Yao, Y. Li, A Review on the Pd-Based Three-Way Catalyst, Catal. Rev. 57 (2014) 79–144. doi:10.1080/01614940.2014.977059.

[44] J.. Holles, R.. Davis, T.. Murray, J.. Howe, Effects of Pd particle size and ceria loading on NO reduction with CO, J. Catal. 195 (2000) 193–206.

[45] Y. Lou, J. Liu, CO Oxidation on Metal Oxide Supported Single Pt atoms : The Role of

the Support, (2017). doi:10.1021/acs.iecr.7b01477.

[46] P. Avila, M. Montes, E.E. Miró, Monolithic reactors for environmental applications, Chem. Eng. J. 109 (2005) 11–36. doi:10.1016/j.cej.2005.02.025.

[47] P. Munnik, P.E. De Jongh, K.P. De Jong, Recent Developments in the Synthesis of Supported Catalysts, (2015). doi:10.1021/cr500486u.

[48] T. Vergunst, F. Kapteijn, J.A. Moulijn, Monolithic catalysts - Non-uniform active phase distribution by impregnation, Appl. Catal. A Gen. 213 (2001) 179–187. doi:10.1016/S0926-860X(00)00896-6.

[49] M.L. Toebes, J.A. Van Dillen, K.P. De Jong, Synthesis of supported palladium catalysts, J. Mol. Catal. A Chem. 173 (2001) 75–98. doi:10.1016/S1381-1169(01)00146-7.

[50] J. Haber, J.H. Block, B. Delmon, Manual of methods and procedures for catalyst characterization (Technical Report), Pure Appl. Chem. 67 (1995) 1257–1306. doi:10.1351/pac199567081257.

[51] C. Perego, P. Villa, Catalyst preparation methods, 34 (1997) 281–305.

[52] N.M. Deraz, The comparative jurisprudence of catalysts preparation methods : I . precipitation and impregnation methods ., 2 (2018) 1–3.

[53] S.A. Malamis, R.J. Harrington, M.B. Katz, D.S. Koerschner, S. Zhang, Y. Cheng, L. Xu, H.-W.W. Jen, R.W. McCabe, G.W. Graham, X. Pan, Comparison of precious metal doped and impregnated perovskite oxides for TWC application, Catal. Today. 258 (2015) 535–542. doi:10.1016/j.cattod.2014.11.028.

[54] N. Labhasetwar, G. Saravanan, S. Kumar Megarajan, N. Manwar, R. Khobragade, P. Doggali, F. Grasset, Perovskite-type catalytic materials for environmental applications, Sci. Technol. Adv. Mater. 16 (2015) 36002. doi:10.1088/1468-6996/16/3/036002.

[55] E. Grabowska, Selected perovskite oxides: Characterization, preparation and photocatalytic properties-A review, Appl. Catal. B Environ. 186 (2016) 97–126.

doi:10.1016/j.apcatb.2015.12.035.

[56] S. Vasala, M. Karppinen, A2B′B″O6 perovskites: A review, Prog. Solid State Chem. 43 (2015) 1–36. doi:10.1016/j.progsolidstchem.2014.08.001.

[57] J. Zhu, A. Thomas, Perovskite-type mixed oxides as catalytic material for NO removal, Appl. Catal. B Environ. 92 (2009) 225–233. doi:10.1016/j.apcatb.2009.08.008.

[58] C. Moure, O. Peña, Recent Advances in Perovskites: Processing and Properties, Prog. Solid State Chem. 43 (2015) 123–148. doi:10.1016/j.progsolidstchem.2015.09.001.

[59] H. Tanaka, M. Uenishi, I. Tan, M. Kimura, J. Mizuki, An intelligent catalyst, (2001). http://papers.sae.org/2001-01-1301/.

[60] J. Zhu, H. Li, L. Zhong, P. Xiao, X. Xu, X. Yang, Z. Zhao, J. Li, Perovskite Oxides: Preparation, Characterizations, and Applications in Heterogeneous Catalysis, (n.d.). doi:10.1021/cs500606g.

[61] H. Tanaka, M. Taniguchi, N. Kajita, M. Uenishi, I. Tan, N. Sato, K. Narita, M. Kimura, Design of the Intelligent Catalyst for Japan ULEV Standard, Top. Catal. 30/31 (2004) 389–396. doi:10.1023/b:toca.0000029780.70319.36.

[62] M. Uenishi, M. Taniguchi, H. Tanaka, M. Kimura, Y. Nishihata, J. Mizuki, T. Kobayashi, Redox behavior of palladium at start-up in the Perovskite-type LaFePdO x automotive catalysts showing a self-regenerative function, Appl. Catal. B Environ. 57 (2005) 267–273. doi:10.1016/j.apcatb.2004.11.011.

[63] S. Solution, P. Particles, P. Metals, G. Growth, F.G. Growth, Self-regeneration of a Pd -perovskite Catalyst : A Philosopher's Stone for Today's Automotive Engine, Environ. Sci. (n.d.) 75–77.

[64] Y. Nishihata, J. Mizuki, T. Akao, H. Tanaka, M. Uenishi, M. Kimura, T. Okamoto, N. Hamada, Self-regeneration of a Pd-perovskite catalyst for automotive emissions control., Nature. 418 (2002) 164–167. doi:10.1038/nature00893.

[65] B. Saruhan, G.C. Mondragón Rodríguez, A.A. Haidry, A. Yüce, S. Heikens, W. Grünert, Integrated performance monitoring of three-way catalytic converters by self-regenerative and adaptive high-temperature catalyst and sensors, Adv. Eng. Mater. 18 (2016) 728–738. doi:10.1002/adem.201500410.

[66] I. Rossetti, O. Buchneva, C. Biffi, R. Rizza, Effect of sulphur poisoning on perovskite catalysts prepared by flame-pyrolysis, Appl. Catal. B Environ. 89 (2009) 383–390. doi:10.1016/j.apcatb.2008.12.017.

[67] J. Gao, L. Li, Z. Yin, J. Zhang, S. Lu, X. Tan, Poisoning effect of SO2 on the oxygen permeation behavior of La0.6Sr0.4Co0.2Fe0.8O3-δ perovskite hollow fiber membranes, J. Memb. Sci. 455 (2014) 341–348. doi:10.1016/j.memsci.2013.12.073.

[68] H. Ziaei-azad, A. Khodadadi, P. Esmaeilnejad-ahranjani, Y. Mortazavi, Effects of Pd on enhancement of oxidation activity of LaBO3 (B = Mn , Fe , Co and Ni) pervoskite catalysts for pollution abatement from natural gas fueled vehicles, Appl. Catal. B Environ. Environ. 102 (2011) 62–70. doi:10.1016/j.apcatb.2010.11.025.

[69] A. Budiman, M. Ridwan, S.M. Kim, J.-W. Choi, C.W. Yoon, J.-M. Ha, D.J. Suh, Y.-W. Suh, Design and preparation of high-surface-area Cu/ZnO/Al2O3 catalysts using a modified co-precipitation method for the water-gas shift reaction, Appl. Catal. A Gen. 462 (2013) 220–226. doi:10.1016/j.apcata.2013.05.010.

[70] A.E. Danks, S.R. Hall, Z. Schnepp, The evolution of “sol-gel” chemistry as a technique for materials synthesis, Mater. Horizons. 3 (2016) 91–112. doi:10.1039/c5mh00260e.

[71] B. Béguin, E. Garbowski, M. Primet, Stabilization of alumina by addition of lanthanum, Appl. Catal. 75 (1991) 119–132. doi:10.1016/S0166-9834(00)83128-0.

[72] E. Tzimpilis, N. Moschoudis, M. Stoukides, P. Bekiaroglou, Ageing and SO2 resistance of Pd containing perovskite-type oxides, Appl. Catal. B Environ. 87 (2009) 9–17. doi:10.1016/j.apcatb.2008.08.020.

[73] X. Tiancun, A. Lidun, Z. Weimin, S. Shishan, X. Guoxin, Mechanism of sulfur poisoning on supported noble metal catalyst - The adsorption and transformation of sulfur on palladium catalysts with different supports, Catal. Letters. 12 (1992) 287–296. doi:10.1007/BF00767211.

[74] T.A. Nijhuis, A.E.W. Beers, T. Vergunst, I. Hoek, F. Kapteijn, J.A. Moulijn, Preparation of monolithic catalysts, Catal. Rev. 43 (2001) 345–380. doi:10.1081/cr-120001807.

[75] S. Govender, H. Friedrich, Monoliths: A Review of the Basics, Preparation Methods and Their Relevance to Oxidation, Catalysts. 7 (2017) 62. doi:10.3390/catal7020062.

[76] E.S.P.B. V, H. Schaper, L.L.V.A.N. Reijen, P. Chemistry, Gamma To Alpha Alumina.Pdf, 77 (1984) 383–393.

[77] T. Zhou, L. Li, J. Cheng, Z. Hao, Preparation of binary washcoat deposited on cordierite substrate for catalytic applications, Ceram. Int. 36 (2010) 529–534. doi:10.1016/j.ceramint.2009.09.027.

[78] P. Jiang, G. Lu, Y.Y. Guo, Y.Y. Guo, S. Zhang, X. Wang, Preparation and properties of a γ-Al2O3 washcoat deposited on a ceramic honeycomb, Surf. Coatings Technol. 190 (2005) 314–320. doi:10.1016/j.surfcoat.2004.05.029.

[79] A. Trovarelli, Catalytic Properties of Ceria and CeO2 -Containing Materials, Catal. Rev. 38 (1996) 439–520. doi:10.1080/01614949608006464.

[80] P. Fornasiero, E. Fonda, R. Di Monte, G. Vlaic, J. Kašpar, M. Graziani, Relationships between Structural/Textural Properties and Redox Behavior in Ce0.6Zr0.4O2 Mixed Oxides, J. Catal. 187 (1999) 177–185. doi:10.1006/jcat.1999.2589.

[81] G. Vlaic, R. Di Monte, P. Fornasiero, E. Fonda, J. Kašpar, M. Graziani, Redox property-local structure relationships in the Rh-loaded CeO2-ZrO2mixed oxides, J. Catal. 182 (1999) 378–389. doi:10.1006/jcat.1998.2335.

[82] M. Melchionna, P. Fornasiero, The role of ceria-based nanostructured materials in

energy applications, Mater. Today. 17 (2014) 349–357. doi:10.1016/j.mattod.2014.05.005.

[83] V. Blachou, D. Goula, Co. Philippopoulos, Wet milling of alumina and preparation of slurries for monolithic structures impregnation, Ind. Eng. Chem. Res. 31 (1992) 364–369.

[84] M.B. Adamowska, P. Da Costa, Structured Pd / γ-Al 2 O 3 Prepared by Washcoated Deposition on a Ceramic Honeycomb for Compressed Natural Gas Applications, J. Nanoparticles. 2015 (2014) 10–12. doi:http://dx.doi.org/10.1155/2015/601941.

[85] N. Mladenov, J. Koop, S. Tischer, O. Deutschmann, Modeling of transport and chemistry in channel flows of automotive catalytic converters, Chem. Eng. Sci. 65 (2010) 812–826. doi:10.1016/j.ces.2009.09.034.

[86] H. Santos, M. Costa, Analysis of the mass transfer controlled regime in automotive catalytic converters, Int. J. Heat Mass Transf. 51 (2008) 41–51. doi:10.1016/j.ijheatmasstransfer.2007.04.044.

[87] H. Santos, M. Costa, The relative importance of external and internal transport phenomena in three way catalysts, Int. J. Heat Mass Transf. 51 (2008) 1409–1422. doi:10.1016/j.ijheatmasstransfer.2007.11.005.

[88] R. Holder, M. Bollig, D.R. Anderson, J.K. Hochmuth, A discussion on transport phenomena and three-way kinetics of monolithic converters, Chem. Eng. Sci. 61 (2006) 8010–8027. doi:10.1016/j.ces.2006.09.030.

[89] R.M. Heck, S. Gulati, R.J. Farrauto, The application of monoliths for gas phase catalytic reactions, Chem. Eng. J. 82 (2001) 149–156. doi:http://dx.doi.org/10.1016/S1385-8947(00)00365-X.

[90] S.T. Sie, H.P. Calis, Structured Catalysts and Reactors, 2005. doi:10.1201/9781420028003.

[91] J.W. Geus, J.C. van Giezen, Monoliths in catalytic oxidation, Catal. Today. 47 (1999) 169–180. doi:10.1016/S0920-5861(98)00297-1.

[92] S. Roy, T. Bauer, M. Al-Dahhan, P. Lehner, T. Turek, Monoliths as multiphase reactors: A review, AIChE J. 50 (2004) 2918–2938. doi:10.1002/aic.10268.

[93] G.L. Vaneman, Comparison of Metal Foil and Ceramic Monolith Automotive Catalytic Converters, in: A. Crucq (Ed.), Stud. Surf. Sci. Catal., Elsevier, 1991: pp. 537–545. doi:http://dx.doi.org/10.1016/S0167-2991(08)63000-1.

[94] F. Tomasic, V., Jovic, State of the art in the monolith catalysts/reactors, Appl. Catal. A Gen. 311 (2006) 112–121.

[95] G.G. Isabella Nova, Alessandra Beretta, and P.F. Luca Lietti, Enrico Tronconi, Monolithic Catalysts for NOx removal from Stationary Sources, in: Struct. Catal. React., n.d.: pp. 171–214.

[96] F. Janssen, Handbook of Heterogeneous Catalysis, in: Handb. Heterog. Catal., Wiley-VCH, 1997: pp. 1633–1668.

[97] A.S. Ivanova, E.M. Slavinskaya, R. V. Gulyaev, V.I. Zaikovskii, O.A. Stonkus, I.G. Danilova, L.M. Plyasova, I.A. Polukhina, A.I. Boronin, Metal-support interactions in Pt/Al2O3and Pd/Al2O3catalysts for CO oxidation, Appl. Catal. B Environ. 97 (2010) 57–71. doi:10.1016/j.apcatb.2010.03.024.

[98] P. Auerkari, Mechanical and physical properties of engineering alumina ceramics, VTT Tied. - Valt. Tek. Tutkimusk. (1996).

[99] C.G.S.F. Frederick B. R., Ceramic catalytic converter substrate, J. Clean. Prod. 6 (1998) 153–170.

[100] P. Biswas, K. Rajeswari, V. Mahendar, R. Johnson, Extrusion processing of dense MgAl2O4 spinel honeycombs with low relative density, Ceram. Int. 39 (2013) 9819–9821. doi:10.1016/j.ceramint.2013.05.091.

[101] C. Emissions, E. Program, UNDERSTANDING CATALYSTS A Handbook for the User Part 2 – Catalysts All Around Us, (n.d.).

[102] J.A.M. Freek Kapteijn, Johan J Heiszwolf, TA van Nijhuis, Monoliths in multiphase catalytic processes: aspects and prospects, Cattech. 3 (1999) 24–40.

[103] M.A. Rahman, F.R. García-García, K. Li, Development of a catalytic hollow fibre membrane microreactor as a microreformer unit for automotive application, J. Memb. Sci. 390–391 (2012) 68–75. doi:10.1016/j.memsci.2011.11.009.

[104] F.R. García-García, M.A. Rahman, B.F.K. Kingsbury, K. Li, Asymmetric ceramic hollow fibres: New micro-supports for gas-phase catalytic reactions, Appl. Catal. A Gen. 393 (2011) 71–77. doi:10.1016/j.apcata.2010.11.028.

[105] B. Kingsbury, J. Stewart, Z. Wu, R. Douglas, K. Li, Advanced Ceramic Substrate with Ordered and Designed Micro-Structure for Applications in Automotive Catalysis, SAE Tech. Pap. 2014–Octob (2014). doi:10.4271/2014-01-2805.

[106] K. Li, Ceramic Membranes for Separation and Reaction, John Wiley & Sons Ltd, 2007.

[107] S.S. Loeb S, No Title, Adv. Chem. Ser. (1962) 117–32.

[108] K. (Krzysztof) Matyjaszewski, M. Möller, Polymer science : a comprehensive reference, Elseiver, 2012.

[109] L.M. Robeson, Polymer blends : a comprehensive review, Hanser, Munich ;;Cincinnati, 2007.

[110] D.F. Sanders, Z.P. Smith, R. Guo, L.M. Robeson, J.E. McGrath, D.R. Paul, B.D. Freeman, Energy-efficient polymeric gas separation membranes for a sustainable future: A review, Polymer (Guildf). 54 (2013) 4729–4761. doi:10.1016/j.polymer.2013.05.075.

[111] H. Strathmann, K. Kock, The formation mechanism of phase inversion membranes, Desalination. 21 (1977) 241–255. doi:10.1016/S0011-9164(00)88244-2.

[112] M. Lee, B. Wang, Z. Wu, K. Li, Formation of micro-channels in ceramic membranes -

Spatial structure, simulation, and potential use in water treatment, J. Memb. Sci. 483 (2015) 1–14. doi:10.1016/j.memsci.2015.02.023.

[113] M.. RAHAMAN, Sintering of Ceramics, CRC Press. i (2007).

[114] E. Mueller, W. Sigmund, 3.1 Forming and Drying, (2003).

[115] Z. Wu, Dual-layer Functional Ceramic Hollow Fibre Membranes for Partial Oxidation of Methane, (2012) 208.

[116] Z. Wu, R. Faiz, T. Li, B.F.K. Kingsbury, K. Li, A controlled sintering process for more permeable ceramic hollow fibre membranes, J. Memb. Sci. 446 (2013) 286–293. doi:10.1016/j.memsci.2013.05.040.

[117] B. Wang, M. Lee, K. Li, YSZ-reinforced alumina multi-channel capillary membranes for micro-filtration, Membranes (Basel). 6 (2015) 5. doi:10.3390/membranes6010005.

[118] M. Lee, Z. Wu, R. Wang, K. Li, Micro-structured alumina hollow fibre membranes – Potential applications in wastewater treatment, J. Memb. Sci. 461 (2014) 39–48. doi:10.1016/j.memsci.2014.02.044.

[119] I.M. Lachman, J.L. Williams, Extruded monolithic catalyst supports, Catal. Today. 14 (1992) 317–329. doi:10.1016/0920-5861(92)80032-I.

[120] V. Tomašić, F. Jović, State-of-the-art in the monolithic catalysts/reactors, Appl. Catal. A Gen. 311 (2006) 112–121. doi:10.1016/j.apcata.2006.06.013.

[121] A. Gouveia Gil, M.H.M. Reis, D. Chadwick, Z. Wu, K. Li, A highly permeable hollow fibre substrate for Pd/Al2O3 composite membranes in hydrogen permeation, Int. J. Hydrogen Energy. 40 (2015) 3249–3258. doi:10.1016/j.ijhydene.2015.01.021.

[122] B. Delmon, J.M. Thomas, R.G. Bell, C.R.A. Catlow, E.J.P. Feijen, J.A. Martens, P.A. Jacobs, W. Souverijns, W. Van Rhun, Preparation of Solid Catalysts: Sections 2.2.2 – 2.3.3, in: Handb. Heterog. Catal., 1997: pp. 264–365. doi:10.1002/9783527619474.ch2c.

[123] J.A.M. T.A. Nijhuis, A.E.W. Beers, T. Vergunst, I. Hoek, F. Kapteijn, Preparation of monolithic catalysts, Catal. Rev. - Sci. Eng. 43 (2001) 345–380. doi:doi:10.1081/CR-120001807.

[124] M. Lee, B. Wang, K. Li, New designs of ceramic hollow fibres toward broadened applications, J. Memb. Sci. 503 (2016) 48–58. doi:10.1016/j.memsci.2015.12.047.

[125] B.F.K. Kingsbury, K. Li, A morphological study of ceramic hollow fibre membranes, J. Memb. Sci. 328 (2009) 134–140. doi:10.1016/j.memsci.2008.11.050.

[126] S. Liu, K. Li, R. Hughes, Preparation of porous aluminium oxide (Al2O3) hollow fibre membranes by a combined phase-inversion and sintering method, Ceram. Int. 29 (2003) 875–881. doi:10.1016/s0272-8842(03)00030-0.

[127] C.K.S. Susan C. Lauderdale, Seth T. Nickerson, Jonathan D. Pesansky, Impact of Ceramic Substrate Web Thicknes On Emission Light-off, Pressure Drop and Strength, SAE Tech. Pap. (2008). doi:10.4271/2008-01-0808.

[128] N.I. Mahyon, T. Li, R. Martinez-Botas, Z. Wu, K. Li, A new hollow fibre catalytic converter design for sustainable automotive emissions control, Catal. Commun. 120 (2019) 86–90. doi:10.1016/j.catcom.2018.12.001.

[129] J. Li, H. Chang, L. Ma, J. Hao, R.T. Yang, Low-temperature selective catalytic reduction of NOx with NH3 over metal oxide and zeolite catalysts—A review, Catal. Today. 175 (2011) 147–156. doi:10.1016/j.cattod.2011.03.034.

[130] B. Kingsbury, J. Stewart, Z. Wu, R. Douglas, K. Li, Advanced Ceramic Substrate with Ordered and Designed Micro-Structure for Applications in Automotive Catalysis, SAE Tech. Pap. 2014–Octob (2014). doi:10.4271/2014-01-2805.

[131] D. Leung R. E. Hayes S. T. Kolaczkowski, Diffusion limitation effects in the washcoat of a catalytic monolith reactor, Can. J. Chem. Eng. 74 (1996).

[132] R.E. Hayes, S.T. Kolaczkowski, Mass and heat transfer effects in catalytic monolith

reactors, Chem. Eng. Sci. 49 (1994) 3587–3599. doi:10.1016/0009-2509(94)00164-2.

[133] J.M.C. Pereira, J.E.P. Navalho, A.C.G. Amador, J.C.F. Pereira, Multi-scale modeling of diffusion and reaction–diffusion phenomena in catalytic porous layers: Comparison with the 1D approach, Chem. Eng. Sci. 117 (2014) 364–375. doi:10.1016/j.ces.2014.06.028.

[134] J. Kašpar, P. Fornasiero, N. Hickey, Automotive catalytic converters: current status and some perspectives, Catal. Today. 77 (2003) 419–449. doi:10.1016/s0920-5861(02)00384-x.

[135] A.T. Bell, G.C. Bond, D.T. Thompson, M. Valden, X. Lai, D.W. Goodman, T. Blasko, J.M.L. Nieto, K. Chen, A.T. Bell, E. Iglesia, T. Koyama, T. Komaya, P.L. Gai, M. Weyland, G. Durscher, N.D. Browning, S.J. Pennycook, F. Besenbacker, P.C. Thune, J. Loss, D. Wonter, P.J. Leustra, J.W. Niemantsverdriet, J. Corker, V. Vidal, A. Theolier, J. Thivolle-Cazat, J.-M. Basset, C. Nozkaki, C.G. Lugmair, A.T. Bell, T.D. Tilley, D. Kolb, K.P. De Jong, J.W. Geus, The impact of nanoscience on heterogeneous catalysis., Science. 299 (2003) 1688–91. doi:10.1126/science.1083671.

[136] J.R. Gaudet, A. De La Riva, E.J. Peterson, T. Bolin, A.K. Datye, Improved low-temperature CO oxidation performance of Pd supported on la-stabilized alumina, ACS Catal. 3 (2013) 846–855. doi:10.1021/cs400024u.

[137] E.J. Peterson, A.T. DeLaRiva, S. Lin, R.S. Johnson, H. Guo, J.T. Miller, J. Hun Kwak, C.H.F. Peden, B. Kiefer, L.F. Allard, F.H. Ribeiro, A.K. Datye, Low-temperature carbon monoxide oxidation catalysed by regenerable atomically dispersed palladium on alumina., Nat. Commun. 5 (2014) 4885. doi:10.1038/ncomms5885.

[138] Q. Dong, S. Yin, C. Guo, X. Wu, T. Kimura, T. Sato, Aluminium doped ceria–zirconia supported palladium-alumina catalyst with high oxygen storage capacity and CO oxidation activity, Mater. Res. Bull. 48 (2013) 4989–4992. doi:10.1016/j.materresbull.2013.05.054.

[139] W. Lang, P. Laing, Y. Cheng, C. Hubbard, M.P. Harold, Co-oxidation of CO and propylene on Pd/CeO2-ZrO2and Pd/Al2O3monolith catalysts: A light-off, kinetics, and mechanistic study, Appl. Catal. B Environ. 218 (2017) 430–442. doi:10.1016/j.apcatb.2017.06.064.

[140] Y. Nagao, Y. Nakahara, T. Sato, S. Nakano, M. Machida, TWC Performance of Honeycomb Catalysts Coated with Pd-Supported 10Al2O3 · 2B2O3 and Its Cation-Substituted Compounds, Emiss. Control Sci. Technol. 2 (2016) 57–65. doi:10.1007/s40825-016-0037-z.

[141] J.R. Theis, A. Getsoian, C. Lambert, The Development of Low Temperature Three-Way Catalysts for High Efficiency Gasoline Engines of the Future, SAE Int. J. Fuels Lubr. 10 (2017) 2017-01–0918. doi:10.4271/2017-01-0918.

[142] R. Caporali, S. Chansai, R. Burch, J.J. Delgado, A. Goguet, C. Hardacre, L. Mantarosie, D. Thompsett, Critical role of water in the direct oxidation of CO and hydrocarbons in diesel exhaust after treatment catalysis, Appl. Catal. B Environ. 147 (2014) 764–769. doi:10.1016/j.apcatb.2013.10.004.

[143] C.L. Li, C.L. Wang, Y.C. Lin, Pd-integrated lanthanum-transition metal perovskites for methanol partial oxidation, Catal. Today. 174 (2011) 135–140. doi:10.1016/j.cattod.2011.01.038.

[144] F. Mudu, U. Olsbye, B. Arstad, S. Diplas, Y. Li, H. Fjellvåg, Aluminium substituted lanthanum based perovskite type oxides, non-stoichiometry and performance in methane partial oxidation by framework oxygen, Appl. Catal. A Gen. 523 (2016) 171–181. doi:10.1016/j.apcata.2016.05.013.

[145] A. Mishra, R. Prasad, Preparation and application of perovskite catalysts for diesel soot emissions control: An overview, Catal. Rev. - Sci. Eng. 56 (2014) 57–81. doi:10.1080/01614940.2014.866438.

[146] H. Zhu, P. Zhang, S. Dai, Recent Advances of Lanthanum-Based Perovskite Oxides for Catalysis, ACS Catal. 5 (2015) 6370–6385. doi:10.1021/acscatal.5b01667.

[147] S. Keav, S. Matam, D. Ferri, A. Weidenkaff, Structured Perovskite-Based Catalysts and Their Application as Three-Way Catalytic Converters—A Review, Catalysts. 4 (2014) 226–255. doi:10.3390/catal4030226.

[148] G.C.M. Rodríguez, K. Kelm, S. Heikens, W. Grünert, B. Saruhan, Pd-integrated perovskites for TWC applications: Synthesis, microstructure and N 2O-selectivity, Catal. Today. 184 (2012) 184–191. doi:10.1016/j.cattod.2011.12.026.

[149] G.C. Mondragón Rodríguez, B. Saruhan, O. Petrova, W. Grünert, Pd-integrated perovskite as effective catalyst for selective catalytic reduction of NOx by propene, Top. Catal. 52 (2009) 1723–1727. doi:10.1007/s11244-009-9326-x.

[150] E. Tzimpilis, N. Moschoudis, M. Stoukides, P. Bekiaroglou, Preparation, active phase composition and Pd content of perovskite-type oxides, Appl. Catal. B Environ. 84 (2008) 607–615. doi:10.1016/j.apcatb.2008.05.016.

[151] V.A. Sadykov, L.A. Isupova, S.F. Tikhov, O.N. Kimkhai, Perovskite Catalysts: High-Surface Area Powders Synthesis, Monoliths Shaping and High-Temperature Applications, ChemInform. 26 (2010) no-no. doi:10.1002/chin.199550238.

[152] A. Christoffel, N. Preller, Numerical modelling of flow through packed beds of uniform spheres, (2011).

[153] Y. Farhang, E. Taheri-Nassaj, M. Rezaei, Pd doped LaSrCuO4 perovskite nano-catalysts synthesized by a novel solid state method for CO oxidation and Methane combustion, Ceram. Int. 44 (2018) 21499–21506. doi:10.1016/j.ceramint.2018.08.211.

[154] B. Kucharczyk, Catalytic Oxidation of Carbon Monoxide on Pd-Containing LaMnO3 Perovskites, Catal. Letters. 145 (2015) 1237–1245. doi:10.1007/s10562-015-1518-3.

[155] U.G. Singh, J. Li, J.W. Bennett, A.M. Rappe, R. Seshadri, S.L. Scott, A Pd-doped

perovskite catalyst, BaCe1-x PdxO3-d, for CO oxidation, J. Catal. 249 (2007) 349–358. doi:10.1016/j.jcat.2007.04.023.

[156] W. Yang, R. Zhang, B. Chen, N. Bion, D. Duprez, S. Royer, Activity of perovskite-type mixed oxides for the low-temperature CO oxidation: Evidence of oxygen species participation from the solid, J. Catal. 295 (2012) 45–58. doi:10.1016/j.jcat.2012.07.022.

[157] S.B. Varandili, A. Babaei, A. Ataie, A.A. Khodadadi, H. Kazerooni, Nano-structured Pd doped LaFe(Co)O3 perovskite; synthesis, characterization and catalytic behavior, Mater. Chem. Phys. 205 (2018) 228–239. doi:10.1016/j.matchemphys.2017.11.030.

[158] N. Russo, P. Palmisano, D. Fino, Pd substitution effects on perovskite catalyst activity for methane emission control, Chem. Eng. J. 154 (2009) 137–141. doi:10.1016/j.cej.2009.05.015.

[159] R. Zhang, H. Alamdari, S. Kaliaguine, Fe-based perovskites substituted by copper and palladium for NO + CO reaction, 242 (2006) 241–253. doi:10.1016/j.jcat.2006.05.033.

[160] G.A. Somorjai, On the mechanism of sulfur poisoning of platinum catalysts, J. Catal. 27 (1972) 453–456. doi:10.1016/0021-9517(72)90183-2.

[161] O.T. Conditions, Comparing Co 2 Emission Levels of a Modern and on-Road Testing Conditions, (2019).

[162] R.E. Hayes, A. Fadic, J. Mmbaga, A. Najafi, CFD modelling of the automotive catalytic converter, Catal. Today. 188 (2012) 94–105. doi:10.1016/j.cattod.2012.03.015.

[163] P. Karuppusamy, R. Senthil, Design, Analysis of Flow Characteristics of Catalytic Converter and Effects of Shape of Catalytic Converter, Int. J. Res. Eng. Adv. Technol. 1 (2013) 1–6. www.ijreat.org.

APPENDIX A

Geometric Surface Area (GSA) Calculation

1. Hollow fibre dimensions (Measurements were taken based on average)

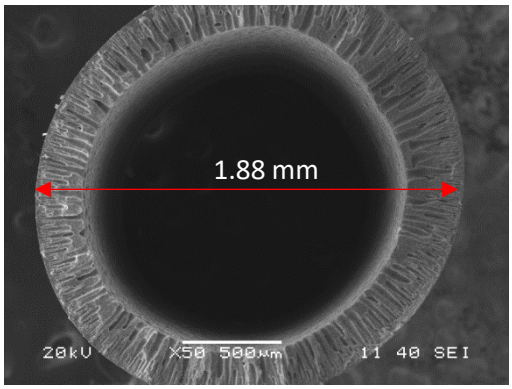

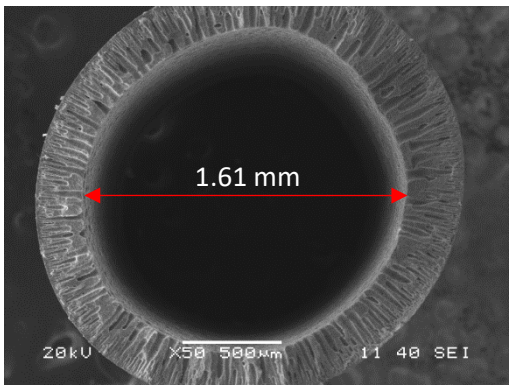

2. Microchannels

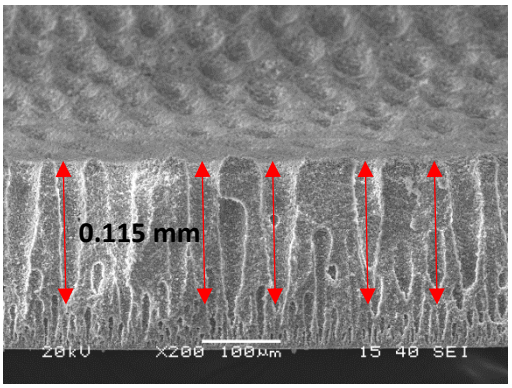

The outer skin-like layer is around

20 micron

Length of micro-channels

= (1.88 mm – 1.61 mm) ÷2 – 20 µm skin

= 0.115 mm

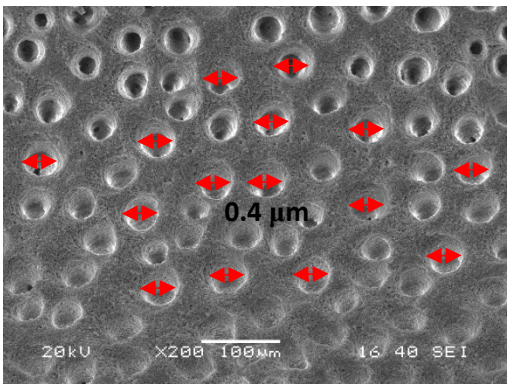

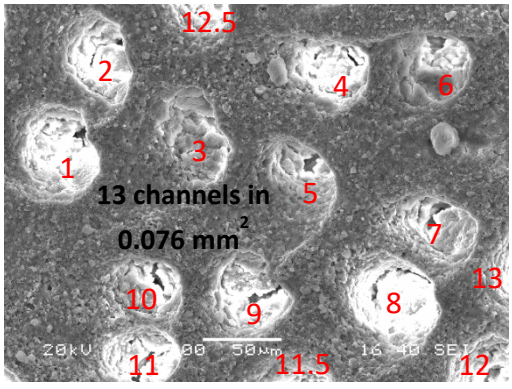

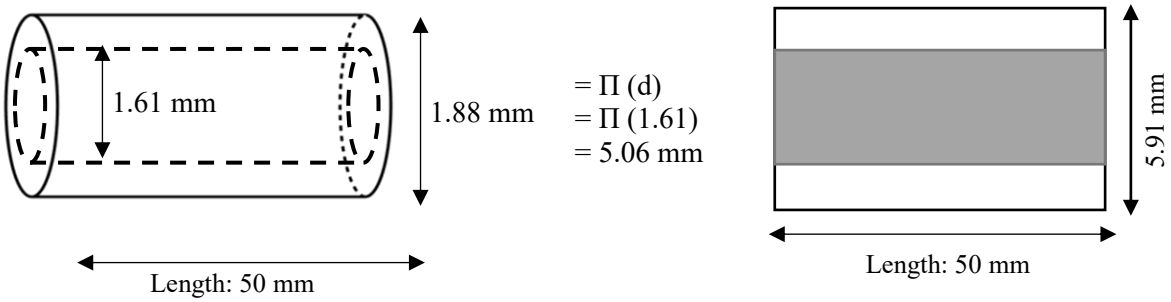

Assumption: Perfect packing in cylinder = 91 fibres

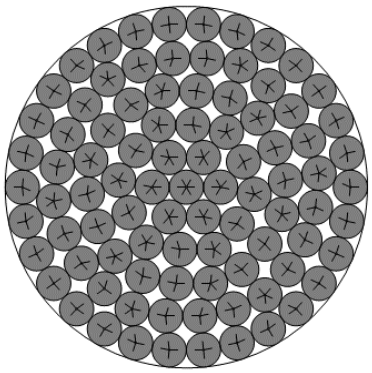

Number of Fibres = 91

Radius of cylinder = 0.09463 x 91 x radius of 1 fibre

= 0.09463 x 91 x (1.88 ÷ 2)

= 8.1 mm

Surface Area Calculations

Total inner surface area A = 50 mm x 5.06 mm

= 253 mm^2

= 253 mm^2 ÷ 0.076 mm^2 = 3328.95 blocks

Thus, 3328.95 x 13 microchannels ~~ 43,276 microchannels per 50 mm fibre.

Area of microchannel entrance (circle) $= \pi r^2 = \pi (0.02^2) = 1.26 \times 10^{-3}$ mm^2

Total area of microchannel entrance $= 43{,}276$ channels $\times 1.26 \times 10^{-3}$ mm^2

$= 54.53$ mm^2

Inner fibre surface area = Area A for inner – microchannels entrance $= 253$ mm^2 – 54.53 mm^2 $= 198.47$ mm^2

1 microchannel

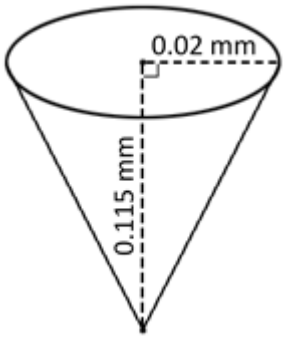

Assumption = cone structure

Surface area for 1 microchannel $= 8.59 \times 10^{-3}$ mm^2

Surface area for all microchannels $= 43{,}276 \times 8.59 \times 10^{-3}$ mm^2

$= 371.74$ mm^2

Surface area of microchannels without entrance area

$= 371.74$ mm^2 - Surface area of microchannel entrance

$= 371.74$ mm^2 – 54.53 mm^2

$= 317.21$ mm^2

Total area = (Area of inner fibre – microchannels entrance area + microchannel cone area) x 91 fibres

$= (198.47$ mm^2 – 54.53 mm^2 + 317.21 mm^2) x 91

$= 461.15$ mm^2 x 91

= 41964.65 mm^2

Volume Calculations

Volume for 91 fibres $= \pi\ r^2\ h$

$= \pi\ (8.1)^2\ (50)$

$= 10305.99\ mm^3$

Geometric Surface Area = Area ÷ volume

$= 41964.65 \div 10305.99$

$= 4.07\ mm^2\ mm^{-3}$

APPENDIX B

Pressure Drop in Hollow Fibre Substrate Calculation

Cross-sectional area of pipe = $\Pi.r^2 = \Pi\ (1.2 \times 10^{-3})^2 = 4.52\ mm^2$

Assumption; Fluid velocity, $u = 10\ m.s^{-1}$

The Reynolds number is given by $Re = (\rho \times u \times d_i) / \mu$

Reynolds number, $Re = (1.225 \times 10 \times 2.4 \times 10^{-3}) / (1.7894 \times 10^{-5}) = 1643.01$ = Laminar

Absolute roughness of the substrate = 0.75

Relative roughness = $0.75 / (2.4 \times 10^{-3}) = 0.3125$

From Moody Chart, friction factor, $f = 0.039$

Table 1 Miscellaneous losses

Fitting / valve	Number of velocity heads, ***K***	Equivalent pipe diameters
Entry	0.5	2.4
Exit	1.0	2.4
Total	1.5	4.8

Method, velocity heads

A velocity head = $u^2 / 2g = 10^2 / (2 \times 9.8) = 5.10$ m

Head loss = $5.10 \times 1.5 = 7.65$ m

As pressure = $7.65 \times 1.225 \times 9.8 = 91.88\ N.m^{-2}$

Friction loss in hollow fibre substrate, ΔP_f = 8 x 0.039 x (120/2.4 x 10^{-3}) x 1.225 x (10^2/2)

= 0.9555 N.m^{-2}

Total pressure loss = 91.88 + 0.9555 = 92.84 ~ 93 N.m^{-2}

Pressure Drop in Commercial Catalytic Converter Substrate Calculation

Cross-sectional area of pipe = Π.r^2 = Π (0.425x 10^{-3})^2 = 0.5675 mm^2

Fluid velocity, u = 10 m.s^{-1}

The Reynolds number is given by $Re = (\rho \times u \times d_i) / \mu$

Reynolds number, Re = (1.225 x 10 x 0.85 x 10^{-3}) / (1.7894 x 10^{-5}) = 581.90 = Laminar

Absolute roughness of the substrate = 0.75

Relative roughness = 0.75 / (0.85 x 10^{-3}) = 0.8824

From Moody Chart, friction factor, f = 0.11

Table 2 Miscellaneous losses

Fitting / valve	Number of velocity heads, ***K***	Equivalent pipe diameters
Entry	0.5	2.4
Exit	1.0	2.4
Total	1.5	4.8

Method, velocity heads

A velocity head = u^2 / 2g = 10^2 / (2 x 9.8) = 5.10 m

Head loss = 5.10 x 1.5 = 7.65 m

As pressure = 7.65 x 1.225 x 9.8 = 91.88 N.m^{-2}

Friction loss in honeycomb substrate, ΔP_f $= 8 \times 0.11 \times (120/0.85 \times 10^{-3}) \times 1.225 \times (10^2/2)$

$= 7.60$ N.m^{-2}

Total pressure loss = 91.88 + 7.60 = 99.48 N.m^{-2} ~ 100 N.m^{-2}